Novel Aromatic Boron-Nitrogen Heterocycles: Synthesis, Properties and Applications in Biomedicine and Optoelectronics

Hannah Hackney

A thesis submitted in partial fulfillment of the requirements for the degree of

Master of Science

Department of Chemistry

University of Alberta

Abstract

Heterocyclic chemistry often calls for an interdisciplinary approach to research. Novel structures invite study from both a fundamental and applied standpoint, and a given scaffold may have properties relevant to synthesis, medicine, catalysis, optoelectronics, and more. In recent decades, boron compounds have become increasingly relevant in these areas, and many simple boronic heterocycles have yet to be comprehensively explored. This work first identifies synthetic strategies to make novel tricoordinate polycyclic aromatic B–N heterocycles. Then, the resulting structures are characterised structurally, using techniques such as pKa measurement, single crystal X-ray crystallography, and NMR spectroscopy. Finally, sample applications are proposed in the areas of optoelectronics and biomedicine.

Chapter 2 describes the synthesis, structure, photophysical properties, and applications of a new luminescent polyaromatic boronic scaffold (DNKs). This scaffold is structurally similar to aryl-Bdan compounds, but it exhibits dramatically different properties. Preliminary synthetic methodology was developed to produce DNKs with differing phenyl and naphthyl substitution patterns in low to moderate yields across two steps. Out of a library of compounds, three DNKs were selected for detailed characterisation and study. X-ray crystallographic study of two DNKs revealed notable structural differences between these compounds and phenyl-Bdan, including markedly shortened C–N bonds and an elongated B–N bond adjacent to the carbonyl, which participated in an intramolecular hydrogen bond. Photophysical data was subsequently collected in the solution and the solid state, with moderate to high quantum yields**.** Compounds within the library exhibit solvatochromism and aggregation-induced emission.

The fluorescence of the DNK compounds appears responsive to various chemical conditions, suggesting DNKs may have potential as a flexible, customizable molecular logic

platform. A simple molecular logic model system was created in solution with 2-inputs and 2-outputs. Additionally, a proof of concept was developed for a system detecting trace boronic acid contaminants at 5-15 ppm level. This method could be useful to pharmaceutical companies concerned with difficult to detect, mutagenic synthetic intermediates in drug samples.

In Chapter 3, an underexplored borazaronaphthalene isomer was envisioned as a product of an enamine cyclisation and an esterification of a boronic acid with a benzylic ketone moiety. In this novel synthetic strategy, the boronic acid is a platform for condensation with easily-accessible and cheap amine modules, generating a diverse library of new structures with aromatic isosterism. Non-classical borylation methods were necessary to produce previously unknown arylboronic building blocks. Enamine adducts could be formed by reaction with many alkyl or aryl amines and aminoalcohols, although notable failures include 1,2-aminoalcohols, aminosulfur compounds and amino acids.

A representative compound was chosen for thorough characterization. Screening suggests that it is effective against methicillin-resistant *S. aureus*, inviting further biological study to assess its medicinal potential. Its pKa of 9 was similar to free arylboronic acids and higher than typical arylboronic cyclic esters, which could be due to partial aromatic character of the B–N containing ring. X-ray crystallographic studies revealed a highly planar structure with unusually short C–N and C–B bonds within the enamine ring, which supported the interpretation of increased π delocalization.

Basic fluorometry data was collected for a few class members, which suggests fluorescence may be general for these species. The qualitative fluorescence is unique compared to naphthalenes and non-enamine phenyl-Bdan, which calls for further investigation and the collection of quantum yields.

Acknowledgments

I am incredibly grateful for my supervisor, Dr. Dennis Hall, who is both a great scientist and caring educator. My time in the Hall lab was a period of great professional and personal growth, and Dennis was instrumental in creating an environment that values creativity, intellectual independence, and the pursuit of nascent ideas. I am very grateful for his support and encouragement.

I must also thank all Hall Group members, past and present. This lab is comprised of down-to-earth, kind people who care deeply and support each other in doing their best work. Especially, I would like to thank Jasmine Bhangu and Carl Estrada for working alongside me every day of the M.Sc. program and providing emotional support. This experience was much richer having done it as a team with two warm, generous people. Thanks also to Dr. Michele Boghi for mentoring me patiently as I began my work and Dr. Burcin Akgun for her advice and joyful friendship. Thanks to Dr. Helen Clement, Rory MacDonald, Dr. Marco Paladino and Jason Rygus, kind people who were generous with their time and formidable expertise when I (frequently) had questions.

Outside of our lab, I'd like to thank Dr. Jeff Stryker for his inspiring intellectual approach and mentorship. His lectures and emphatic encouragement helped shape my relationship, and future, with chemistry. Thank you to Dr. Dave Scott, whose enthusiastic technical advice, experimental support, and friendship brightened many days in Edmonton. Thanks to Hayley Wan, who is a pleasure to work with and one of the best parts of teaching assistantship. My work was also made possible by Wayne Moffat and Jennifer Jones of the Analytical and Instrumentation Lab; Ed Fu and his HPLC expertise; Dr. Michael Ferguson and Dr. Yuqiao Zhu and their incredible crystallographic work, and the entire staff of the Mass Spectroscopy Facilities.

There are also people in my personal life that made this thesis possible by filling me up and shaping the values I treasure. Thanks to my family and especially to my three engineers: my sister Rachel, for defining family for me since the day I was born; my father Steve, for providing me intellectual outlets and companionship, and teaching me integrity and self-discipline; and my mother Lori, for providing me with an example of what it means to be fierce and independent, but retain compassion, and to fight for one's own future and education. Finally, I must thank my best friend, Aurelie Frenette-Araujo, for her daily conversation and companionship throughout this

work. Her loyalty, emotional insight, and love through the toughest parts made everything possible.

Table of Contents

List of Tables

List of Figures

List of Abbreviations

9-BBN	9-borabicyclo[3.3.1]nonane
Å	Ångstrom(s)
Ac	acyl
AIE	aggregation induced emission
Ar	aryl
B_2pin_2	bis(pinacolato)diboron
BAHC	boronic acids and heteroatom condensates
Bdan	1,8-diaminonaphthalene boron adduct
BINAM	1,1'-bi(2-naphthylamine)
Bn	benzyl
BODIPY	4,4-difluoro-4-bora-3a,4a-diaza-s-indacene
Bpin	boron pinacolate ester
calcd.	calculated
CO-ADD	Community for Open Antimicrobial Drug Discovery
cod	1,5-cyclooctadiene
comp m	complex multiplet
conc	concentration
d	doublet
D_2O	deuterium oxide
DAN	1,8-diaminonaphthalene
dba	dibenzylideneacetone
DBU	1,8-diazabicyclo[5.4.0]undec-7-ene
o-DCB	*ortho*-dichlorobenzene
DCM	dichloromethane
dd	doublet of doublets
ddd	doublet of doublet of doublets
dddd	doublet of doublet of doublet of doublets
DDQ	2,3-dichloro-5,6-dicyano-1,4-benzoquinone

DFT	Density Functional Theory
DIPEA	*N,N*-diisopropylethylamine
DMF	dimethylformamide
DMSO	dimethyl sulfoxide
DNK	diazaborolyl naphthyl ketone
dppf	1,1′-ferrocenediyl-bis(diphenylphosphine)
EI	electron ionization
ε	molar extinction coefficient
equiv	equivalent(s)
ESI	eletrospray ionization
ESIPT	excited state intramolecular proton transfer
Et	ethyl
Et_3N	triethylamine
EtOAc	ethyl acetate
g	gram(s)
h	hour(s)
HBBC	hexa-peri-hexabenzoborazinocoronene
HBC	hexa-peri-hexabenzocoronene
HOMO	highest occupied molecular orbital
HPLC	high performance liquid chromatography
HRMS	high resolution mass spectroscopy
Hz	Hertz
IR	infrared
*i*Pr	isopropyl
λ	wavelength
LC-MS	liquid chromatography-mass spectroscopy
LG	leaving group
LED	light emitting diode
LiTMP	lithium tetramethylpiperidine
LUMO	lowest unoccupied molecular orbital
M	molar

m/z	mass to ion ratio
Me	methyl
MeCN	acetonitrile
MeOH	methanol
Mes	mesityl
mg	milligram(s)
MHz	megahertz
MIDA	*N*-methyliminodiacetic acid
min	minute(s)
mL	milliliter
ML	mechanoluminescence
mM	millimolar
mmol	millimole
mol	mole
MRSA	methicillin-resistant *S. aureus*
NBS	*N*-bromosuccinimide
*n*Bu	butyl
*n*Pr	propyl
NICS	nucleus-independent chemical shift
NMR	nuclear-magnetic resonance
ORTEP	oak ridge thermal ellipsoid plot
PAH	polyaromatic hydrocarbon
Ph	phenyl
Φ	quantum yield of luminescence
ppb	parts per billion
PPTS	pyridinium *p*-toluenesulfonate
*p*TsOH	*para*-toluene sulfonic acid
pyr	pyridine
R_f	retention factor
rt	room temperature
RTP	room temperature phosphorescence

SPhos	2-dicyclohexylphosphino-2',6'-dimethoxybiphenyl
τ	phosphorescence lifetime
*t*Bu	tertiary butyl
TEA	triethylamine
Tf	triflic
TfOH	triflic acid
THF	tetrahydrofuran
TLC	thin layer chromatography
TNT	2,4,6-trinitrotoluene
tmphen	3,4,7,8-tetramethyl-1,10-phenanthroline
TMS	trimethylsilyl
UV	ultraviolet
Vis	visible
XPhos	2-dicyclohexylphosphino-2′,4′,6′-triisopropylbiphenyl
XPhos Pd G2	chloro(2-dicyclohexylphosphino-2′,4′,6′-triisopropyl-1,1′-biphenyl)[2-(2′-amino-1,1′-biphenyl)]palladium(II)

List of Schemes

A literature survey of the luminescence of arylboronic acids and their heteroatom condensates

1.1 Introduction

In recent years, boron has gained considerable traction in organic optoelectronics.[1] For example, it can act as a heteroatom dopant in graphene fragments.[2] Replacement of C–C double bonds with the isoelectronic and isosteric B–N bond can dramatically tune the performance of familiar aromatic hydrocarbons, as has been shown by a long tradition of studies started by Michael Dewar 60 years ago.[3,4] Four-coordinate organoboron compounds have demonstrated potential for a variety of technologies, but they are most widely used in the high performing family of BODIPY dyes.[5] These applications can be contextualized in terms of the organoboron functional groups shown in Figure 1-1.

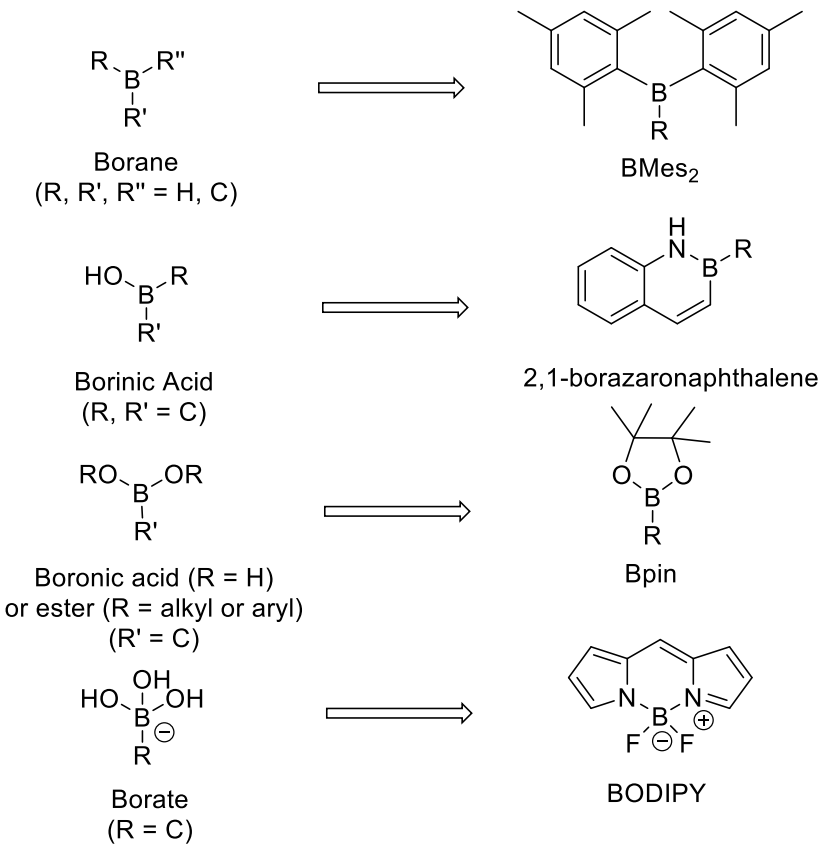

Figure 1-1. The functional groups of boron at left can be correlated to popular boron motifs in optoelectronics.

Arylboronic esters and acids show markedly superior stability compared to boranes and borinic acids.[6] They are generally stable to oxygen, water, and can tolerate broad pH ranges, making for robust compounds that can be handled in ambient conditions. Further, most boronates present little toxicity, and this fact combined with their slow oxidation into boric acid makes them environmentally friendly. Many of these properties can be related to boron's vacant p orbital. When boron is bonded to atoms bearing lone pairs, such as oxygen or nitrogen, its vacant orbital accepts electron density through π conjugation, giving the B–X moiety partial double bond character. Though there is evidence for B-C π conjugation in B–C(sp^2) as well, lone pair conjugation helps give boronates their unique properties in contrast to other boron species. These

interactions have a dramatic effect on the properties for which organoboron compounds are known, such as Lewis acidity, thermodynamic stability, and key electronic phenomena like reactivity and luminescence.

In luminescence chemistry, boron seems to get its widest usage in patterns like $BMes_2$ and boron difluorides, and for good reason. In each respect these boron groups have attractive electronic characteristics that appear to translate well into new contexts. The steric bulk of -$BMes_2$ kinetically stabilizes the vacant p orbital and prevents close molecular packing, giving high solid-state quantum yields.[7] The difluoride motif has gone beyond BODIPY to act as a robust design strategy for creating novel luminescent materials on a variety of scaffolds (Figure 1-2).[8,9]

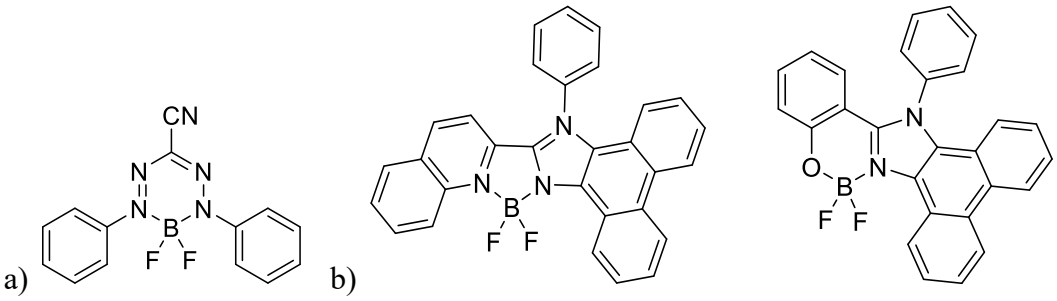

Figure 1-2. a) An example of a boron formazanate dye, pioneered by Gilroy and coworkers.[8] b) Two dyes synthesized by Luo and coworkers; one features an N–B–O motif that is growing in popularity.[9]

Between the electron-poor boranes and electron-rich tetrahedral borates lies the middle ground of boronic esters and acids, which have received far less attention in luminescence chemistry. This void may be explained by their 'moderated' electronic poorness, which makes them less applicable to popular donor-acceptor designs where electron withdrawing groups are required, and boranes perform excellently in this capacity. Compared to azaborines (R_2BN), boronates are not good electronic analogies for C=C bonds towards the precise and controlled alteration of polyaromatic hydrocarbon (PAH) properties, as their additional pair of electrons

renders them no longer isoelectronic. Moreover, with our current level of understanding, it is difficult to predict if or how a boronate will luminesce, in turn making them difficult to apply in rational design. As suggested by the recent discovery that phenyl-Bpins (boron pinacolate esters) are capable of room-temperature phosphorescence in air,[10] the field is at a stage where the basic luminescence of arylboronates is only beginning to be appreciated. In spite of these challenges, there has been an upsurge in the study of boronate luminescence in the last couple decades, following varied reports of their unique optical attributes and efficient performance. Considering their advantages of stability and modularity, we hope that a survey and analysis of trends can facilitate their application as they assume their place in luminescence chemistry amidst other organoborons.

This short review will survey the literature on the inherent luminescence of tricoordinate arylboronates, or boronic acids and heteroatom condensates (BAHCs), of the type shown in Figure 1-3. The contents are arranged by bond motif, with azaborolines (Ar–BNY) grouped into structural trends, followed by boronic acids and esters (Ar-BO_2). Polymers, inorganic and alkynyl boronates will not be covered. A few examples of intrinsically luminescent BAHC sensors will be described, but the focus must be restricted in this respect as well. As shown in Fang and coworkers' comprehensive 2018 review,[11] boronic acids and esters have received a lot of attention as sensors that form luminescent species *in situ*, for the detection or tagging of glucose, sialic acid, endogenous hydrogen peroxide, fluoride ion, and so on. Because the luminescence often follows oxidation of the C-B bond, or tetrahedral coordination of the boron, that literature will not be discussed.

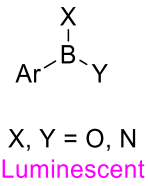

Figure 1-3. Schematic of the structures surveyed in this review.

1.2 Ar–BNY

1.2.1 Diazaborolines

Diazaborolines, or 5-membered N–B–N rings (Figure 1-4), are 6π-electron compounds demonstrated to be heteroaromatic by NMR spectroscopy, photoelectron spectroscopy and theoretical study.[12] In addition to their relevance to ligand chemistry and electrochemistry, they are some of the best-studied of all BAHC luminophores, owing to their high quantum yields, thermodynamic stability, and large Stokes shifts. For this reason, their luminescence has already been the subject of an excellent, comprehensive review by Weber and Bohling, released in 2015 and covering the previous two decades during which most of the research has been accomplished.[7] Since then, one important paper on the subject has been published,[13] which can serve to introduce their interesting properties in the context of this review.

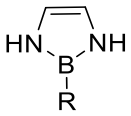

Figure 1-4. The core structure of 1,3,2-diazaborolines.

In this work, Weber and coworkers disclosed some push-pull (or donor-acceptor) systems: this is a popular and effective design strategy where electron accepting and electron donating

substituents are separated in space by a π conjugated system (D–π–A), yielding efficient luminophores with tuned Stokes shifts (Figure 1-5).

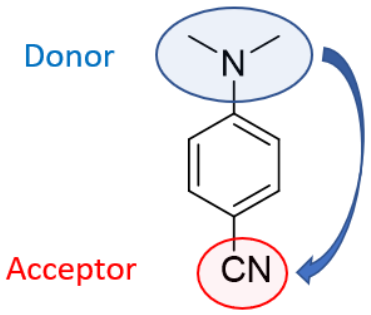

Figure 1-5. Donor-pi-acceptor systems. If, during excitation, electron density is transferred into a spatially distant orbital, the resulting dramatic change in the molecule's dipole can give a large Stokes shift as the molecule is forced to reorganize itself with respect to its environment, losing energy in the excited state.

One of the most familiar boron groups for the purpose of D–π–A, and indeed in organic optoelectronics generally, is $BMes_2$. Diazaborolines, however, have been increasingly explored. It is worth noting that, assessing the p orbitals of the NBN unit, this motif is isoelectronic with the electron-rich allyl anion. While the common expectation of tricoordinate boron species is that they are good π acceptors, owing to the vacant p orbital on boron, calculations on the diazaboroline system have suggested that this heterocycle is a π donor comparable to $-NMe_2$ or -OMe, unless strong electron withdrawing groups are placed onto the nitrogen atoms.[13] In addition to their performance and efficiency, these systems expand our basic conceptions about the behaviour of boron luminophores, and this fact, combined with their potential as a bifunctional, π donating or accepting module, justifies the explosion of interest.

Weber and coworkers produced select D–π–A diazaborolinyl-substituted thiophenes and their indole congeners to help elucidate the fundamental properties of diazaborolines and the

impact of the B–N bond replacement.[13] While two structures, with alkynyl spacers, are outside the scope of this review, multiple comparator compounds for their thiophenyl example were included to allow for good comparison (Figure 1-6).

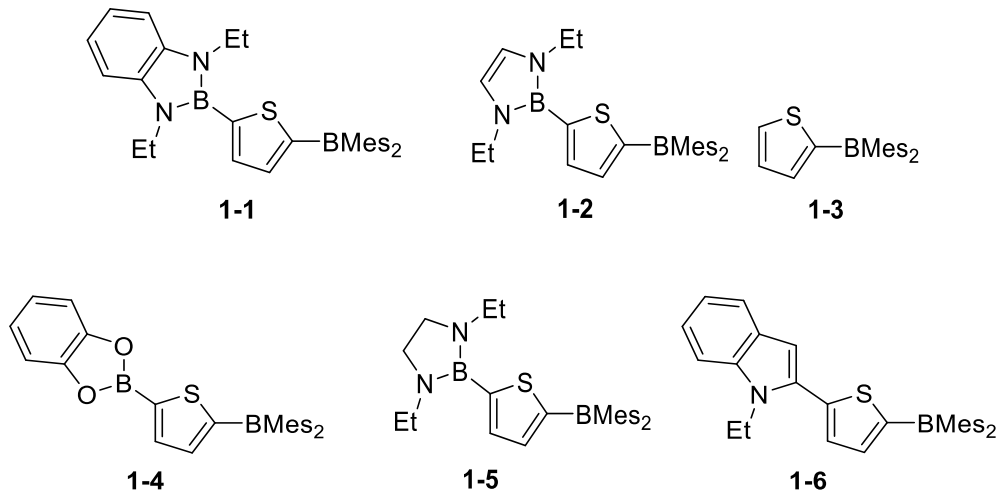

Figure 1-6. The diazaboroline **1-1** and its five comparators.

X-ray crystallographic data showed that, in key bond lengths and angles, diazaboroline **1-1** is almost identical to its indole counterpart **1-6**, though with a smaller twist between the donor motif and the thiophene ring, suggesting that the diazaboroline may have better electronic communication across the π structure (at least in the solid state). In the photophysical data (Table 1-1), addition of the diazaboroline group (structure **1-1** versus **1-3**) red-shifted the absorption maximum, shrinking the HOMO-LUMO gap compared to the π-A system. In lieu of computations on this control, an interpretation of this result could be that the addition of the donor diazaboroline results in more extensive pi conjugation and charge transfer character. Next, diazaboroline **1-1** can be compared with the set of its non-benzannulated **1-2**, saturated **1-5**, and even catecholboron **1-4** counterparts. Apparently, the Ar–N connections are important, as it gave a red shift in the absorption and emission maxima compared to this entire set of controls, probably due to the

diazaboroline group being a better donor. This connection also gave a massive increase in quantum yield, from 0.01 for the controls in both solvents to 0.81 and 0.46 in cyclohexane and THF, respectively. Interestingly, these good quantum yields were trumped by the Ar–N indolyl control **1-6** (0.97 in cyclohexane and 0.93 in THF), which demands separate consideration. While the absorption of the indolyl **1-6** was red shifted, its emission wavelength was blue-shifted compared to the diazaboroline **1-1**. The authors proposed that, in contrast to the solid state results, the ground state of compound **1-6** may be more planar: therefore, to achieve a planar excited state, it would require less geometric reorganization than **1-1**. It is conceivable that these molecular motions required of the diazaboroline **1-1** could be related to its greater rate of nonradiative relaxation and lower quantum yield.

Table 1-1. Selected photophysical data for compounds **1-1** to **1-6**

Compound	Solvent	λ_{abs} (nm)	λ_{em} (nm)	Φ_F
1-1	Cyclohexane	345	439	0.81
	THF	350	482	0.46
1-2	Cyclohexane	331	383	0.01
	THF	331	400	0.01
1-3	Cyclohexane	323	360	0.01
	THF	323	384	0.01
1-4	Cyclohexane	335	387	0.01
	THF	333	410	0.01
1-5	Cyclohexane	331	381	0.01
	THF	331	396	0.01
1-6	Cyclohexane	392	428	0.97
	THF	395	472	0.93

λ_{abs} and λ_{em} are wavelengths of the absorption and fluorescence emission maxima, respectively; Φ_F is the relative fluorescence quantum yield compared to 2,2'-benzene-1,4-diylbis(5-phenyl-1,3-oxazole) in anhydrous and distilled solvent.

1.2.2 Borazines and their fragments

While Stock was the first to discover borazine, or 'inorganic benzene',[14] it was the work of Dewar and Koster that bridged the gap into organic chemistry by positioning this subunit within polyaromatic hydrocarbon structures.[15,16] This weakly-aromatic[17] analogue shows markedly different properties and reactivity than benzene, which can be modulated by where the motif is placed. When embedded in a carbon framework, the BN bond shows good stability, but as recent nanographene research has demonstrated, an arene's optoelectronics can be effectively controlled by manipulating the shape and heteroatom doping at the edge.[18] Researchers in the last 15 years have produced structures and disconnections using both embedded and edge motifs.

Yamaguchi and coworkers were the first to closely examine the luminescent potential of aryl borazines. They published a paper in 2005 showcasing a sterically congested "bundle" scaffold with aryl substituents orthogonal to the borazine core (Figure 1-7a).[19] The close proximity of the arenes' neighbouring pi orbitals could permit through-space and through-bond interactions, two theoretical phenomena first described in 1968 that can be applied to modulate electronic structure.[20] Manipulating molecular topology to give novel optoelectronic and theoretical properties remains a popular and powerful strategy,[21] and in this endeavor, the authors stated that borazine possessed crucial advantages over the conventional benzene ring. In addition to the greater efficiency and synthetic simplicity in making highly substituted systems, the alternating nitrogen and boron atoms allow regioselective placement of two different aryl substituents in C_3 symmetry around the core. Anthracenes **1-7** were chosen for one of these arene subunits, probably due to their benchmark optoelectronic performance in several respects (particularly in the solid state; Figure 1-7b).

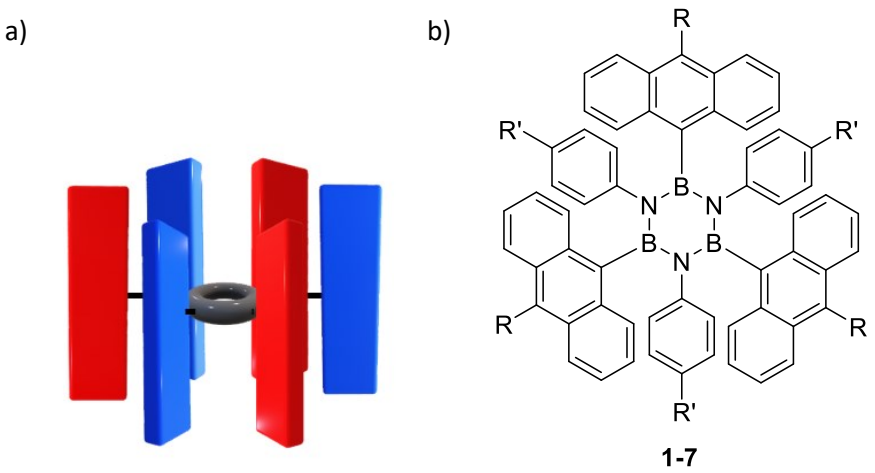

Figure 1-7. Design of the N-aryl borazines. a) This cartoon depicts the bundle topology design. The black ring represents the borazine core and the coloured blocks signify the alternating aryl substituents. The authors hoped that steric congestion would force the π subunits orthogonal to the plane of the borazine ring, close enough for stacking and through-space interactions. b) The design of the borazine bundle library **1-7**.

The photophysics of borazines **1-7**, furnished by a simple one-pot procedure with common reagents, were assessed in contrast with that of anthracene. Compared to this standard, their UV-vis absorption and fluorescence showed bathochromic shifts that can be attributed to the electron-withdrawing nature of the core. Theoretical calculations also showed that the HOMO, while mainly centralized on the anthryl subunits, received some contribution from the B–N–B moiety in the form of a through-bond interaction between anthracenes. The remaining analysis focused on the effects of the bundle structure, where dramatic increases in quantum yield (0.62 for the simplest borazine **1-7** versus 0.27 for anthracene) were rationalized by the decrease in nonradiative relaxation within a more rigid and constrained structure.

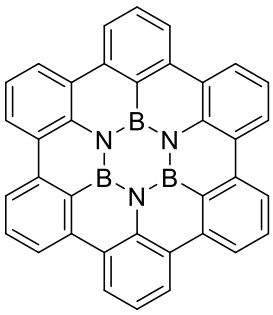

1-8

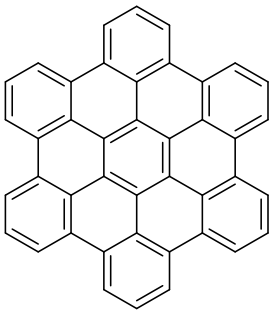

1-9

Figure 1-8. Hexabenzoborazinocoronene (HBBC) **1-8** and its all-carbon congener, the strongly aromatic hexabenzocoronene (HBC) **1-9**.

Following this early paper, borazines that were further studied for their luminescence can be grouped as derivatives of the more conventional, planar structure of hexabenzoborazinocoronene (HBBC, Figure 1-8). Though HBBC **1-8** was first discovered by Bettinger and coworkers in 2015,[22] a thorough optoelectronic study of an HBBC **1-10** was published by Bonifazi and coworkers in 2017. This latter study was enabled by modifications that overcame the solubility issues of HBBC **1-8** in the original work (Scheme 1-1).[23] Their HBBCs showed dramatically different performance than the all-carbon congener of type **1-9**. Consistent with prediction on borazine's nonaromaticity, and the observed effect of heteroatom doping in nanographenes, the borazine moiety widened the optical band gap, giving blue-shifted emissions. Compared to **1-9,** the HBBC **1-10** also had dramatically increased luminescence quantum yields (0.43 versus 0.03, or 0.77 versus 0.05 in oxygen-free solvent), while low temperature phosphorescence studies revealed long-lasting blue emission. Though quantum yields were not reported, the solid form was said to fluoresce violet-blue light at room temperature.

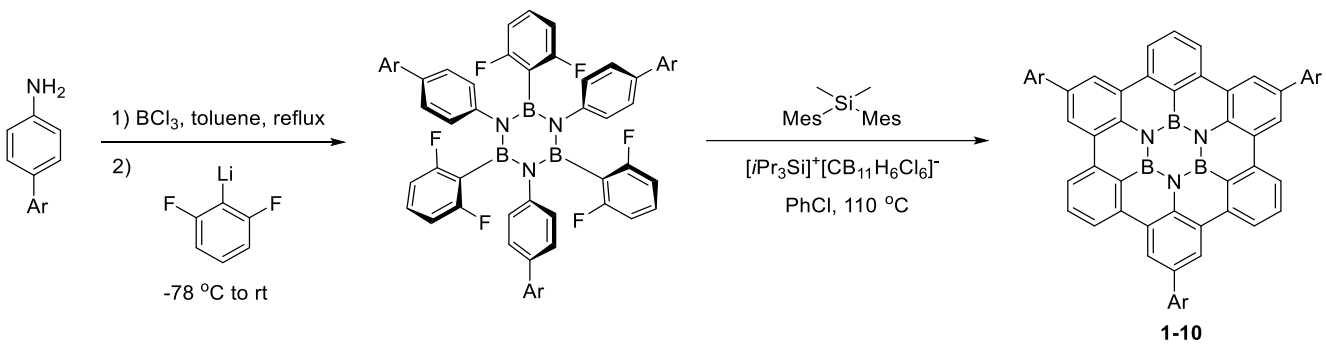

Scheme 1-1. Bonifazi and coworkers' synthesis, in solution, of an HBBC **1-10**.[23]

Numerous other disconnections of HBBC **1-8** can be envisioned, and the Bettinger laboratory has contributed a few papers of interest over the last several years.[24] In 2012, they revived a piece of fundamental boron chemistry from the mid-20th century by synthesizing the racemate of propeller-like trimer **1-11** (Figure 1-9) for photophysical study, which was originally, and sparsely, described by Koster.[25] Consistent with the work of Bonifazi and coworkers, they observed blue-shifted absorption and emission bands compared to the all-carbon congener **1-12**. However, there was only a slight shift in emission for solid state fluorescence (385 nm) when compared to solution (379 nm for the borazine **1-11**; 480 nm for the PAH **1-12**), possibly due to the nature of the packing mode.

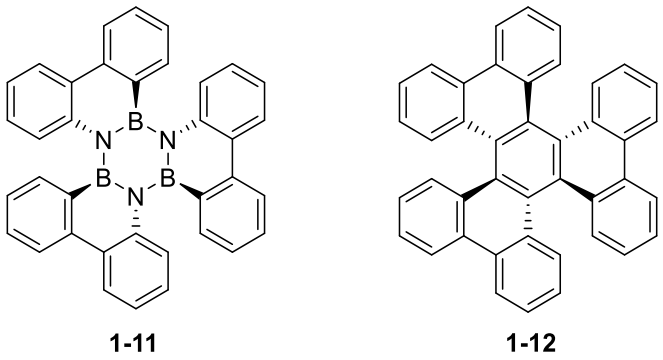

Figure 1-9. The propeller-like trimer **1-11** and its all-carbon congener **1-12**.

The Bettinger laboratory would later apply this trimer as a synthetic precursor to create two borazines bearing a perylene motif.[26] Following photochemically-induced oxidative C–C bond formation, one compound, **1-13**, could have its central B_3N_3 core hydrolyzed to give a BNBN fragment **1-14** (Figure 1-10a). Recalling the other work on borazines in this review, the absorbance bands of these two compounds were markedly blue-shifted in comparison to dibenzoperylene **1-15** (by 70 nm, Figure 1-10b). Interestingly, the fluorescence emission of the larger borazine **1-13** bore a slight blue shift in comparison to the smaller fragment **1-14**, both emitting in the deep blue portion of the spectrum. Recently, a gram-scale bottom-up route to access structure **1-14** was disclosed. This synthesis featured interesting intermediates whose synthesis and photophysics were developed by Hatakeyama and coworkers (see Section 1.3.1).[27] Preliminary analysis of the product **1-14** revealed an exceptional quantum yield of 0.84 for its deep-blue emission band. Meanwhile, NICS (nucleus-independent chemical shift) computations suggested the aromaticity pattern resembled that of a quaterphenyl **1-16** (Figure 1-10c), with weak aromaticity on the heteroatom rings and the azaborine bonds acting mainly as rigidifying linkers. Further study could shed light on the effect of the unprecedented N–B–N–B bay region motif, with tuning via functionalization expected to be synthetically straightforward.

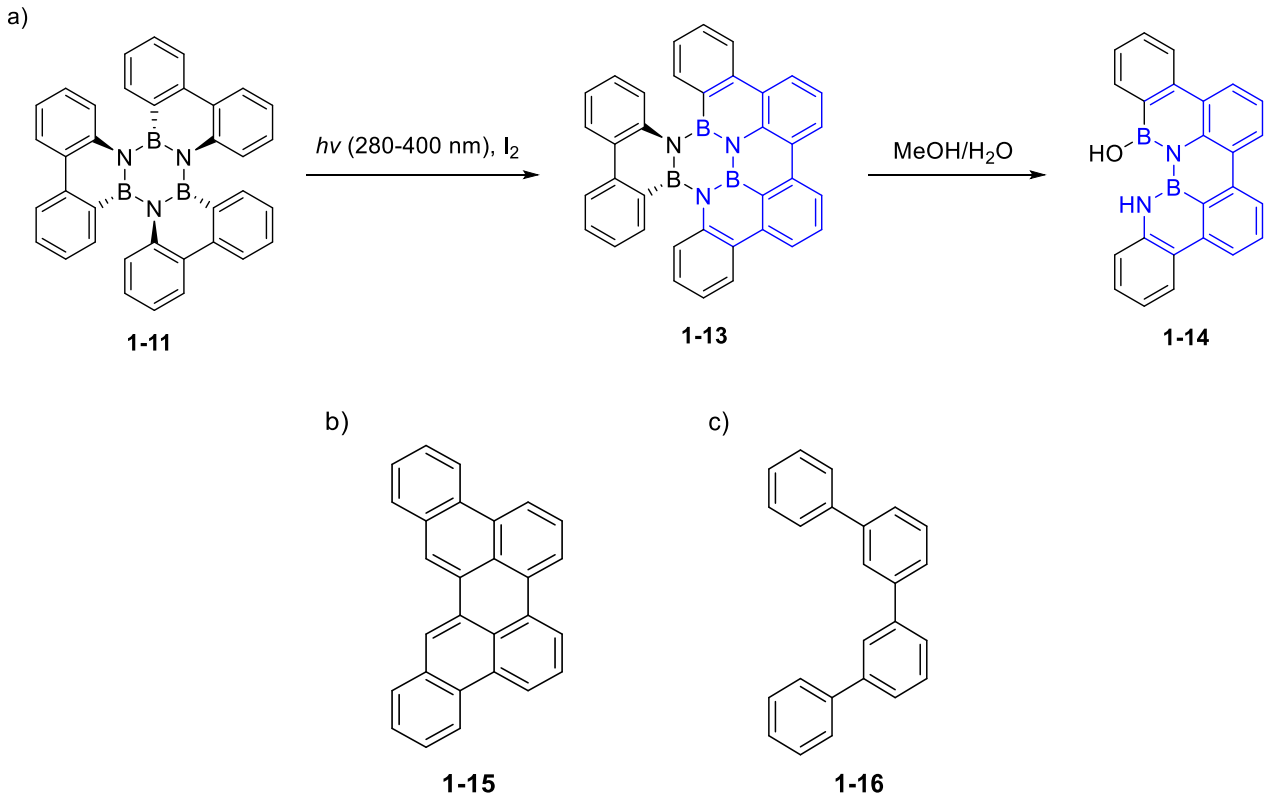

Figure 1-10. Bettinger's borazine fragments and all-carbon comparators. a) The borazines **1-13** and **1-14** exhibit a perylene motif (outlined in blue). The truncated derivative **1-14** could be formed by hydrolysis of **1-13**. b) The dibenzoperylene comparator **1-15**. c) NICS computations indicate the aromaticity pattern of the truncated derivative **1-14** resembles a quaterphenyl **1-16**.

1.2.3 Novel scaffolds

In addition to the borazine disconnections disclosed in two papers by the Bettinger laboratory, one report mentions, briefly, the luminescence of aromatic N–B–OH acids. Groziak and coworkers noticed that a poorly soluble pentacyclic dione **1-17** fluoresced strongly at 486 nm when an aqueous solution was irradiated with 400 nm light.[28] Interestingly, when dissolved in

aqueous NH_4OH, green-yellow light was emitted with irradiation at 366 nm. While the authors did not speculate on the cause of the red shift, a hydroxylated form of **1-17** (Figure 1-11) could exist in basic solution. In contrast to **1-17**, this species would differ in the coordination number of the boron, the involvement of the boron's p orbital in delocalization, and extent of intramolecular hydrogen bonding, all of which might contribute to the shift in optical performance.

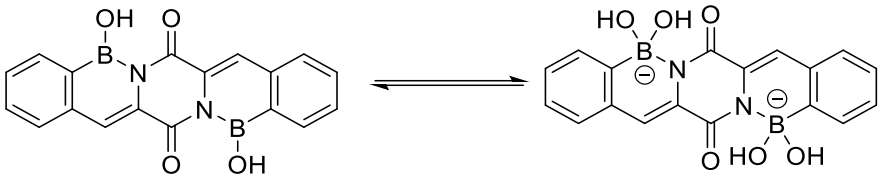

1-17

Figure 1-11. Possible equilibrium of dione **1-17** in the presence of aqueous base.

In fact, these intramolecular hydrogen bonds may be particularly related: one can imagine that, analogous to indigo, they improve optical performance and stability by enforcing planarity, at the expense of reducing solubility in water.[29,30] Further study would be needed to understand, and tune, the functional relevance of this scaffold.

About a year before Groziak's report, Wang, in collaboration with Wakamiya and their coworkers, produced a class of fluorescent N–B–N fused compounds and studied their structure-property relationships (Figure 1-12).[31]

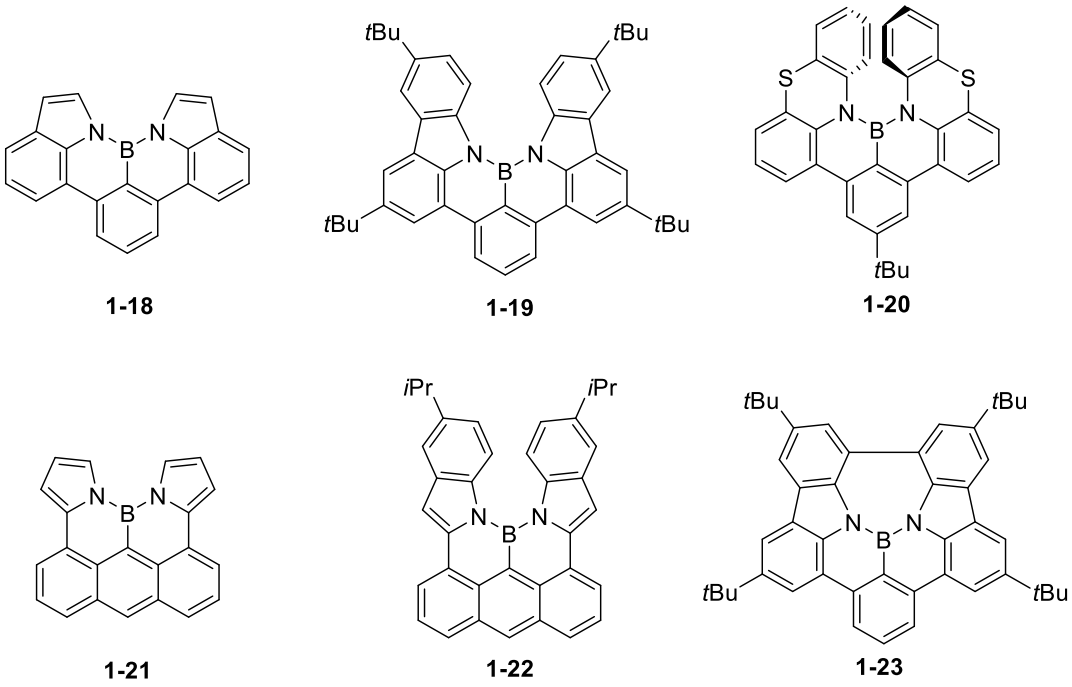

Figure 1-12. Wang's N-B-N doped PAHs.[31]

Electrophilic C–H borylation with boron trihalides was employed as a viable synthetic strategy to access this scaffold, and, in one example, a Scholl-like coupling was used to construct the embedded 7-membered N–B–N ring of **1-23**, demonstrating the utility of an essential PAH reaction[32] in the underdeveloped methodology of this area (Scheme 1-2). This work is a rare instance of deliberate, focused study on the impact of the unique –BXY motif on the luminescence of aromatic molecules. Featuring helicene motifs, distinct backbones, and heterocycles, the authors' small library displayed a corresponding diversity in photophysical properties (Table 1-2).

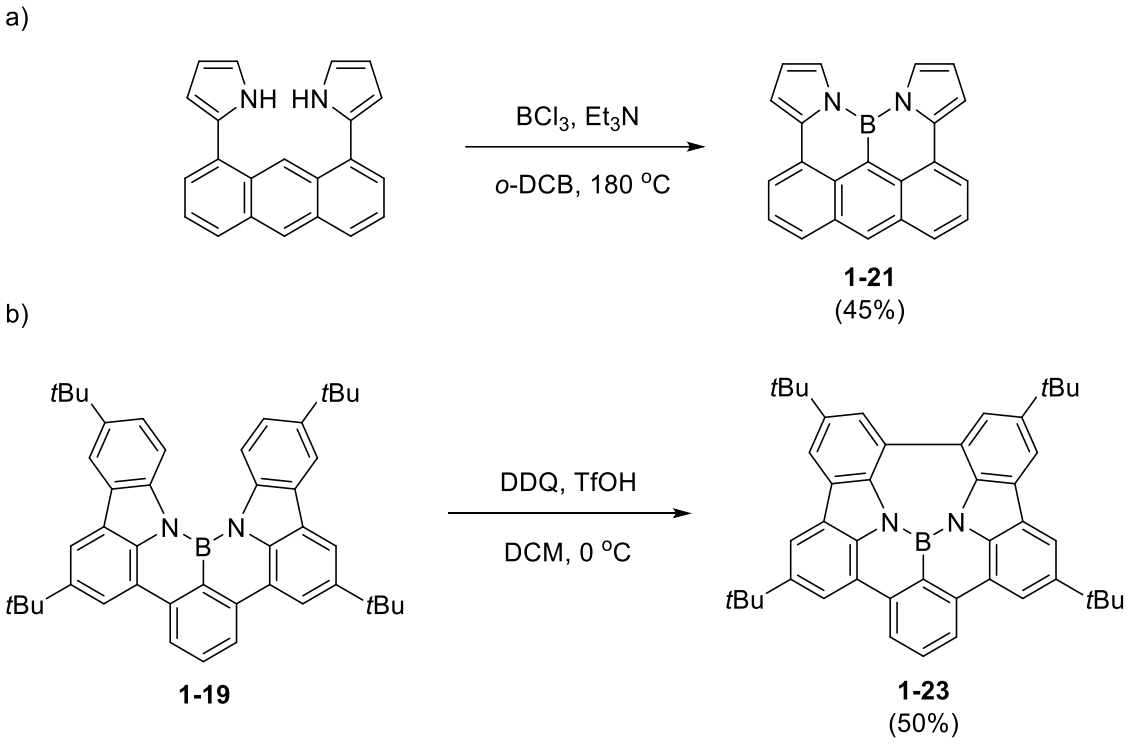

Scheme 1-2. Representative reaction conditions used to synthesize the structures in Figure 1-12**.** a) Electrophilic borylations of this type are well described in the literature; the nitrogen atoms are effective regiodirectors. b) DDQ has become a popular reagent for oxidative C–C couplings (the Scholl reaction).

These properties were in turn contextualized by X-ray crystallography and DFT computations. The calculations showed that boron made significant contribution to the LUMO spatial distributions of all structures. Structures **1-18** and **1-19** showed similar blue fluorescence with high quantum yields (0.65 and 0.63), resulting from a π–π^* transition. In spite of the presence of heteroatoms, the high quantum yields and defined vibrational spectral features suggested no charge transfer in the excited state, which agreed with DFT calculations: the HOMO and LUMO change little in spatial distribution. Interestingly, the planar structure **1-18** is an isoelectronic analogue of a known B-doped helicene cited by Wang, and so this invites comparison between the B–N and B–C bond: though the analogy is not perfect, the B–N bond may contribute to the blue

shift and slight reduction in quantum yield. The anthracenyl structures **1-21** and **1-22** had significant red shifts, probably due to extended π conjugation, though with low and moderate quantum yields. Comparing structures **1-18** and **1-21**, changing the backbone may be the most effective means to tune fluorescence emission into longer wavelengths for varied applications. Structure **1-23**, which bears an interesting 7-membered ring, has only a modest red shift following annulation when compared to **1-19**. In spite of its solubilizing groups, π stacking in solution, leading to aggregation-induced quenching, is likely to blame for its reduced quantum yield. NICS calculations confirmed that, as expected from its eight-electron count, the seven-membered NBN ring of **1-23** is strongly antiaromatic. Conversely, the B–N rings were essentially nonaromatic in compounds **1-18** to **1-22**.

Table 1-2. Selected photophysical data for compounds **1-18** to **1-23**

Compound	λ_{abs} (nm)	λ_{em} (nm)	Φ
1-18	385, 366, 349	387, 407, 427	0.65
1-19	387, 369	384, 404, 431	0.63
1-20	381	431	0.05
1-21	505	601	0.07
1-22	505, 537	565, 602	0.39
1-23	385, 404, 419, 439	450, 478, 510	0.25

λ_{abs} and λ_{em} are wavelengths of the absorption and fluorescence emission maxima. Φ is absolute photoluminescence quantum yield.

Bao and coworkers, in contrast, studied the well-established, cyclic N-B-N motifs of diazaborolines and Bdans (tricoordinate boron adducts with 1,8-diaminonaphthalene) with a focus on application (Figure 1-13).[33] While diazaborolines presented the typical, attractive luminescence that has made them such an active area of study, this paper was unique for being the first to treat Bdans as interesting optical materials in their own right; they were known primarily as a protecting group for boronic acids following Suginome's pioneering work in 2007.[34] Excitingly, the results

suggest Bdans may be a platform for aggregation induced emission (AIE), a rapidly growing area of study that dramatically adds to the applicability of organic materials. In contrast to the majority of organic molecules, AIEgens luminesce weakly in solution but more strongly as solids or aggregates,[35] creating application in diverse areas, from solid state electronics[36] to bioimaging,[37] that was previously impossible.

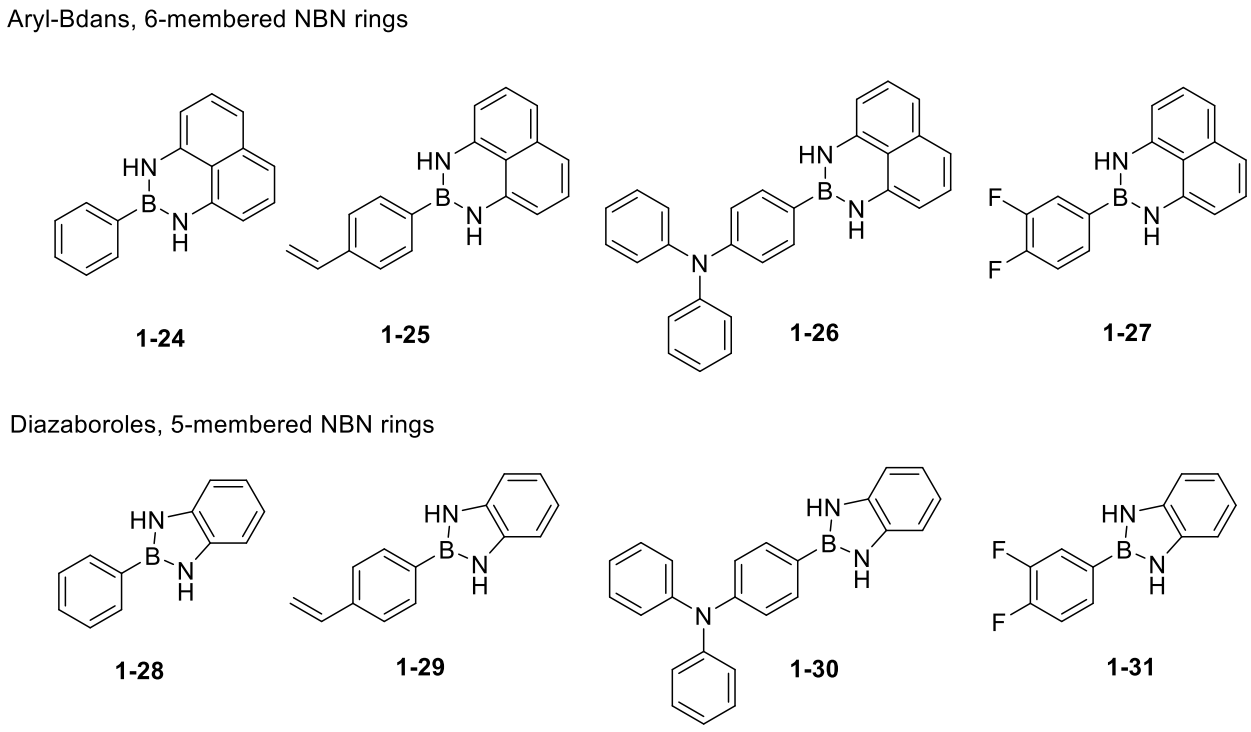

Figure 1-13. Cyclic NBN compounds synthesized by Bao and coworkers.[33]

In this work, the authors synthesized the target compounds by condensation of boronic acids with diamines in excellent yields using simple mix-and-stir conditions in THF, a departure from Suginome's classic method for DAN protection with a Dean-Stark apparatus and toluene. The diazaborolines showed high quantum yields (35.0-96.6%) for deep blue luminescence, with reduced, but still good, quantum yields in the solid state (2.5-47.9%). The four Bdans **1-24-27**, however, showed negligible fluorescence in methanol, but quantum yields around 2% when in the

solid state. Compared to the four diazaborolines, the Bdans had bathochromically-shifted, cyan-coloured solid state emissions (Table 1-3).

Table 1-3. Selected photophysical data for 6- and 5-membered NBN compounds

Compound	λ_{abs} (nm, methanol)	λ_{em} (nm, methanol)	λ_{em} (nm, solid)	Φ (%, methanol)	Φ (%, solid)
1-24	327	-	462	0.32	2.59
1-28	297	387	362	88.2	27.6
1-25	338	-	506	0.24	3.11
1-29	315	445	399	96.64	47.91
1-26	330	-	449	0.16	1.83
1-30	325	373	397	35.00	2.48
1-27	331	-	464	0.12	1.69
1-31	300	376	367	95.96	29.13

λ_{abs} and λ_{em} are wavelengths of the absorption and fluorescence emission maxima. Φ is absolute photoluminescence quantum yield.

The 5- and 6- membered NBN rings could be compared with each other and their corresponding C=C congeners. Electrostatic potential maps of the unsubstituted NBN compounds were very similar to their C=C congeners. However, these maps also showed that the five membered rings had less electrostatic potential (more homogenous electron distribution) than the six membered homologs: this was considered evidence for differing aromaticity in the two ring systems. This analysis matched NICS data, which assigned positive values to the 6-membered NBN ring. Antiaromatic character is expected of this ring system based on the Huckel rule's prediction on its seven-electron count (Figure 1-14). In contrast, the 5-membered NBN ring of the diazaborolines were computed by NICS to be aromatic.

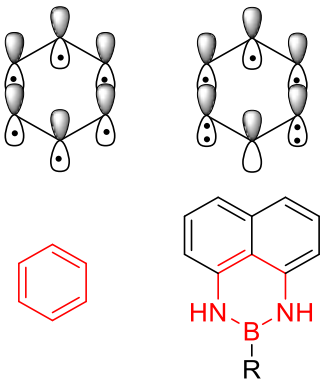

Figure 1-14. Orbital diagrams of Bdan compared to benzene. The red rings are depicted with molecular orbital schematics above them. In a normal carbon-carbon π bond, one electron can be assigned to each participating p orbital. However, nitrogen contributes 2 electrons with its lone pair and boron contributes a vacant p orbital.

The simplest Bdan, 1a, was demonstrated to be an extremely sensitive (ppb) turn-off fluorescence detector for TNT, both in 90% water solution and in the solid phase with test strips, with good anti-interference for various other analytes with ions or nitro groups. Computations indicated that TNT quenches its fluorescence by accepting charge transfer, after which the excitation energy decays nonradiatively.

1.3 Ar-BO_2: acids and esters

While there has been considerable study into the B–N bond motif in materials and optoelectronics, the B–O bond has received much less interest. Though they are both strong, stable bonds that bear resemblance to the C–C double bond, the B–O bond is not as close an electronic analogy due to oxygen's additional lone pair of electrons. Simultaneously, the ubiquity of the nitrogen atom in dye chemistry may have also biased the faster development of the B–N moiety.

Regardless, this dramatic difference in interest appears to be arbitrary, as the work from a handful of researchers in the last several years demonstrates the unique and promising optical properties of arylboronic acids and their esters.

1.3.1 Fluorescence: substituent and scaffold

In 2015, a theoretical and spectroscopic study was published on the solution fluorescence of the simplest member of this class: phenylboronic acid.[38] With absorption wavelengths of around 230 nm and emissions ranging from 270-380 nm in various solvents, the authors used this solvatochromic data to calculate ground and excited state dipole moments for this well-studied molecule that had previously received little to no optoelectronic interest in its own right.

Crawford and coworkers also chose boronic esters as a key substituent in their own fundamental study of a familiar compound, pyrene.[39] This work examined how functional groups affect pyrene's photophysics when placed in different positions. The paper complemented the authors' work on iridium-catalyzed borylation of the 2- and 7- positions of pyrene:[40] the nodal plane passing through these sites on both the HOMO and LUMO makes substitution both synthetically challenging and highly interesting in terms of effect on electronic structure. The resulting pinacol boronic esters were both applied as synthetic intermediates to affix substituents, and also included in the resulting library for computational and experimental study. For comparison, the better-studied 1-functionalized pyrenes were included in the work (Table 1-4).

Table 1-4. Selected photophysical data for boron-substituted pyrenes

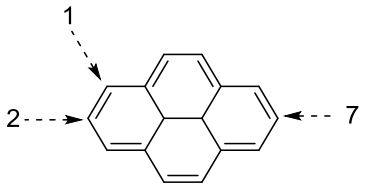

	ε (M^{-1} cm^{-1})	λ_{abs} (nm)	λ_{em} (nm)	Φ
Pyrene	600	362	372	0.64
2-$BMes_2$-pyrene	2000	413	434	0.68
2-Bpin-pyrene	1900	385	386	0.72
2,7-$(Bpin)_2$-pyrene	5000	398	400	0.88
1-Bpin-pyrene	7000	378	379	0.81

ε is the molar extinction coefficient. λ_{abs} and λ_{em} are wavelengths of the absorption and fluorescence emission maxima. Φ is absolute fluorescence quantum yield.

The authors found that Bpin substitution increased the molar extinction coefficients and the fluorescence quantum yields. Though the S_1–S_0 absorptions and emission were bathochromically shifted and more so in the 2- and 2,7- derivatives, the compounds retained small Stokes shifts between 70-250 cm^{-1}. In contrast, more dramatic modulation of pyrene's optical behaviour was seen with the stronger π accepting $B(Mes)_2$, which had greater bathochromic shifts of absorption and emission bands. The authors did not offer further reasoning on the role of boron.

These authors' strategy resembles a recent paper from Scott, Itami, and coworkers on their commercially available warped nanographene (WNG) scaffold.[41] With the use of specially modified iridium-catalysed borylation, a species **1-33** was produced that served both as synthetic intermediate and member of the resulting library for photophysical study (Scheme 1-3).

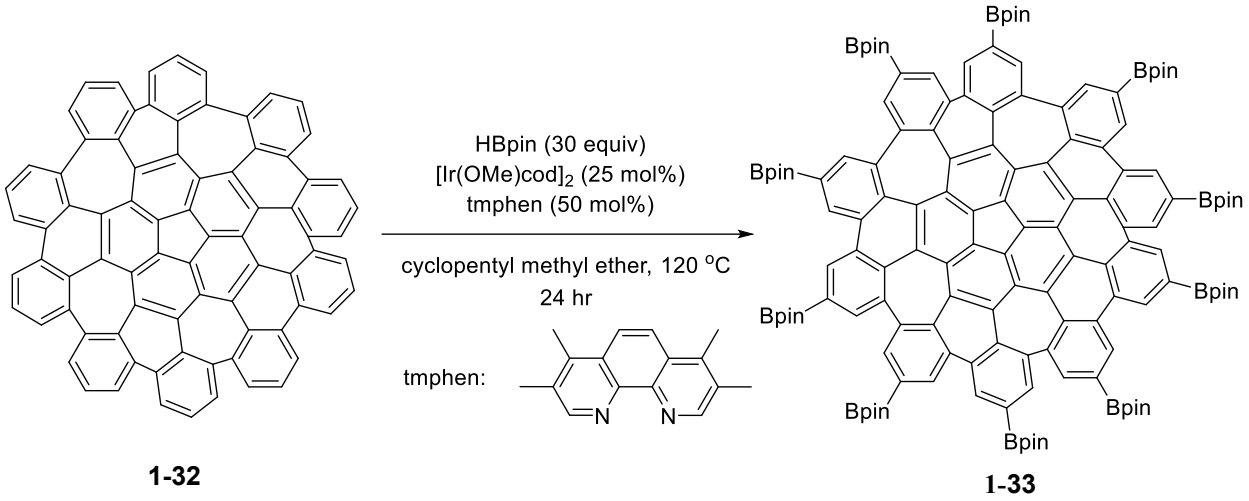

1-32 **1-33**

Scheme 1-3. Preparation of WNG **1-32** by polyborylation. The 5 and 7 membered rings decorating the WNG **1-32** induce a significant amount of warping for this π surface. This record-breaking decaborylation was achieved by screening for optimal conditions and ultimately modifying the solvent (cyclopentyl methyl ether) and ligand (tmphen).

This collaborative paper adds to a rich body of work between these two laboratories, which includes the methodology of one-shot C-H polyborylation and the WNG scaffold **1-32** with applications in bio-imaging and cancer phototreatment. In one step, ten boronyl functionalities were affixed to the $C_{80}H_{30}$ polyaromatic hydrocarbon (PAH), a new record for pristine PAHs. This study bridges a gap in the function of WNG **1-32** by tuning its fluorescence for the first time; while previous functionalization produced little perturbation in its characteristic green fluorescence, both absorption and emission bands could here be bathochromically shifted. This work expands the potential for WNG's application in chemical biology. Specifically, longer wavelength analytical or therapeutic dyes benefit from deeper tissue penetration, less noise from the auto-fluorescence of endogenous fluorophores, and diminished DNA damage from its short-wavelength excitation.[42] Of the three WNG derivatives studied, the Bpin substituted **1-33** offered a relatively modest loss

of quantum yield (0.20 down from 0.26 of the WNG **1-32**) with a bathochromic shift of absorption and emission peaks. The authors did not speculate on the mechanism or role of the BAHC motif.

Beyond simple pinacolates, other researchers have created new BAHC scaffolds for fluorescence study.[43] In a crystallographic journal article, Kutniewska and coworkers disclosed the blue fluorescence of an unusual 1,2-diboronyl compound with a tetrahedral boron at the spiro junction (Figure 1-15a). Given boron's presence in many attractive functional materials, these researchers saw an opportunity to generate new chemical diversity by condensing 1,2-phenylenediboronic acid with the known luminogen system of imidazo[1, 2-a]pyridines, with a strategy that recalls the well-established N,O-chelation chemistry of 8-hydroxyquinoline with various metal ions as well as boron (Figure 1-15b).[44,45] Interestingly, computations on **1-34** showed that the HOMO and LUMO remained localized on the pyridine ligand, without charge transfer into the boron subunit. Condensation of the ligand with boron also blocked excited-state intramolecular proton transfer (ESIPT) by inserting into the site of keto-enol isomerization that could lead to the weak, long-wavelength emission band associated with this phenomenon in imidazo[1, 2-a]pyridines.

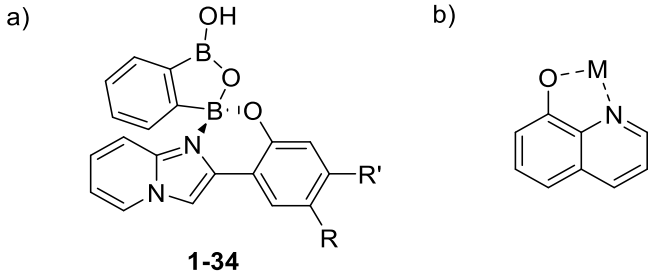

Figure 1-15. a) A spiro diboryl chelate **1-34** with both tetrahedral and tricoordinate boron condensates. b) The basic structure of metal chelation complexes of 8-hydroxyquinoline.

Two teams of researchers, led by Hatakeyama and Mullen, also disclosed synthetic protocols and characterisation of a boron-embedded PAH scaffold. In 2016 they independently published papers with variations on the symmetrical edge-doped OBO ditetracene unit **1-35** shown in Figure 1-16.

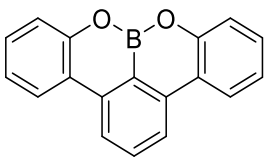

1-35

Figure 1-16. The core pattern common to the work of Hatakeyama, Mullen and their coworkers.[46,27]

Mullen and coworkers studied both the helicene-like compounds in Figure 1-17a and, uniquely, the annulated counterpart **1-37** (Table 1-5).[46] However, the latter is what makes this work so interesting. A Scholl-like coupling using DDQ/TfOH enabled a planarization of the helicene **1-38** through ring annulation, and photophysical study revealed a blue fluorescence quantum yield of 27%, with sharp vibronic features and a very small Stokes shift of 7 nm attributed to its rigid structure. The paper also included DFT computations that facilitate interpretation of the effects of the BAHC motif. Evidently, the BAHC edge significantly perturbs the pattern of aromaticity across the rings of the structure (NICS calculations, Table 1-5).

Table 1-5. NICS(1) calculations for **1-36** and **1-37**

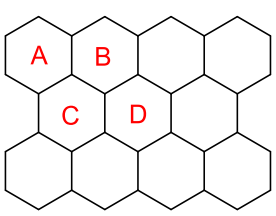

1-36

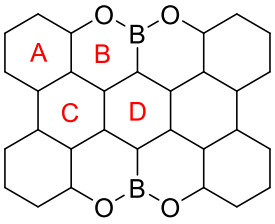

1-37

Structures are fully unsaturated; double bonds are omitted for clarity. Negative values indicate aromaticity; positive, antiaromaticity. Values of small magnitude are considered nonaromatic.

Ring	Compound **1-36**	Compound **1-37**
A	-6.7	-10.0
B	-5.6	+0.1
C	+2.7	-3.8
D	-0.5	-11.6

These results can be considered in parallel with another paper Mullen and Feng published in 2018, featuring real experimental data for a peritetracene of type **1-36**:[47] the hitherto unknown PAH has singlet biradical character and a decomposition half-life of about 3 hours in ambient conditions, with no fluorescence reported. The authors rationalized the difference in electronic character by the differing counts of the C-C-C (3 p_z electrons) and O-B-O (4 p_z electrons) patterns in **1-36** and **1-37**, respectively. Since BAHCs replace two carbon strings, **1-37** should have 2 additional electrons, and indeed the computed HOMO and LUMO densities of the OBO-peritetracene **1-37** resemble the LUMO and LUMO+1 of the carbon congener **1-36**.

The formal addition of two electrons onto a biradical, plus the lowering of the HOMO, could be the reason for the dramatic difference in the kinetic stability of the structures. The HOMO itself of **1-37** might be stabilized by the electronegativity of oxygen; noting the electron density on

both B and O in the LUMO, this molecular orbital could be stabilized by the π accepting capacity of the boron atom. Why the BAHC endows this PAH with fluorescence is unclear, although this study also reported weak (φ = 15%) red fluorescence of a boron-free, cyano-substituted derivative of **1-36**, so perhaps, for these structures, a heteroatom effect is at play.

Though Mullen and coworkers also produced helicenes **1-38** and **1-39** (Figure 1-17a), the optical isomers were not separated. This was probably due to the low barrier for interconversion, but they could still be observed in X-ray crystal structures of the racemates. Here, the B–O bonds were of normal length (1.37 Å) for boronic esters, though the central benzene ring was remarkably distorted, with a torsion angle of 24.5 degrees from one B-ipso carbon to another. The helicene racemates **1-38** and **1-39** fluoresced blue with quantum yields of 61% and 52% at similar wavelengths.

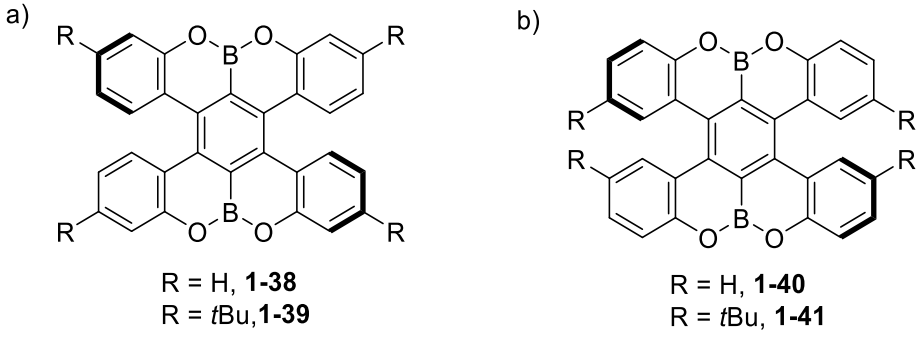

Figure 1-17. R = H, *t*Bu: the helicenes of a) Mullen[46] and b) Hatakeyama.[48]

In contrast to Mullen's work, Hatakeyama and coworkers focused on the axially chiral BAHCs **1-40** and **1-41** (Figure 1-17b).[48] Their structures displayed fluorescence with Commission Internationale de l'Éclairage coordinates of (0.15, 0.08) and (0.15, 0.06) for **1-40** and **1-41**, close to standard coordinates for pure blue (0.15, 0.06) and therefore within the margin for application in OLEDs. Further, the quantum yields neared 70%, which are record setting values for helicenes

and contrast sharply with the nonfluorescent, unstable, all-carbon congener. The unique placement of the R groups enhanced the molecules' potential as chiral materials: addition of *t*Butyl groups onto **1-41** discouraged optical racemization, and the separated enantiomers exhibited circularly polarized luminescence with good anisotropy factors, a measurement of the proportional chirality of emitted light. The rigidity conferred by the placement of the *t*Butyl groups may also explain the improved quantum yield in solution of **1-41** over Mullen's regioisomer **1-39** (68% versus 52%).

Hatakeyama's second paper with a similar embedded scaffold followed soon after, detailing the methodology and expanding upon the structural scope (Scheme 1-4), with boron diamide (**1-43**) and dithioester (**1-42**) substructures in addition to the diesters (**1-35**).[27] The sulfur compound **1-42** luminesced only weakly, possibly due to a heavy atom effect that could accelerate nonradiative intersystem crossing. Meanwhile, the B-O compound **1-35** had almost double the quantum yield of the B-N **1-43** (0.60 vs 0.31), though with emission blue-shifted into the deep violet region of the spectrum. The electron distribution of both compounds' (**1-35** and **1-43**) HOMO and LUMO orbitals appeared similar, though the dioxaborinine compound **1-35** had lower energy orbitals, presumably due to the lower atomic orbital energy of oxygen when compared to nitrogen.

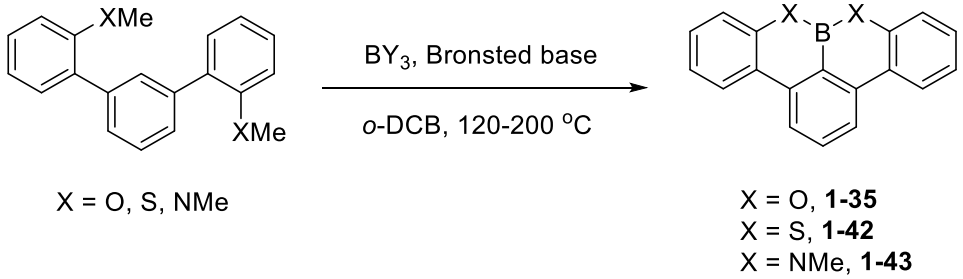

Scheme 1-4. Hatakeyama's demethylative synthesis towards XBX structures.[27]

The authors closed the report with the description of an interesting boroxahexacene **1-44**, stable even at 300 °C in the presence of light and air (Figure 1-18). While highly unusual for regular long acenes, they attribute this kinetic stability to the low-lying HOMO (-5.64 eV) and large optical band gap (3.36 eV), which would discourage oxidation and photoreactivity in ambient conditions. As long acenes are known to have reactive, diradical character, it is possible that the increased electron count in the OBO motif could disrupt this electronic pattern.

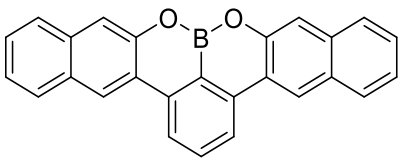

1-44

Figure 1-18. The boroxahexacene **1-44**.

1.3.2 Phosphorescence and mechanoluminescence

In late 2016, Kuno,[10] Shoji,[49] and their respective coworkers independently published articles demonstrating that simple arylboronic acids and esters, remarkably, exhibit fluorescence and phosphorescence in the solid state when exposed to UV light. While solid state fluorescence is somewhat unusual for organic molecules, owing to electronic interactions in aggregation induced quenching, the room temperature phosphorescence (RTP) is exceptionally remarkable. Common understanding, from basic theory on spin-orbit coupling and El Sayed's rule, is that RTP is observed in materials with heavy atoms, nitrogen heterocycles, or carbonyl groups.[50] The two laboratories both confirmed phosphorescence lasting several seconds, but they focused on different structures (Figure 1-19). Kuno and coworkers reported unique data on boronic acids **1-61** and **1-**

62, while Shoji presented a 20-compound survey of esters, mostly pinacolates, in conjunction with computational study (Table 1-6).

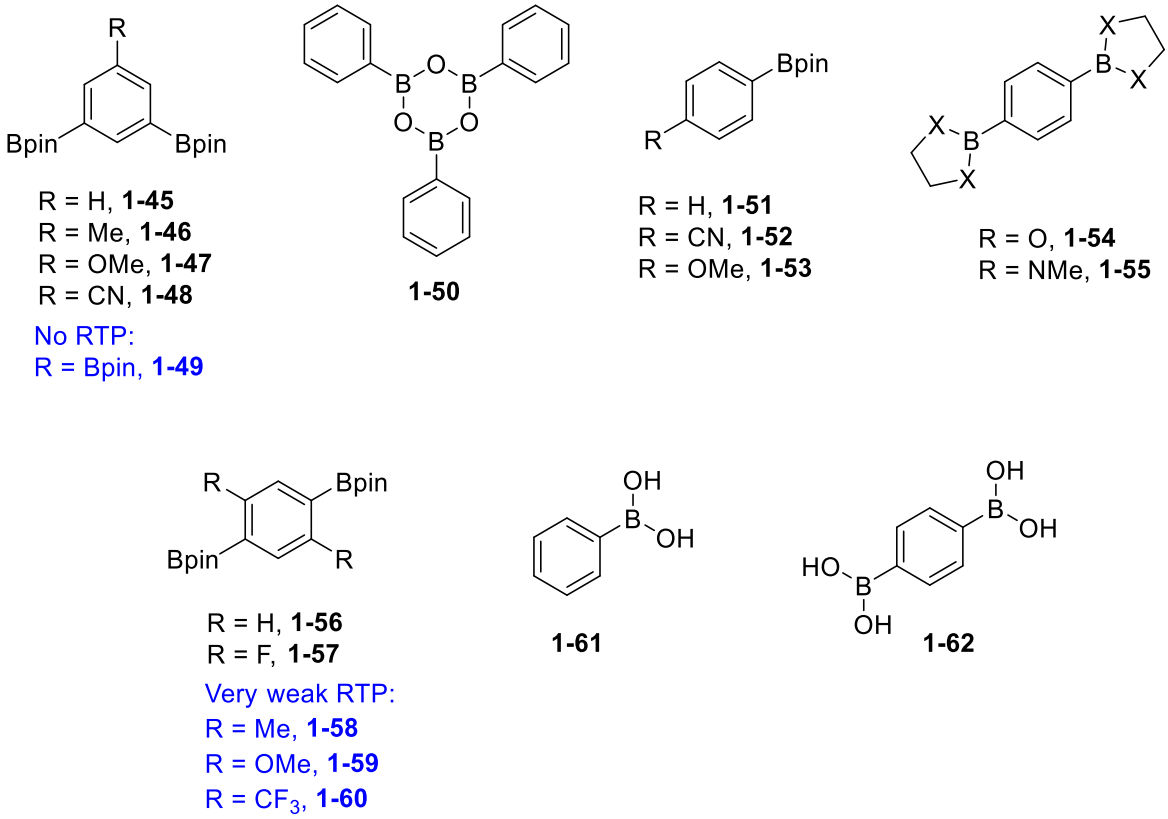

Figure 1-19. A selection of the compounds studied by Kuno[10] (the boronic acids **1-61** and **1-62**) and Shoji[49] (**1-45** to **1-60**). All exhibited RTP except where otherwise noted.

In Shoji's work, comparison with their non-borylated control in low temperature studies made it clear that the boronic ester functionality suppresses nonradiative transition from triplet to ground state. Computations suggested that the out-of-plane distortion of the pinB–C(ipso) moiety, when excited, may encourage mixing of this sigma orbital with the benzene's pi orbitals thus promoting spin-orbit coupling. This theoretical work also showed that, as is commonly seen with heteroatoms, the introduction of Bpin shrinks the HOMO–LUMO gap for the singlet transition. Their compound survey showed that long-lived RTP is general for aryl-BAHCs, with 14 more

samples exhibiting the phenomenon. A few that did not display RTP had bulky substituents around the ring, which were speculated to increase the free volume around the BAHC group in the crystalline state and promote molecular motions, leading to nonradiative relaxation. Interestingly, replacing oxygen with nitrogen in **1-55** did not perturb the phosphorescence; nor did groups like methoxy (**1-52**) or cyano (**1-53**). Another highlight in this work was the demonstrated phosphorescence of well-known boroxine **1-50**, hinting at the potential for developing this simple scaffold in optoelectronics.

Table 1-6. Emissive properties of selected phosphorescent boronic acids and esters

Compound	λ_{Fluor} (nm)	λ_{Phos} (nm)	τ_{Phos} (s)
1-45	297	469, 500	1.57
1-46	305	452, 478	0.49
1-47	329	480	0.69
1-48	306	449, 473	0.42
1-49	306	-	-
1-50	302	461, 495	0.46
1-51	290	465	1.79
1-52	306	519	0.44
1-53	298	502	1.39
1-54	316	471, 506	1.65
1-55	400	457	0.79
1-56	305	460, 500	1.85
1-57	351	507	0.56
1-58	328	528 (very weak)	-
1-59	385	514 (very weak)	-
1-60	301	456 (very weak)	-
1-61	322	482	1.2
1-62	329	494	0.95

Measurements performed on crystalline samples sandwiched between KBr plates at room temperature, exposed to air. λ_{Fluor} is the peak wavelength of fluorescence emission and $\lambda_{Phos\ is}$ the peak wavelength of phosphorescence emission. τ_{Phos} is luminescence decay lifetime.

Boronic esters are among a handful of compounds at the intersection of new research on AIE and mechanoluminescence (ML). Two papers published shortly before the work on RTP

showed that not only were these compounds able to emit light at higher quantum yields as solids, the hallmark of AIE and a rare and valuable property for organic compounds, but their emission could be stimulated by mechanical stress. In both articles, explanation of the compounds' properties tended to focus on crystal packing, with little attention to the role of the boron atom.

Bai and coworkers showed that Bpin substitution on well-studied pyrene affords a material **1-63** that fluoresces green in the solid state when mechanical stress is applied, then recovers its original blue fluorescence within minutes (Figure 1-20).[51] Most examples in the relatively sparse literature of organic ML require fuming solvent vapours or heating to speed a recovery time of several hours. The authors speculate that this unique feature of their system could make it eligible for application in frequent data read-write situations. They attribute the ML of Bpin-pyrene **1-63** to one of pyrene's hallmark luminescent properties, its tendency to form excimers (excited-state dimers with distinct photophysical properties compared to the monomer). The fast-recovering green fluorescence state is due to the metastable, sandwich-shaped packing, which slowly rearranges to the offset stack packing, giving blue fluorescence. Interestingly, ML was not exhibited by the related neopentyl boronic ester **1-64**. The crystal of the pinacolate ester **1-63** was softer and more amenable to plastic deformation, allowing rearrangement into the metastable mode, while the neopentyl ester crystal **1-64** was brittle and prone to fracture.

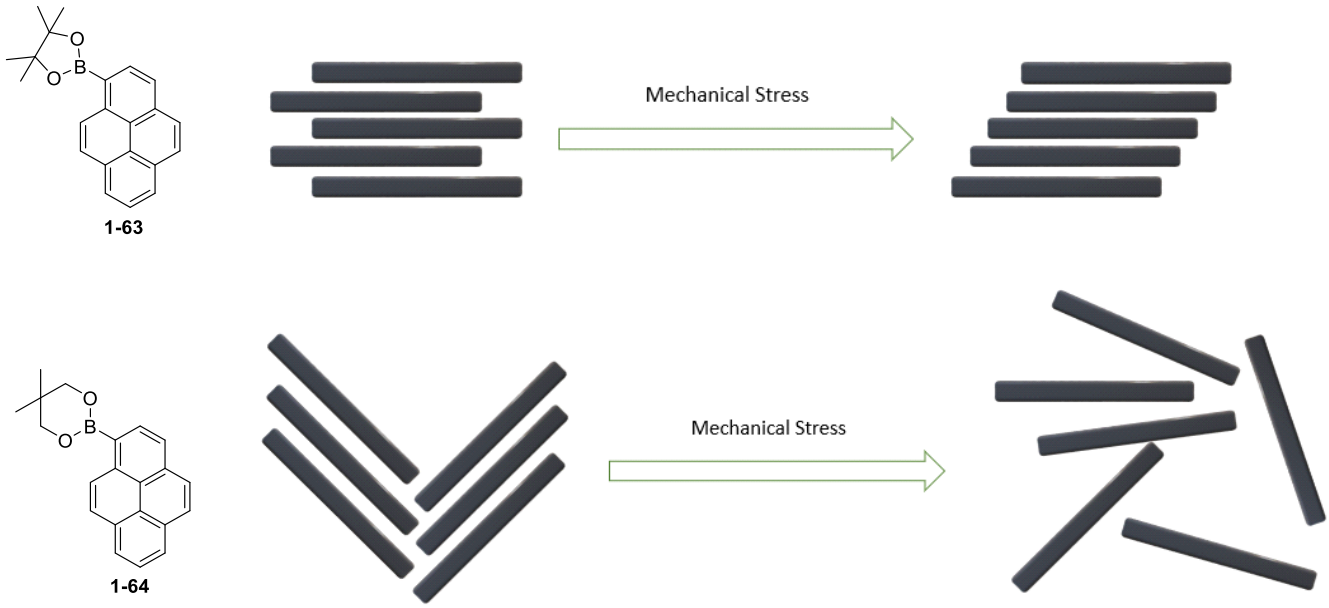

Figure 1-20. The effect of mechanical stress on the planar stacking modes of each pyrene crystal.

Li and coworkers also found ML in a Bpin compound of unrelated structure, an m-terphenyl **1-65** (Figure 1-21).[52] It exhibited highly unusual dual fluorescence-phosphorescence upon mechanical stimulation, which also corresponded to the singlet and triplet states observed from photoexcitation. Additionally, this was the first time mechanophosphorescence had been observed for an AIE luminogen. Strong intermolecular interactions enhanced rigidity and therefore reduced nonradiative relaxation; simultaneously, the interaction of oxygen's lone pairs with adjacent molecules promoted n–π* transitions in **1-65** and enhanced intersystem crossing, in keeping with El-Sayed's rule. This molecule is attractive as a model compound for studying the basic photophysics of ML, just as chemiluminescence and electroluminescence deserve study as distinct processes: the researchers produced data to support the existence of inherent energy states, like singlets and triplets, for the ML process.

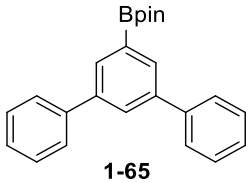

1-65

Figure 1-21. The m-terphenyl luminogen studied by Li and coworkers.[52]

1.3.3 Sensors

An excellent synopsis has been written recently on boronic acid-based luminescent sensors.[11] While most of the work is outside of the scope of this review, a few papers are of interest and will be mentioned briefly (Figure 1-22). Srikun and coworkers introduced a pinacol boronic ester to modulate the fluorescence of a biological H_2O_2-sensing dye **1-66**, which was dimmed and red-shifted upon the loss of the BAHC-containing substructure.[53] Li and coworkers also used the naphthalimide structure with boronic acid (**1-67**) and pinacol boronic ester (**1-68**) derivatives, which acted as a 'turn-off' fluorescent chemosensor for Cu^{2+} for biological applications.[54] Wang and coworkers produced a boronic acid, 'turn-off' fluorescence sensor **1-69** with good selectivity for cyanide anion in comparison with ten others.[55] Finally, Lampard and coworkers disclosed a variety of Bpin fluorescence probes of type **1-70** for H_2O_2, a few of which had their intrinsic luminescence decreased by the presence of the analyte.[56] The reader is encouraged to consult the review by Wu for more details.[11]

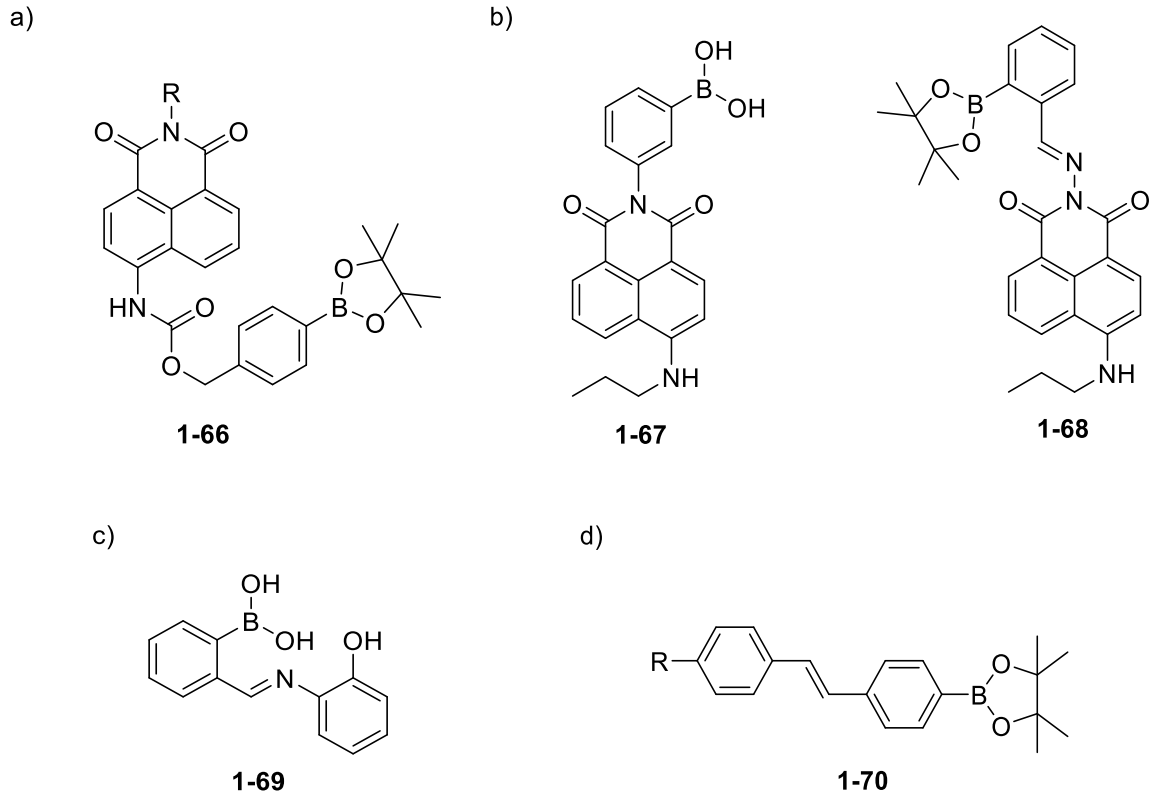

Figure 1-22. Intrinsically fluorescent boronic acid and ester sensors. The work of a) Srikun, b) Li, c) Wang, and d) Lampard.

1.4 Summary & outlook

BAHCs have unique advantages, both in their practical properties and their photophysics, that earn them a place in luminescence chemistry amidst their well-studied organoboron counterparts. While diazaborolines, with their aromaticity, varied possibilities for substitution, and electron richness, continue to receive the widest usage of the class, new focus has come on other structural motifs in the past few years. The familiar borazine scaffold, with its nonaromaticity, can applied both as an embedded substitution in large PAHs and also as a formal scaffold upon which

disconnections can be envisioned. These edge-doped nanographene patterns seem to be associated with increased band gap and characteristic electronic behaviour that is distinct from internally doped materials.

Meanwhile, using common BAHCs to decorate scaffolds can give a range of effects: for example, a Bpin group can tune existing luminescence in a manner common to heteroatoms or dramatically confer RTP and mechanoluminescence. These latter phenomena are attributed variously to crystal packing or the promotion of spin-orbit coupling, either from structural distortions or lone pairs on the BAHC unit.

There are several challenges ahead as this research area widens out. As is generally true for heteroatom doping in PAHs and nanographenes, efficient synthetic methodologies are still needed to produce novel BAHC scaffolds, especially with unique embedded or edge patterns. While efficient methods improve the chance that these materials can be commercially or practically applied, larger libraries for wide evaluation can also improve our theoretical understanding so that BAHCs can be used as tools in rational design. In this pursuit, computational study is indispensable: clearly, the diversity of compounds will not succumb to inspection or simplistic models of electron donor or acceptor. In the current climate of optoelectronics research, computationally informed design goes hand in hand with chemical intuition and creative proposal. In complement, these strategies could help establish BAHCs as powerful tools with diverse, rich electronic properties.

1.5 References

(1) Mellerup, S. K.; Wang, S. Boron-Doped Molecules for Optoelectronics. *Trends Chem.* **2019**, *1* (1), 77–89. https://doi.org/10.1016/j.trechm.2019.01.003.

(2) Wang, X.-Y.; Yao, X.; Narita, A.; Müllen, K. Heteroatom-Doped Nanographenes with Structural Precision. *Acc. Chem. Res.* **2019**, *52* (9), 2491–2505. https://doi.org/10.1021/acs.accounts.9b00322.

(3) Campbell, P. G.; Marwitz, A. J. V.; Liu, S.-Y. Recent Advances in Azaborine Chemistry. *Angew. Chem. Int. Ed.* **2012**, *51* (25), 6074–6092. https://doi.org/10.1002/anie.201200063.

(4) Bosdet, M. J. D.; Piers, W. E. B-N as a C-C Substitute in Aromatic Systems. *Can. J. Chem.* **2009**, *87* (1), 8–29. https://doi.org/10.1139/v08-110.

(5) Loudet, A.; Burgess, K. BODIPY Dyes and Their Derivatives: Syntheses and Spectroscopic Properties. *Chem. Rev.* **2007**, *107* (11), 4891–4932. https://doi.org/10.1021/cr078381n.

(6) Hall, D. G. *Boronic Acids. Preparation and Applications in Organic Synthesis, Medicine and Materials*, 2nd Completely Revised ed.; Hall, D. G., Ed.; Wiley-VCH: Weinheim, Germany, 2011.

(7) Weber, L.; Böhling, L. The Role of 2,3-Dihydro-1-H-1,3,2-Diazaboroles in Luminescent Molecules. *Coord. Chem. Rev.* **2015**, *284*, 236–275. https://doi.org/10.1016/j.ccr.2014.09.022.

(8) Barbon, S. M.; Reinkeluers, P. A.; Price, J. T.; Staroverov, V. N.; Gilroy, J. B. Structurally Tunable 3-Cyanoformazanate Boron Difluoride Dyes. *Chem. – Eur. J.* **2014**, *20* (36), 11340–11344. https://doi.org/10.1002/chem.201404297.

(9) Luo, H.-X.; Niu, Y.; Jin, X.; Cao, X.-P.; Yao, X.; Ye, X.-S. Indolo-Quinoline Boron Difluoride Dyes: Synthesis and Spectroscopic Properties. *Org. Biomol. Chem.* **2016**, *14* (18), 4185–4188. https://doi.org/10.1039/C6OB00623J.

(10) Kuno, S.; Kanamori, T.; Yijing, Z.; Ohtani, H.; Yuasa, H. Long Persistent Phosphorescence of Crystalline Phenylboronic Acid Derivatives: Photophysics and a Mechanistic Study. *ChemPhotoChem* **2017**, *1* (3), 102–106. https://doi.org/10.1002/cptc.201600031.

(11) Fang, G.; Wang, H.; Bian, Z.; Sun, J.; Liu, A.; Fang, H.; Liu, B.; Yao, Q.; Wu, Z. Recent Development of Boronic Acid-Based Fluorescent Sensors. *RSC Adv.* **2018**, *8* (51), 29400–29427. https://doi.org/10.1039/C8RA04503H.

(12) Weber, L. Recent Developments in the Chemistry of 1,3,2-Diazaborolines-(2,3-Dihydro-1H-1,3,2-Diazaboroles). *Coord. Chem. Rev.* **2008**, *252* (1), 1–31. https://doi.org/10.1016/j.ccr.2007.02.014.

(13) Weber, L.; Eickhoff, D.; Chrostowska, A.; Darrigan, C.; Stammler, H.-G.; Neumann, B. Synthesis, Structure, and Properties of Luminescent Diazaborole and Indole Systems. *Chem. Heterocycl. Compd.* **2017**, *53* (1), 54–65. https://doi.org/10.1007/s10593-017-2021-0.

(14) Stock, A.; Pohland, E. Borwasserstoffe, VIII. Zur Kenntnis Des B2H6 Und Des B5H11. *Berichte Dtsch. Chem. Ges. B Ser.* **1926**, *59* (9), 2210–2215. https://doi.org/10.1002/cber.19260590906.

(15) Dewar, M. J. S.; Kubba, V. P.; Pettit, R. 624. New Heteroaromatic Compounds. Part I. 9-Aza-10-Boraphenanthrene. *J. Chem. Soc. Resumed* **1958**, 3073–3076. https://doi.org/10.1039/JR9580003073.

(16) Davies, K. M.; Dewar, M. J. S.; Rona, Peter. New Heteroaromatic Compounds. XXVI. Synthesis of Borazarenes. *J. Am. Chem. Soc.* **1967**, *89* (24), 6294–6297. https://doi.org/10.1021/ja01000a054.

(17) Islas, R.; Chamorro, E.; Robles, J.; Heine, T.; Santos, J. C.; Merino, G. Borazine: To Be or Not to Be Aromatic. *Struct. Chem.* **2007**, *18* (6), 833–839. https://doi.org/10.1007/s11224-007-9229-z.

(18) Narita, A.; Wang, X.-Y.; Feng, X.; Müllen, K. New Advances in Nanographene Chemistry. *Chem. Soc. Rev.* **2015**, *44* (18), 6616–6643. https://doi.org/10.1039/C5CS00183H.

(19) Wakamiya, A.; Ide, T.; Yamaguchi, S. Toward π-Conjugated Molecule Bundles: Synthesis of a Series of *B,B ‘* , *B ‘ ‘* -Trianthryl- *N,N ‘* , *N ‘ ‘* -Triarylborazines and the Bundle Effects on Their Properties. *J. Am. Chem. Soc.* **2005**, *127* (42), 14859–14866. https://doi.org/10.1021/ja0537171.

(20) Hoffmann, R.; Imamura, A.; Hehre, W. J. Benzynes, Dehydroconjugated Molecules, and the Interaction of Orbitals Separated by a Number of Intervening Sigma Bonds. *J. Am. Chem. Soc.* **1968**, *90* (6), 1499–1509. https://doi.org/10.1021/ja01008a018.

(21) Majewski, M. A.; Stępień, M. Bowls, Hoops, and Saddles: Synthetic Approaches to Curved Aromatic Molecules. *Angew. Chem. Int. Ed.* **2019**, *58* (1), 86–116. https://doi.org/10.1002/anie.201807004.

(22) Krieg, M.; Reicherter, F.; Haiss, P.; Ströbele, M.; Eichele, K.; Treanor, M.-J.; Schaub, R.; Bettinger, H. F. Construction of an Internally B3N3-Doped Nanographene Molecule. *Angew. Chem. Int. Ed.* **2015**, *54* (28), 8284–8286. https://doi.org/10.1002/anie.201412165.

(23) Dosso, J.; Tasseroul, J.; Fasano, F.; Marinelli, D.; Biot, N.; Fermi, A.; Bonifazi, D. Synthesis and Optoelectronic Properties of Hexa- *Peri* -Hexabenzoborazinocoronene. *Angew. Chem. Int. Ed.* **2017**, *56* (16), 4483–4487. https://doi.org/10.1002/anie.201700907.

(24) Biswas, S.; Müller, M.; Tönshoff, C.; Eichele, K.; Maichle-Mössmer, C.; Ruff, A.; Speiser, B.; Bettinger, H. F. The Overcrowded Borazine Derivative of Hexabenzotriphenylene Obtained through Dehydrohalogenation: The Overcrowded Borazine Derivative of Hexabenzotriphenylene. *Eur. J. Org. Chem.* **2012**, *2012* (24), 4634–4639. https://doi.org/10.1002/ejoc.201200322.

(25) Köster, R.; Hattori, S.; Morita, Y. 1,2:3,4:5,6-Tris-(2,2′ -Biphenylylene) Borazole a Trimer of 9,10-Azaboraphenanthrene. *Angew. Chem. Int. Ed. Engl.* **1965**, *4* (8), 695–695. https://doi.org/10.1002/anie.196506951.

(26) Fingerle, M.; Stocker, S.; Bettinger, H. F. New Synthesis of a Dibenzoperylene Motif Featuring a Doubly Boron–Nitrogen-Doped Bay Region. *Synthesis* **2019**, *51* (22), 4147–4152. https://doi.org/10.1055/s-0039-1690687.

(27) Numano, M.; Nagami, N.; Nakatsuka, S.; Katayama, T.; Nakajima, K.; Tatsumi, S.; Yasuda, N.; Hatakeyama, T. Synthesis of Boronate-Based Benzo[Fg]Tetracene and Benzo[Hi]Hexacene via Demethylative Direct Borylation. *Chem. – Eur. J.* **2016**, *22* (33), 11574–11577. https://doi.org/10.1002/chem.201602753.

(28) de Lescure, L. R.; Jesse, T.; Groziak, M. P.; Powers, X. B.; Olmstead, M. M. Polycyclic Aromatic Heterocycles with a Benzo[c][1,2]Azaborinine Core. *J. Heterocycl. Chem.* **2019**, *56* (10), 2960–2965. https://doi.org/10.1002/jhet.3651.

(29) Seixas de Melo, J.; Moura, A. P.; Melo, M. J. Photophysical and Spectroscopic Studies of Indigo Derivatives in Their Keto and Leuco Forms. *J. Phys. Chem. A* **2004**, *108* (34), 6975–6981. https://doi.org/10.1021/jp049076y.

(30) Ma, C.; Li, H.; Yang, Y.; Li, D.; Liu, Y. TD-DFT Study on Electron Transfer Mobility and Intramolecular Hydrogen Bond of Substituted Indigo Derivatives. *Chem. Phys. Lett.* **2015**, *638*, 72–77. https://doi.org/10.1016/j.cplett.2015.08.012.

(31) Yang, D.-T.; Nakamura, T.; He, Z.; Wang, X.; Wakamiya, A.; Peng, T.; Wang, S. Doping Polycyclic Arenes with Nitrogen–Boron–Nitrogen (NBN) Units. *Org. Lett.* **2018**, *20* (21), 6741–6745. https://doi.org/10.1021/acs.orglett.8b02850.

(32) King, B. T.; Kroulík, J.; Robertson, C. R.; Rempala, P.; Hilton, C. L.; Korinek, J. D.; Gortari, L. M. Controlling the Scholl Reaction. *J. Org. Chem.* **2007**, *72* (7), 2279–2288. https://doi.org/10.1021/jo061515x.

(33) Wan, W.-M.; Tian, D.; Jing, Y.-N.; Zhang, X.-Y.; Wu, W.; Ren, H.; Bao, H.-L. NBN-Doped Conjugated Polycyclic Aromatic Hydrocarbons as an AIEgen Class for Extremely Sensitive Detection of Explosives. *Angew. Chem.* **2018**, *130* (47), 15736–15742. https://doi.org/10.1002/ange.201809844.

(34) Noguchi, H.; Hojo, K.; Suginome, M. Boron-Masking Strategy for the Selective Synthesis of Oligoarenes via Iterative Suzuki−Miyaura Coupling. *J. Am. Chem. Soc.* **2007**, *129* (4), 758–759. https://doi.org/10.1021/ja067975p.

(35) Hong, Y.; Lam, J. W. Y.; Tang, B. Z. Aggregation-Induced Emission: Phenomenon, Mechanism and Applications. *Chem. Commun.* **2009**, No. 29, 4332–4353. https://doi.org/10.1039/B904665H.

(36) Mei, J.; Hong, Y.; Lam, J. W. Y.; Qin, A.; Tang, Y.; Tang, B. Z. Aggregation-Induced Emission: The Whole Is More Brilliant than the Parts. *Adv. Mater.* **2014**, *26* (31), 5429–5479. https://doi.org/10.1002/adma.201401356.

(37) Zhu, C.; Kwok, R. T. K.; Lam, J. W. Y.; Tang, B. Z. Aggregation-Induced Emission: A Trailblazing Journey to the Field of Biomedicine. *ACS Appl. Bio Mater.* **2018**, *1* (6), 1768–1786. https://doi.org/10.1021/acsabm.8b00600.

(38) Patil, S. S.; Muddapur, G. V.; Patil, N. R.; Melavanki, R. M.; Kusanur, R. A. Fluorescence Characteristics of Aryl Boronic Acid Derivate (PBA). *Spectrochim. Acta. A. Mol. Biomol. Spectrosc.* **2015**, *138*, 85–91. https://doi.org/10.1016/j.saa.2014.11.028.

(39) Crawford, A. G.; Dwyer, A. D.; Liu, Z.; Steffen, A.; Beeby, A.; Pålsson, L.-O.; Tozer, D. J.; Marder, T. B. Experimental and Theoretical Studies of the Photophysical Properties of 2- and 2,7-Functionalized Pyrene Derivatives. *J. Am. Chem. Soc.* **2011**, *133* (34), 13349–13362. https://doi.org/10.1021/ja2006862.

(40) Crawford, A. G.; Liu, Z.; Mkhalid, I. A. I.; Thibault, M.-H.; Schwarz, N.; Alcaraz, G.; Steffen, A.; Collings, J. C.; Batsanov, A. S.; Howard, J. A. K.; et al. Synthesis of 2- and 2,7-Functionalized Pyrene Derivatives: An Application of Selective C-H Borylation. *Chem. – Eur. J.* **2012**, *18* (16), 5022–5035. https://doi.org/10.1002/chem.201103774.

(41) Kato, K.; Lin, H.-A.; Kuwayama, M.; Nagase, M.; Segawa, Y.; Scott, L. T.; Itami, K. Two-Step Synthesis of a Red-Emissive Warped Nanographene Derivative via a Ten-Fold C–H Borylation. *Chem. Sci.* **2019**, *10* (39), 9038–9041. https://doi.org/10.1039/C9SC03061A.

(42) Lavis, L. D.; Raines, R. T. Bright Ideas for Chemical Biology. *ACS Chem. Biol.* **2008**, *3* (3), 142–155. https://doi.org/10.1021/cb700248m.

(43) Kutniewska, S. E.; Jarzembska, K. N.; Kamiński, R.; Stasyuk, A. J.; Gryko, D. T.; Cyrański, M. K. Structural, Energetic and Spectroscopic Studies of New Luminescent Complexes Based on 2-(2′-Hy-droxy-phenyl)-imidazo[1,2-a]Pyridines and 1,2-Phenyl-ene-diboronic Acid. *Acta Crystallogr. Sect. B Struct. Sci. Cryst. Eng. Mater.* **2018**, *74* (6), 725–737. https://doi.org/10.1107/S2052520618015469.

(44) Soroka, Krystyna.; Vithanage, R. S.; Phillips, D. A.; Walker, Brian.; Dasgupta, P. K. Fluorescence Properties of Metal Complexes of 8-Hydroxyquinoline-5-Sulfonic Acid and Chromatographic Applications. *Anal. Chem.* **1987**, *59* (4), 629–636. https://doi.org/10.1021/ac00131a019.

(45) Sadu, V. S.; Bin, H.-R.; Lee, D.-M.; Lee, K.-I. One-Pot Synthesis of Four-Coordinate Boron(III) Complexes by the Ligand-Promoted Organic Group Migration between Boronic Acids. *Sci. Rep.* **2017**, *7*. https://doi.org/10.1038/s41598-017-00236-2.

(46) Wang, X.-Y.; Narita, A.; Zhang, W.; Feng, X.; Müllen, K. Synthesis of Stable Nanographenes with OBO-Doped Zigzag Edges Based on Tandem Demethylation-Electrophilic Borylation. *J. Am. Chem. Soc.* **2016**, *138* (29), 9021–9024. https://doi.org/10.1021/jacs.6b04092.

(47) Ajayakumar, M. R.; Fu, Y.; Ma, J.; Hennersdorf, F.; Komber, H.; Weigand, J. J.; Alfonsov, A.; Popov, A. A.; Berger, R.; Liu, J.; et al. Toward Full Zigzag-Edged Nanographenes: Peri-Tetracene and Its Corresponding Circumanthracene. *J. Am. Chem. Soc.* **2018**, *140* (20), 6240–6244. https://doi.org/10.1021/jacs.8b03711.

(48) Katayama, T.; Nakatsuka, S.; Hirai, H.; Yasuda, N.; Kumar, J.; Kawai, T.; Hatakeyama, T. Two-Step Synthesis of Boron-Fused Double Helicenes. *J. Am. Chem. Soc.* **2016**, *138* (16), 5210–5213. https://doi.org/10.1021/jacs.6b01674.

(49) Shoji, Y.; Ikabata, Y.; Wang, Q.; Nemoto, D.; Sakamoto, A.; Tanaka, N.; Seino, J.; Nakai, H.; Fukushima, T. Unveiling a New Aspect of Simple Arylboronic Esters: Long-Lived Room-Temperature Phosphorescence from Heavy-Atom-Free Molecules. *J. Am. Chem. Soc.* **2017**, *139* (7), 2728–2733. https://doi.org/10.1021/jacs.6b11984.
(50) Valeur, B. *Molecular Fluorescence: Principles and Applications*; Wiley-VCH, 2001.
(51) Wang, T.; Zhang, N.; Zhang, K.; Dai, J.; Bai, W.; Bai, R. Pyrene Boronic Acid Cyclic Ester: A New Fast Self-Recovering Mechanoluminescent Material at Room Temperature. *Chem. Commun.* **2016**, *52* (62), 9679–9682. https://doi.org/10.1039/C6CC03248F.
(52) Yang, J.; Ren, Z.; Xie, Z.; Liu, Y.; Wang, C.; Xie, Y.; Peng, Q.; Xu, B.; Tian, W.; Zhang, F.; et al. AIEgen with Fluorescence–Phosphorescence Dual Mechanoluminescence at Room Temperature. *Angew. Chem. Int. Ed.* **2017**, *56* (3), 880–884. https://doi.org/10.1002/anie.201610453.
(53) Srikun, D.; Miller, E. W.; Domaille, D. W.; Chang, C. J. An ICT-Based Approach to Ratiometric Fluorescence Imaging of Hydrogen Peroxide Produced in Living Cells. *J. Am. Chem. Soc.* **2008**, *130* (14), 4596–4597. https://doi.org/10.1021/ja711480f.
(54) Li, M.; Ge, H.; Arrowsmith, R. L.; Mirabello, V.; Botchway, S. W.; Zhu, W.; Pascu, S. I.; James, T. D. Ditopic Boronic Acid and Imine-Based Naphthalimide Fluorescence Sensor for Copper(II). *Chem Commun* **2014**, *50* (80), 11806–11809. https://doi.org/10.1039/C4CC03453H.
(55) Wang, S.-T.; Sie, Y.-W.; Wan, C.-F.; Wu, A.-T. A Reaction-Based Fluorescent Sensor for Detection of Cyanide in Aqueous Media. *J. Lumin.* **2016**, *173*, 25–29. https://doi.org/10.1016/j.jlumin.2015.12.041.
(56) Lampard, E. V.; Sedgwick, A. C.; Sun, X.; Filer, K. L.; Hewins, S. C.; Kim, G.; Yoon, J.; Bull, S. D.; James, T. D. Boronate-Based Fluorescence Probes for the Detection of Hydrogen Peroxide. *ChemistryOpen* **2018**, *7* (3), 262–265. https://doi.org/10.1002/open.201700189.

A novel luminescent N–B–N aromatic polycycle: synthesis, properties and applications

2.1 Introduction

Heteroatom doping is a popular strategy to modulate the properties of graphene, nanographenes, and polyaromatic hydrocarbons (PAHs).[1] One area of study, beginning with the pioneering work of Dewar and coworkers in the 1960s, applies the B–N bond as a replacement for C=C bonds in aromatic structures.[2] Though the two moieties are isoelectronic and isosteric, the B–N replacement can significantly alter the photophysical, aromatic and electronic properties of the molecule, thereby enriching the chemical space of aromatics and diversifying their optoelectronic applications.

In elaboration of this strategy, N–B–N bond patterns have the potential to offer considerable advantage. Analogous to boronic esters, the nitrogen lone pairs electronically shield the boron's vacant p orbital, substantially improving thermodynamic and kinetic stability when compared to borinic B–N compounds.[3] With its 4-electron count, the N–B–N unit can act as a heteroarene replacement (Figure 2-1). As a functional group, they are also versatile for further functionalization, as N–B–N rings can orthogonally tolerate the Suzuki-Miyaura cross-coupling reaction without being consumed.[4]

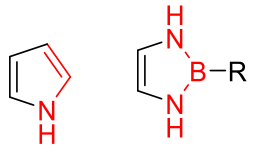

Figure 2-1. Pyrrole and a 1,3,2-diazaboroline. The structures are isosteric and isoelectronic, while the same can be said of the substructures in red when substituted into other rings.

Over the last couple of decades, the best-established motif has been 1,3,2-diazaborolines, or five-membered, pyrrole-isosteric rings, discussed extensively in a review by Weber,[5,6] who has made considerable experimental contributions to the field (Figure 2-2). In addition to their attractive properties as ligands and for electrochemistry, these compounds often exhibit extremely high (near 100%) luminescence quantum yields in solution and the solid state. A recent paper by Wan and coworkers applied 1,3,2-diazaborolines in conjunction with their six-membered ring counterparts, naphthodiazaborinines (Bdans).[7] Aryl-Bdans are familiar compounds in organoboron chemistry, since the pioneering work of Suginome developed 1,8-diaminonaphthalene (DAN) as a protecting group for boronic acids.[4] However, these stable, colourless solids, which display very weak fluorescence in solution, have been largely unexplored as interesting optoelectronic materials in their own right. Though Wan's work showed their solution and solid quantum yields were low, the aryl-Bdans exhibited unusual aggregation-induced emission (AIE) and promising application as highly sensitive (ppb) detectors for explosives.

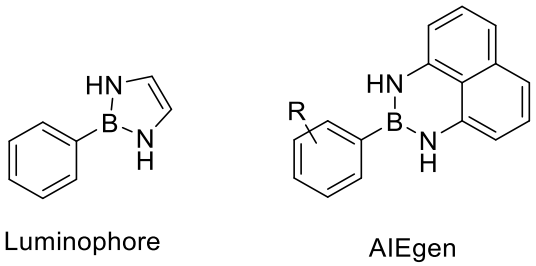

Figure 2-2. Basic aryl 1,3,2-diazaboroline (left) and aryl Bdans (right) have demonstrated use as luminogens and AIEgens.

2.2 Objective

In the course of a reaction performed on an aryl-Bdan for an unrelated heterocycle project, the primary products were two intensely hued compounds that fluoresced blue under visible light and hand-held UV lamp (Scheme 2-1). This optical behaviour was dramatically different from the expected product and starting material.

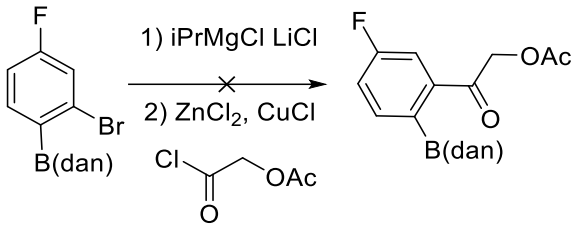

Scheme 2-1. DAN was selected as a boronic acid protecting group for this acylation reaction, which led to the formation of unexpected products.

In interest of improving the reaction, and out of basic curiosity, the products were characterised as the naphthyl ketones **2-1** and **2-2** (Figure 2-3). Following preparation of some derivatives, the simplest scaffold with these optical properties was determined (Figure 2-4).

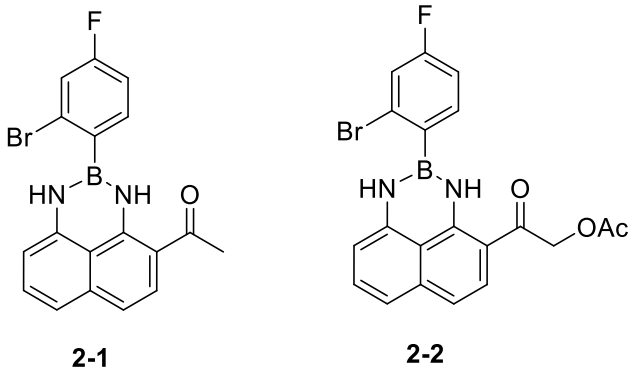

Figure 2-3. The naphthyl ketone products isolated from the failed reaction in Scheme 2-1.

To our knowledge, this diazaborolyl-naphthyl-ketone (DNK) structure, and the 1,8-diaminonaphthalene-ketone substructure, have not been reported in the literature. This simple modification of familiar phenyl-Bdan **2-3** has dramatically altered the optical performance of the scaffold.

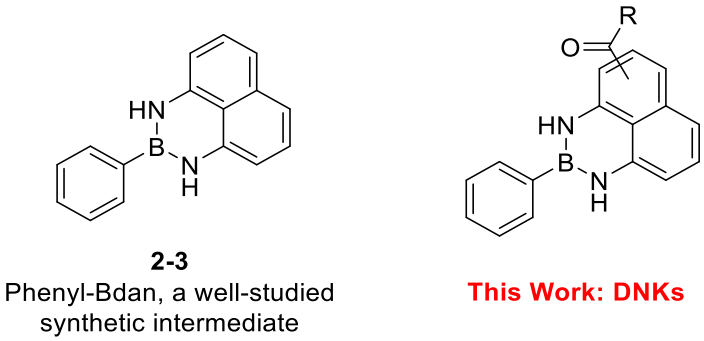

Figure 2-4. The basic scaffold associated with this luminescence behaviour features a ketone-substituted naphthyl diazaborole motif. This platform, and its behaviour, is the subject of this chapter.

The objective of the project is primarily to characterise the photophysics and structure of this new class of luminophores, both in solution and in the solid state. Comparator compounds, such as phenyl-Bdan **2-3**, are used wherever possible to clarify the impact of key structural patterns on the photophysical properties. In addition, basic methodologies are developed to access a small

library for eventual studies of structure-property relationships. Photophysical data is used to identify potential applications for DNK class members as well as the novel DAN-ketone.

2.3 Results

2.3.1 Synthesis of DNK compounds

Two main synthetic strategies were used to produce DNK compounds. At this stage, the reactions have not undergone optimization, and so the yields are low to moderate. However, the methods benefit from a degree of modularity that can assist in the generation of small libraries of analogs. In the first strategy, Suginome's DAN protection is used,[4] followed by acylation using a strong base like *n*BuLi or DBU, giving predominantly the ortho product (Scheme 2-2).

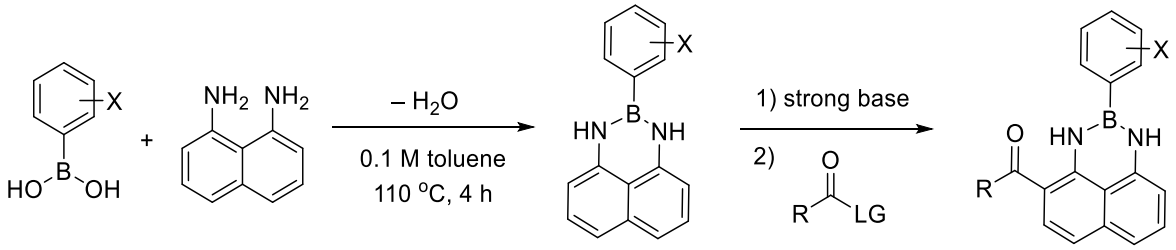

Scheme 2-2. The strong base promoted acylation method.

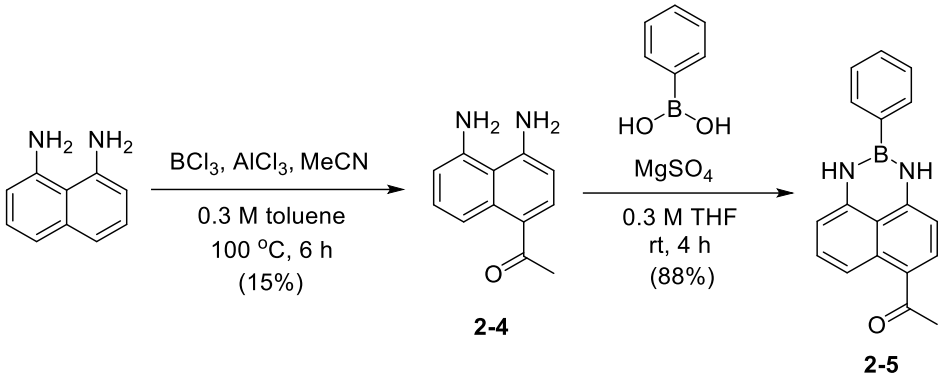

Scheme 2-3. The Sugasawa method to affix the acyl substituent first.

The second strategy begins with Sugasawa reaction conditions, which were disclosed in 1978 as an alternative to Friedel-Crafts chemistry. The reaction occurs regioselectively to give the ortho-substituted anilines[8] from various nitriles. However, in Scheme 2-3, the reaction furnishes exclusively the para-substituted DAN derivative **2-4**. It is possible that boron trichloride functions as an *in situ* cyclic protecting group for the peri-diamines, allowing a Friedel-Crafts-like acylation to proceed in the para position.

The reaction's low yield could relate to an unexpected perimidine side product **2-6**, which was identified using 1D and 2D NMR spectroscopy and HRMS (Figure 2-5). Perimidines may be formed in the presence of boron trihalides and water with ketones.[9] Though it resembles an *N,N*-ketal with acetone, the mechanism leading to such a side product is unclear as the substrate is not exposed to this solvent.

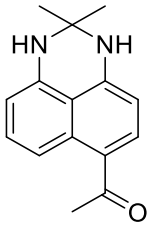

2-6

Figure 2-5. The perimidine **2-6**, which appears to fluoresce, unlike the desired product **2-4**.

Additionally, an isomeric compound **2-7** was designed with the ketone functionality placed on the phenyl ring. It was prepared using an α-bromination reaction (Scheme 2-4), a modification of a procedure previously developed in the Hall Group to yield a cyclic species. The bromide intermediate shown had never been isolated, but it could be observed in the crude mixture based on ^{1}H NMR data.

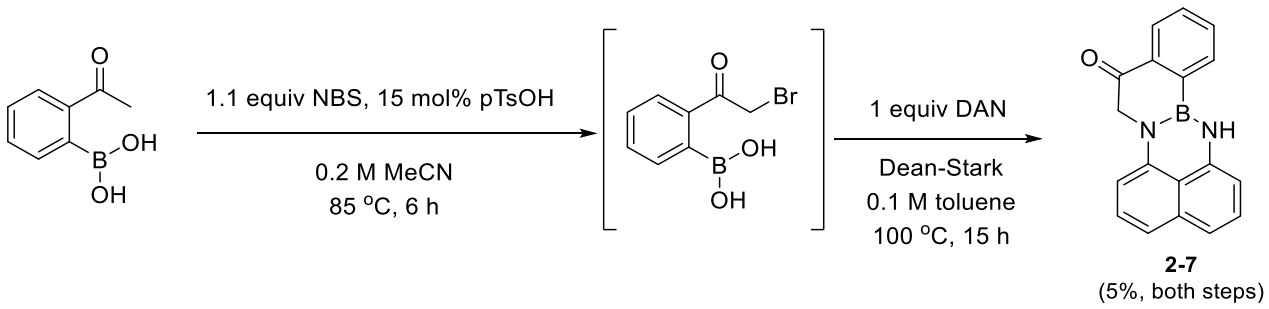

2-7
(5%, both steps)

Scheme 2-4. Synthesis of a cyclic ketone **2-7**; the yield is across both steps.

2.3.2 DNK compound library

In addition to heterocycles **2-7** and **2-5,** several candidates were synthesized using the protocol described in Scheme 2-2. As described in Suginome's work, the yields for the first step are good to quantitative; the yields for the second step are shown beneath their code numbers

(Figure 2-6). The notably low yield of phenylated **2-10** could relate to the sterically-influenced dihedral angle between the naphthyl moiety and the phenone, analogous to the conformation of benzophenones described in the literature:[10] this could interrupt the formation of a favourable hydrogen bond between amine and carbonyl. Consistent with this observation is the formation of the para-substituted isomer, analogous to **2-5**, in significant proportion.

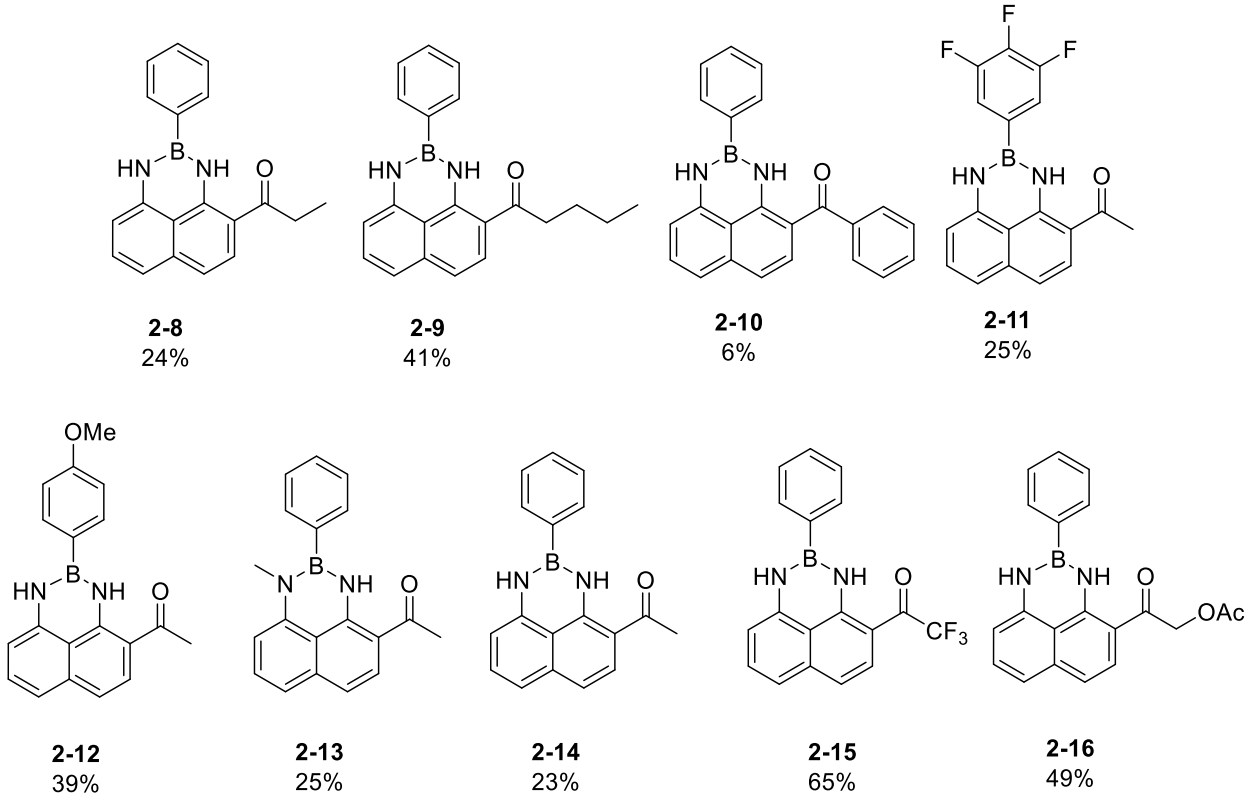

2-8 24%

2-9 41%

2-10 6%

2-11 25%

2-12 39%

2-13 25%

2-14 23%

2-15 65%

2-16 49%

Figure 2-6. A library of DNK compounds was generated to screen for interesting optoelectronic properties.

Qualitatively, almost all the class members showed similar fluorescence behaviour, with a few notable exceptions. The cyclic ketone **2-7** was a vivid orange colour with very weak fluorescence in solution. Addition of the –OAc group onto the ketone, as in **2-16** and **2-2**, gave a marked red shift in the emission. The methoxy class member **2-12** showed very bright fluorescence in the solid state. The phenyl ketone **2-10** had relatively weak, yellow fluorescence. Interestingly,

substitution on the B-phenyl ring did not make significant qualitative impact on the fluorescence in solution.

A few compounds could not be synthesized successfully (Figure 2-7, Scheme 2-5). Preparation of the dimethylaniline **2-17** was attempted according to Scheme 2-2. During the acylation step, DBU did not react with the starting material (probably due to the strong electron richness of the species), while treatment with *n*BuLi resulted in decomposition. The axially chiral BINAM adduct **2-18** also utilized the strategy of Scheme 2-2, but the problem arose in step 1, as condensation products appeared not to form. Concurrently, when the binaphthyl diamine precursor BINAM was subjected to Sugasawa reaction conditions in Scheme 2-3, the reaction gave a complex mixture of unidentifiable products.

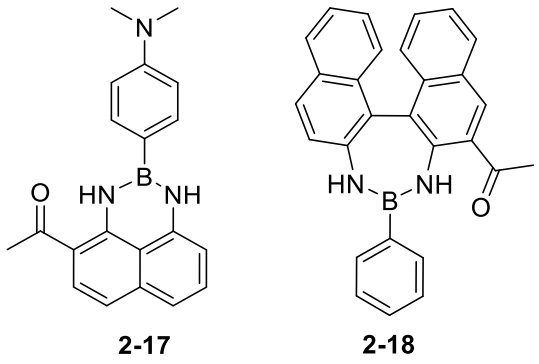

2-17 **2-18**

Figure 2-7. The dimethylaniline **2-17** decomposed into several vividly-coloured products during acylation, while an adduct between BINAM and boronic acid could not be isolated.

An aminoalcohol adduct **2-20** was also proposed. The subunit **2-19** was prepared according to a literature procedure in a ten gram-scale reaction with molten sodium and potassium hydroxide.[11] However, the condensation reaction conditions in Scheme 2-2 were not efficient, the product was difficult to purify by column chromatography and subsequent acylation with DBU resulted in a complex mixture of products (Scheme 2-5).

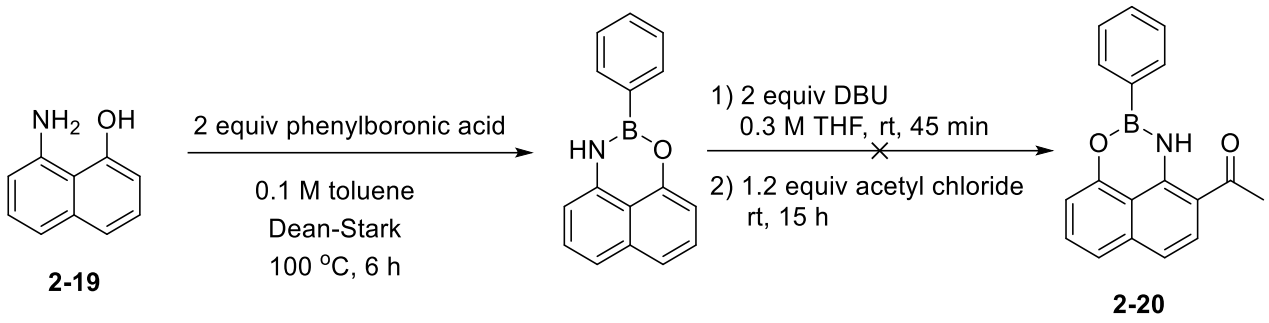

Scheme 2-5. The procedure from Scheme 2-2 was applied towards the synthesis of an oxazaborolidine analogue **2-20**.

In addition to the challenges presented by unoptimized syntheses, purification was an obstacle for many of the members of this class. The compounds appear to stick to 'grease' present in pentanes and hexanes, and several techniques to remove the grease (trituration, use of HPLC-grade hexanes, co-evaporation with toluene or acetonitrile, repeating column chromatography) proved ineffectual. It also presented an issue if grease was present in synthetic intermediates, such as diamine **2-4.** HPLC-grade toluene was eventually determined to be an effective choice of eluent for column chromatography. Nonetheless, pervasive impurities in many compound samples made it difficult to collect comprehensive, quantitative photophysical data sets, as these measurements should be performed on samples of high purity. Further, as this class of luminophores has received no attention to date, detailed structure-property relationship studies were deemed outside of the scope of the current work. Instead, at this stage, the focus was to choose a few representative class members and characterise them thoroughly.

Three DNKs (Figure 2-8) were selected as focus compounds for thorough characterisation and study. They were chosen based on their optical performance, ease of synthesis and handling, and the selection of unique properties they represented for the class. To begin study, detailed structural information would be obtained by single crystal X-ray crystallography.

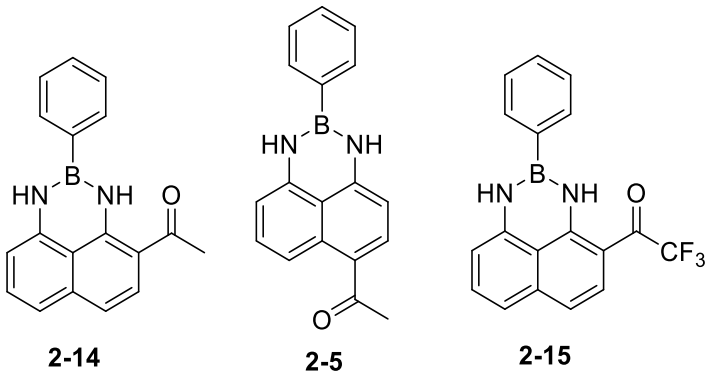

Figure 2-8. The DNK structures chosen as representative class members.

2.3.3 Crystal structures

The ^{1}H NMR spectra of the ortho-acylated **2-14** and **2-15** show characteristic downfield shifts for the N–H proton (~12 ppm) intramolecularly hydrogen-bonded to the carbonyl. The ^{11}B NMR shifts are typical for arylboronic acids and esters (28.9 ppm in deuterated chloroform and acetone). To further elucidate the structure, single crystals of these two compounds were grown by the slow evaporation of ethyl acetate and dichloromethane, respectively, allowing X-ray diffraction studies (Figure 2-9).

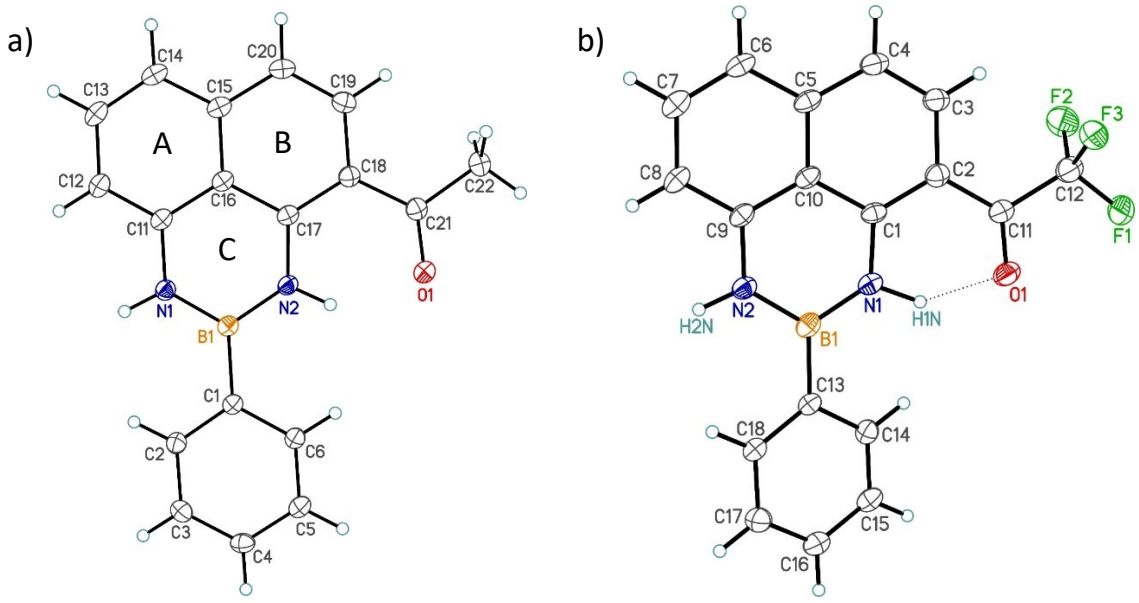

Figure 2-9. ORTEP drawings of DNKs a) **2-14** and b) **2-15**, with the ABC ring system (the diazaborolyl substructure) indicated on the structure of one molecule.

Both compounds are highly planar through the ABC ring system but exhibit some deviations throughout the larger structures. There is a small dihedral angle of 5.8° between the B-phenyl ring and the ABC ring system of DNK **2-14**. This deviation is much more pronounced in fluorinated DNK **2-15**, where the angle is 18.7°. The intramolecular hydrogen bond between the carbonyl oxygen and the N–H moieties is clearly visible, holding the ketone coplanar with the naphthyl substructure. The hydrogen bond length in this interaction is significantly different (1.953 Å for DNK **2-14**, 1.77 Å for **2-15**), as expected from the inductive effect of the fluorine atoms. Unlike the $-CF_3$ in **2-15**, the methyl group in DNK **2-14** is also slightly out of the plane of the ABC ring system, which could relate to the differences in crystal packing between these compounds. The methyl group hydrogens of **2-14** have contacts with neighbouring molecules, and the carbonyl exhibits a long intermolecular hydrogen bond of 2.687 Å. These interactions are absent in fluorinated analog **2-15**, though its carbonyl is aligned for interaction with an adjacent naphthyl ring. However, both exhibit herringbone packing with offset π stacking. The boron atom

of both species also interacts with the π orbital of an adjacent naphthyl ring, potentially enriching the vacant p_z orbital. (Figure 2-10).

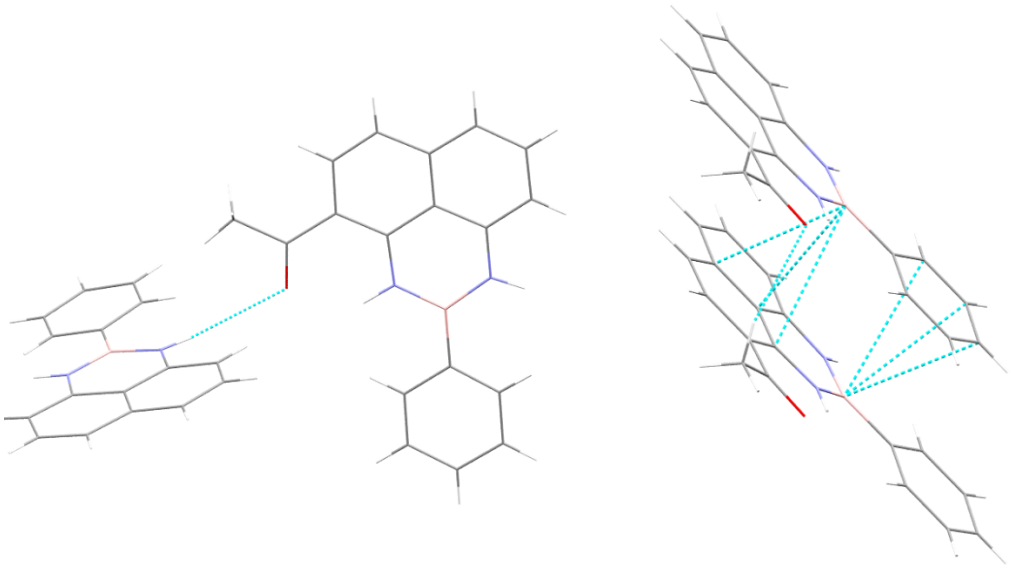

Figure 2-10. Diagrams of selected short contacts (indicated by teal lines) in DNK **2-14**, depicting the intermolecular hydrogen bond and the boron atom interaction.

It is also instructive to contrast **2-14** with the published crystal structure of phenyl-Bdan **2-3**.[12] Specifically, DNK **2-14** is planar through the ABC rings, suggesting π delocalization for these molecules, though recent NICS calculations published by Wan and coworkers suggest the N–B–N ring in these compounds is antiaromatic. Bdan **2-3** has a markedly different packing mode, dominated with T-shaped π stacking, and fewer short contacts, though the boron atom also interacts with neighbouring aryl rings. In terms of molecular structure, the dihedral angle between the planes of the ABC and the phenyl rings is similar (9°), but there are differences in the lengths of key bonds in the ABC ring system. The N–C bonds of DNK **2-14** (1.3872 and 1.3701 Å) are markedly shortened from symmetrical Bdan **2-3** (1.400 Å), with the shorter of the two bonds positioned ortho to the carbonyl site. This could be ascribed to the electron withdrawing effect of

the acyl group or perhaps the modulation of electron density due to the intramolecular hydrogen bond. The B–N bond beside this carbonyl is also elongated, measuring 1.429 Å compared to the 1.412 Å B–N bond in phenyl-Bdan **2-3**.

2.3.4 Photophysical characterisation

2.3.4.1 Photophysics in solution

Confirming our qualitative observations of fluorescence under UV and visible light irradiation, the absorption and fluorescence emission spectrum of DNK **2-14** revealed that absorptions in both wavelength ranges gave the same cyan emission at 455 nm (Figure 2-11).

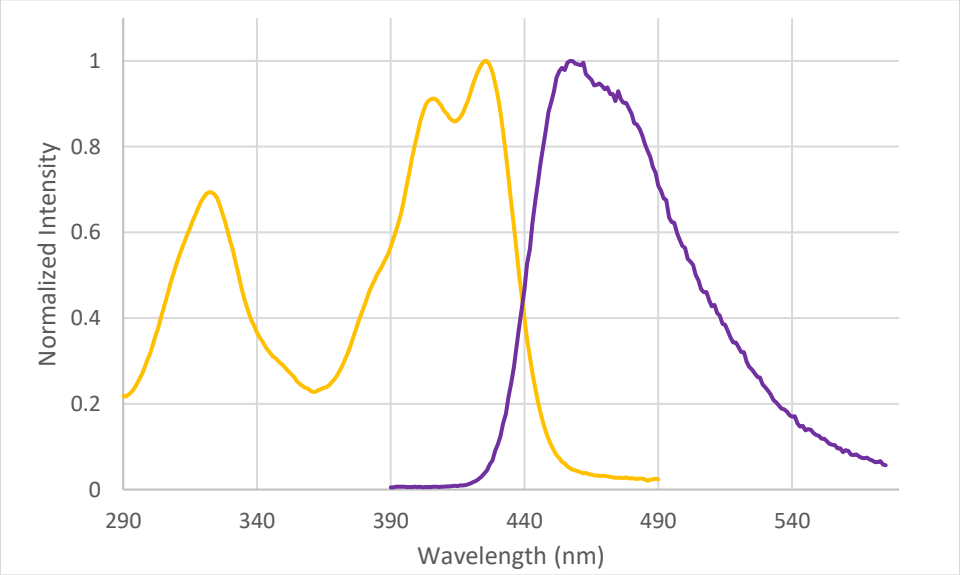

Figure 2-11. Absorption (yellow trace) and fluorescence emission (purple trace) of DNK **2-14** in acetonitrile, 15 μM.

Comprehensive photophysical data was subsequently collected for the three DNKs (**2-14, 2-15, 2-5)** and two comparator compounds, the synthetic intermediate **2-4** and phenyl Bdan **2-3**,

to assist in the preliminary analysis of structure-property relationships in these new compounds (Figure 2-12).

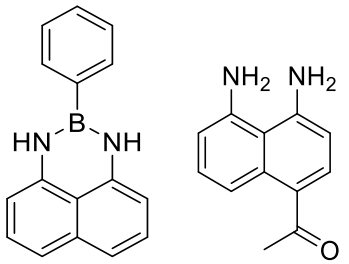

2-3 **2-4**

Figure 2-12. Phenyl-Bdan and diamine **2-4**, synthetic intermediates and comparator compounds.

Our studies confirmed that this new DNK scaffold presents unique fluorescence properties and markedly improved quantum yields over both comparators in both solution (Table 2-1) and the solid (Table 2-2) state, with one class member exhibiting an extremely high fluorescence quantum yield of 89% in toluene.

Table 2-1. Photophysical data for three DNKs and two comparators in solution

	In MeCN (15 μM)					In Toluene (15 μM)					
	λ_{abs} (nm)	λ_{em} (nm)	ε (M^{-1} cm^{-1})	Stokes Shift (cm^{-1})	φ (%)	λ_{abs} (nm)	λ_{em} (nm)	ε (M^{-1} cm^{-1})	Stokes Shift (cm^{-1})	φ (%)	Solvato-chromic Shift (cm^{-1})
2-14	425	455	16400	1550	51	426	442	11500	850	37	646
2-15	449	540	12000	3750	4	454	507	11900	2300	9	1210
2-5	399	471	13500	3830	84	391	460	9530	3840	89	508
2-3	328	516	13600	11100	2	330	467	13000	8890	3	2030
2-4	377	538	11000	7930	8	371	540	7140	8440	16	-68.8

Quantum yields were collected in nitrogen-degassed solvent and determined using an integrating sphere. Solvatochromic shift was calculated as the difference in cm^{-1} between the emission bands for toluene and acetonitrile.

In acetonitrile, DNK **2-14** presented a relatively small Stokes shifts in contrast to **2-15** and **2-5**. Consistent with these values, solvent studies performed on two of these compounds (Figure 2-13) revealed positive solvatochromism in their emission bands, suggesting a change in dipole moment of the molecule in transition from ground to excited state. Comparators **2-4** and **2-3** show dramatically different optical profiles with very large Stokes shifts and broad, red-shifted emission bands, demonstrating that both the boron and ketone moieties are key to the observed optical behaviour.

a)

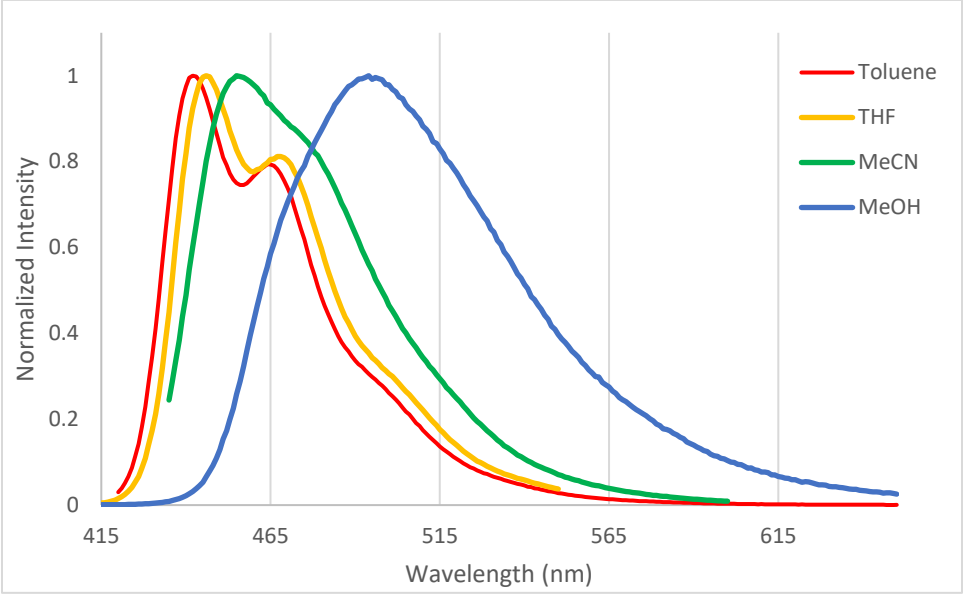

b)

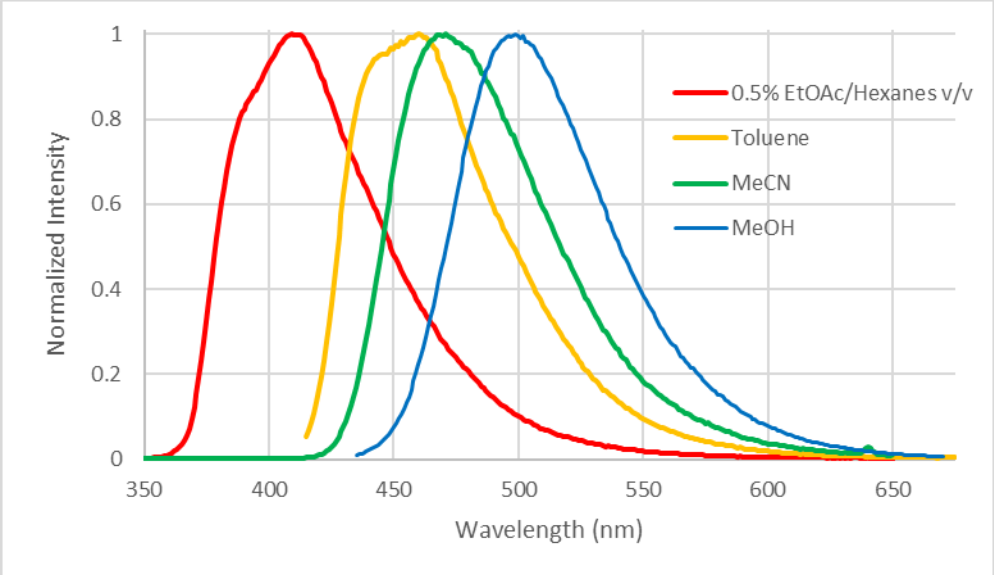

Figure 2-13. Fluorescence emission spectra of (a) **2-14** and (b) **2-5** collected in 4 solvents, 15 μM.

With respect to the diamine **2-4**, this data, complemented by its markedly reduced quantum yield, suggests one role of the boronate moiety may be to restrict internal rotation of the C–N

bonds, modulating conformation that could effect an n → π^* transition and reducing channels for internal conversion that would reduce quantum yield. This echoes the classical explanation for the high quantum yield of indole[13] and it could also explain the apparent fluorescence of the perimidine side product **2-6** that is not observed in the diamine **2-4.**

The small negative solvatochromism of diamine **2-4** could be attributed to a ground state that is more dipolar than the excited state, as has been reported for some compounds with push-pull structures or quinoidal resonance forms.[14] The very large Stokes shift and solvatochromic shift of phenyl-Bdan **2-3** allow the possibility of an excited state characterised by intramolecular charge transfer. Recalling the crystal structures of **2-14** and **2-3**, it is possible that the differences in key C–N and B–N bond lengths reflect alterations in the electronic character of N-lone pair or π orbitals of the boron-containing ring, which could lead to the differences in their fluorescence profiles.

Comparing the DNKs, it is evident that the nature and placement of the acyl group has a marked effect on the fluorescence. Though para-substituted DNK **2-5**'s emission band is slightly red shifted compared to ortho-substituted DNK **2-14**, its absorption band is at markedly shorter wavelengths. Somewhat unusually, **2-14** has a higher quantum yield in the more polar solvent, which could be due to a favourable disruption of the intramolecular hydrogen bond. While the CF_3 group gives **2-15** pronounced red shifts in both bands and greater solvatochromism between the two solvents, there is a concomitant drop in the solution phase quantum yields, possibly due to the relationship between solvent relaxation and non-radiative decay. These effects, and its large Stokes shifts, are probably due to a larger excited state dipole and more geometric reorganization than **2-14**, and more generally, the special properties of fluorine in organic molecules (such as C–F bond strength and electronegativity).

2.3.4.2 Photophysics of solids

The solid-state luminescence emission peaks for **2-14** and **2-15** were red shifted and broadened compared to the spectra in solution, presumably due to π interactions (Table 2-2). The quantum yields may also have been lowered by the π interactions, or possibly those experienced by the carbonyl and boron motifs that are also observed in the single crystal X-ray structures (Figure 2-10). However, the degree of crystallinity of the measured solids is unclear. They were prepared by concentrating solutions on a rotary evaporator, which suggests a low degree of order, but X-ray diffraction studies would be required to provide a more definitive answer. Qualitatively, single crystals of DNKs **2-14** and **2-15** appeared to fluoresce under UV light.

Table 2-2. Solid state photophysical data for two DNKs and phenyl-Bdan **2-3**

Compound	λ_{em} (nm)	φ (%)
2-14	550	8
2-15	525	7
2-3	462[7]	2.6[7]

Solid state quantum yield measurements were performed on powdered solids in glass tubes under argon atmosphere, with barium sulfate as a scattering standard, and determined using an integrating sphere.

Noting that the solution and solid quantum yields for **2-15** are remarkably similar, it appeared possible this compound is a potential platform for AIE. To investigate the fluorescence of aggregates in solution, water was chosen as the poor solvent and acetonitrile the good solvent. Solutions of equal concentration in DNK **2-15** were prepared with varying proportions of water to acetonitrile and their absolute fluorescence intensity compared (Figure 2-14). The data confirm DNK **2-15** exhibits aggregation-induced emission, and at superior quantum yields to the phenyl-Bdan AIEgens studied by Wan and coworkers.[7]

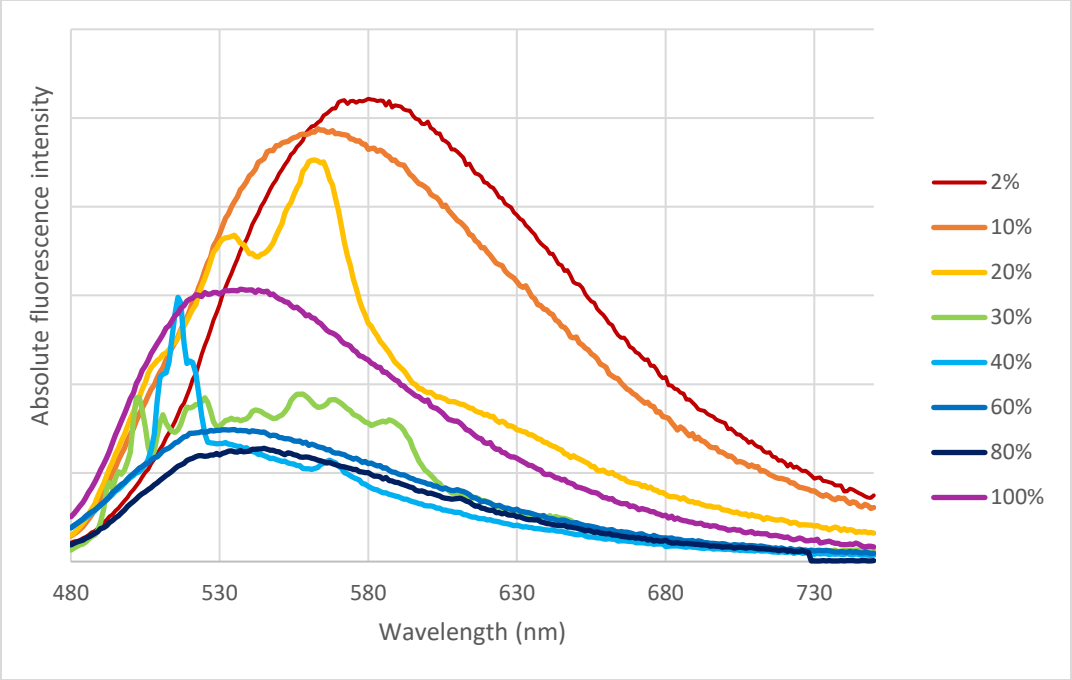

Figure 2-14. Percentages indicate v/v percentage of acetonitrile to water. All solutions were measured at equal concentration of fluorophore (15 μM) and identical instrument settings, including excitation wavelength (450 nm).

However, unlike the classical behaviour expected of AIEgens, there is a non-linear relationship between proportion of water and fluorescence intensity: note that, though the 2% solution has the strongest fluorescence, fluorescence intensity is lowest around 80%, not 100%, acetonitrile. Furthermore, there appears to be fine structure to the emission bands for solvent systems of intermediate ratio (20-60%). This outcome suggests that there is more than one mechanism affecting fluorescence as aggregates form, or the nature of the aggregate structure may qualitatively change along the solvent gradient. The structureless emission bands towards the two solvent composition extremes could indicate wider conformational distribution and relatively amorphous, large aggregates at 2% acetonitrile concentration, while the two peaks at 20% acetonitrile/water could indicate two favourable conformational modes that DNK **2-15** can adopt.

The sharp peak at 40% acetonitrile concentration could correlate to an ordered, rigid aggregate packing mode. Further study[15] is required for more concrete interpretation. Nonetheless, the existence of an AIE effect increases the relevance of this new compound class to biological[16] or solid state materials[17] applications.

2.3.5 Applications

2.3.5.1 Ion sensing

To explore if DNKs could be used as chemosensors, a screening array was designed to quickly and qualitatively assess response to a variety of chemicals. DNK **2-5** was chosen for its high quantum yield. We were particularly interested in a turn-off fluorescence sensor, as this could give higher sensitivity. Supposing that the electronic phenomenon responsible for fluorescence was an $n \rightarrow \pi^*$ transition, we could modulate or quench the fluorescence by physical or chemical environments that interacted with the electron lone pair. Either the diamine **2-4** or the adduct **2-5** could interact with Lewis acids at this site. Alternately, a Lewis base or anion could affect the p_z orbital of boron. Various metal species were prioritized as analytes, due to their relevance to some subfields of analytical chemistry.

Dilute (10 μM) solutions of DNK **2-5** and diamine **2-4** were prepared in acetonitrile and distributed into small vials. Concentrated (~0.5 M) solutions of analytes in acetonitrile or water were also prepared and 1-2 drops were added to the vials of **2-5** and **2-4**. Qualitative observations were recorded (Table 2-3).

Table 2-3. Chemosensing screening qualitative results for **2-5** and **2-4**

Analyte	DNK **2-5**	Diamine **2-4**
KCN		
$AlCl_3$		
$Hg(OAc)_2$		
$HgCl_2$		
$ZnCl_2$		
KCl		
6 M HCl	Quench	Quench
Ag_2CO_3 + 6 M HCl		Quench
$CuCl_2$		
Boric acid		
Fructose		
$Cu(NO_3)_2$	Quench	Quench
$CuBr_2$	Quench	Quench
NaCl		
$MnCl_2$		
$MgCl_2$		
$CoCl_2$		
$Fe(NO_3)_3$	Quench	Quench
$FeCl_3$	Quench	Quench
$AgNO_3$		
$CdCl_2$		
$NiCl_2$		
AuCl	Quench	
$CrCl_3$		
$PtCl_2$		
$CoCl_2$		
$CeCl_3$		

Blank entries indicate no change in fluorescence behaviour; grey entries were not performed.

Follow-up experiments revealed that fairly high concentrations of AuCl are required for the quenching effect to be significant. Additionally, the fluorescence of DNK **2-14** was tested in the presence of copper, iron, and aluminum species. Its response differed from **2-5** only with respect to aluminum, which only slightly diminished the fluorescence intensity. Evidently, the compounds nonselectively detect the presence of multiple, low-toxicity metals, which is

unattractive for many analytical chemosensing applications that involve complex mixtures of analytes.

2.3.5.2 Molecular logic

Logic gates are the basic building blocks of electronics and computing. They are physical devices that perform logical operations (specifically, Boolean functions), or to put more simply, take one or more inputs and produce a single output according to a logical principle.[18] In 1993, de Silva and coworkers published a seminal article in *Nature* describing the design of the first molecular logic gate.[19] Their molecule featured a tertiary amine and a crown ether module attached to an anthracene and functioned as a turn-on fluorophore, fluorescing strongly only in the presence of both protons and sodium ions based on the principle of photoinduced electron transfer (Figure 2-15).

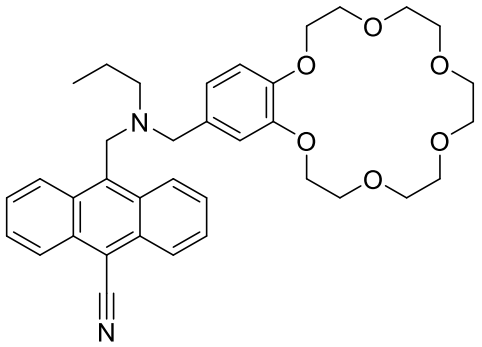

Figure 2-15. The first molecular logic gate by de Silva and coworkers.

In addition to translating ionic to photonic signal, the system also modeled an AND operator, one of the most fundamental logic gates in computing. The mathematical definitions of two operator examples, AND and OR, are given in Table 2-4.

Table 2-4. Truth tables for two different logical operators

Input		Output	Output
p	*q*	AND	OR
0	0	0	0
0	1	0	1
1	0	0	1
1	1	1	1

AND gives output only when it receives both inputs, while OR gives output when it receives at least one input.

de Silva's work launched an active area of study in organic materials. Similar to chemosensing, diverse physical, optical, chemical, electrical, or pH inputs can generate outputs, and applications are soon to be ready in areas ranging from biotechnology[20] to user authentication.[21]

The screening results for chemosensing shown in Section 2.3.5.1 were disappointing in the sense that they barred the possibility of application as a selective sensor for interesting analytes. However, the compounds' response to diverse stimuli suggests that their photochemistry is rich with potential for multiple inputs in a molecular logic system.

Parameters that could non-destructively quench or alter the fluorescence appeared most interesting, as they could conceptually demonstrate a platform for a reversible system or real-time sensing. Copper and iron species are known to be able to insert into the B–C bond, potentially quenching fluorescence by protodeboronation.[3] In order to investigate if copper, iron or aluminum species were reversibly quenching the fluorescence, three samples of fluorophore **2-5** were prepared at equal concentration, to which the metal species were added at about 0.1 M concentration, ensuring the fluorescence was completely quenched. These samples were assessed by LC-MS. In only the aluminum trichloride solution was DNK **2-5** still detectable.

To quantitate the extent of fluorescence quenching, two samples of equal fluorophore concentration were prepared, one with 10 mM $AlCl_3$ added (Figure 2-16). The addition of aluminum trichloride gave a thirty-fold decrease in fluorescence emission at peak wavelength.

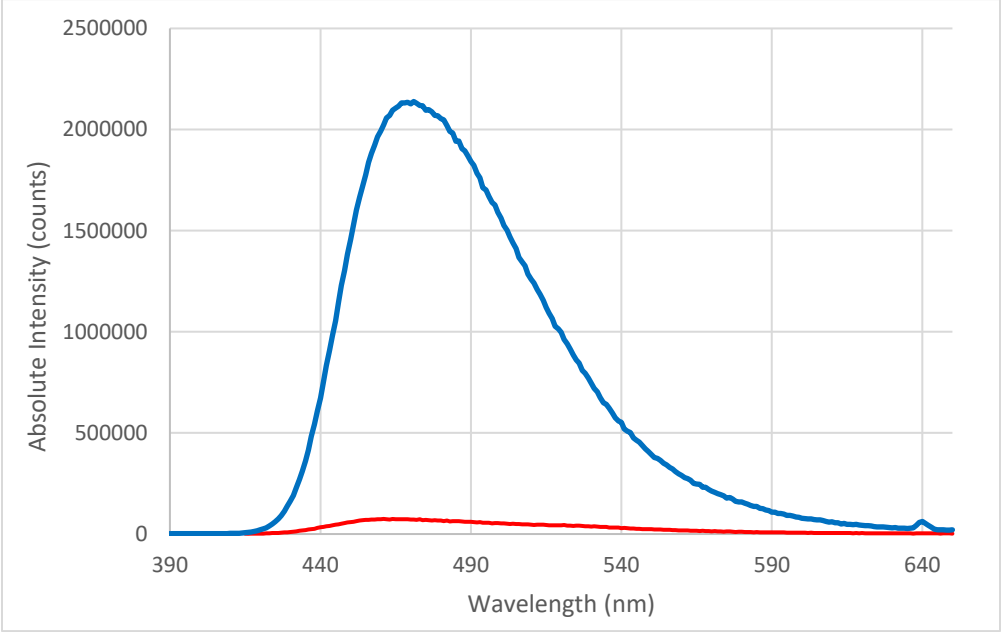

Figure 2-16. Both solutions were of equal concentration of the fluorophore **2-5** (15 μM in acetonitrile). The red trace represents sample with 10 mM $AlCl_3$. All instrument parameters (slit widths, excitation wavelength) were equal.

For the second chemical input, the solvatochromic effect was chosen. Increasing solvent polarity for DNK, or adding water to solution, red-shifts the absorption band, while the Lewis acid in acetonitrile efficiently quenches any fluorescence, with a simultaneous appearance of a new UV-vis absorption band around 500 nm as another potential output. These varied, qualitative changes indicate the system could perform combinational logic, integrating multiple inputs to simultaneously produce multiple output signals. Physical systems such as these are the means by which computers perform logical operations like addition and subtraction.

One model logic system was designed as a proof of concept: $AlCl_3$ concentration was set to 10 mM, acetonitrile and methanol were chosen as the solvents, and the output parameters were set as separate emission wavelengths for simultaneous data output. The truth table correspondences are shown in adjacent columns (Table 2-5).

Table 2-5. Application of DNK **2-5** in a 2-input 2-output logic system

Lewis acid		**Solvent polarity**		**Blue fluorescence**		**Green fluorescence**	
$AlCl_3$ (mM)	*p*	Solvent	*q*	Fluorescence, λ_{em} = 450 nm	AND	Fluorescence, λ_{em} = 500 nm	¬q
0	0	MeCN	0	Yes	0	No	1
0	0	MeOH	1	No	1	Yes	0
10	1	MeCN	0	No	1	No	1
10	1	MeOH	1	No	1	Yes	0

Fluorescence measurements collected at 15 μM concentration of **2-5**. ¬q is the q inverter operator.

This simple 2-input 2-output system is a combination of 'AND' and ¬q, or q inverter ('NOT' with respect to q) gates. Interestingly, aluminum chloride has no effect on the fluorescence in methanol. This could be attributed to ligand exchange in this solution: the literature suggests that, in acetonitrile, the complexes $AlCl_3 \cdot n$MeCN (n = 1, 2, 3) exist in solution,[22] but in methanol, the solvent may displace a chloride ion,[23] giving one or more complexes of the type $[Al(MeOH)_4Cl_2]^+$ and significantly perturbing the nature of its Lewis acidity. Different combinations of solvents could give qualitatively distinct logic gates. Looking forward, the diverse photophysical properties of DNKs indicate potential for modified solvent-ion system designs, and solid state molecular logic, which call for more detailed study.

2.3.5.3 Boronic acid sensing

In recent years, evidence has emerged that suggests some boronic acids are mutagenic and present a peril to human health.[24,25] This finding is cause for alarm in the pharmaceutical industry, as boronic acids are one of the most common synthetic intermediates:[3] The Suzuki-Miyaura cross-coupling accounts for an incredible 12% of all reactions performed for drug discovery and development.[26] There is particular concern when the Suzuki-Miyaura reaction is used late in synthesis, as low concentration (<10 ppm) boronic acids are difficult to detect by HPLC and NMR spectroscopy, but may still pose a health hazard. The straightforward mix-and-stir reaction conditions in Scheme 2-3 suggested that the diamine **2-4** could form DNK structures *in situ* with boronic acids and act as a fluorescent chemosensor. The strong fluorescence of DNK **2-5**, and the observation that phenyl ring substitution does not seem to make a significant difference to fluorescence in solution, indicate that this fluorescent chemosensor system could be both sensitive and robust to a wide variety of boronic acid substrates.

To eliminate background noise from diamine **2-4** fluorescence, HPLC was chosen for purification and fluorescence detection in the boronic acid chemosensing procedure. DNK adduct **2-5** demonstrated good kinetic stability to a variety of HPLC conditions, including acidic eluent. In fact, the acid stability of these compounds is worthy of remark: though typical aryl-Bdans are hydrolyzed with dilute acid at room temperature,[4] compound **2-14** was highly resistant to hydrolysis, even when heated to 60 °C in the presence of 2 M hydrochloric acid over several days.

Next, samples were prepared and reaction conditions were designed to imitate a pharmaceutical company's quantitation of trace boronic acid starting material in a Suzuki-Miyaura reaction product. A solid "cake" of 10 ppm phenylboronic acid in biphenyl was prepared. To

ensure quantitative conversion to DNK **2-5** in reasonable time, a large excess of diamine **2-4** and concentrated solution were found to be essential. Acetonitrile was chosen as the solvent with gentle heating (Scheme 2-6).

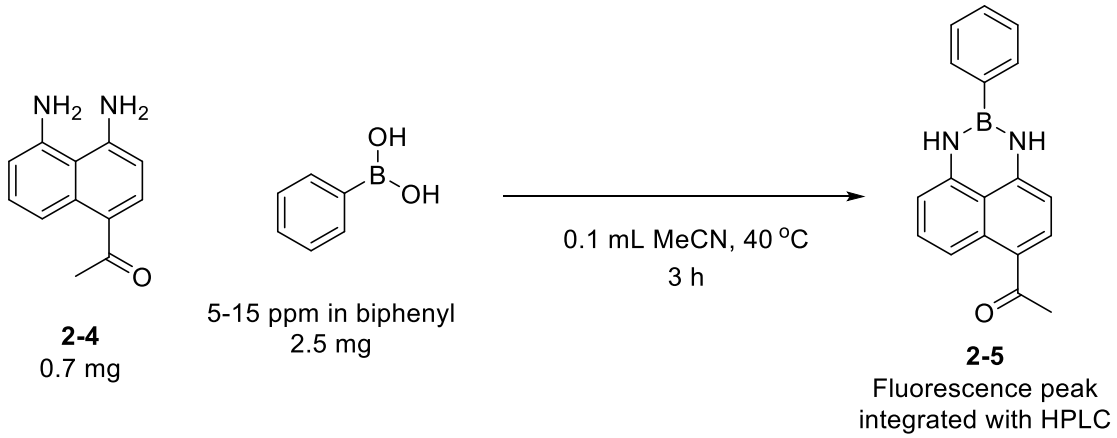

Scheme 2-6. The reaction conditions used to detect boronic acid contaminant in an unknown sample along with a set of standard samples.

To infer the quantity of boronic acid in an unknown sample, the integration of the fluorescent peak corresponding to a DNK adduct could be compared with the integration of a known sample. A calibration curve was deemed the most rigorous and robust standard. All four samples were prepared at the same time, in small scale, and underwent identical treatment. The calibration curve is constructed with boronic acid in a range of concentrations (Figure 2-17).

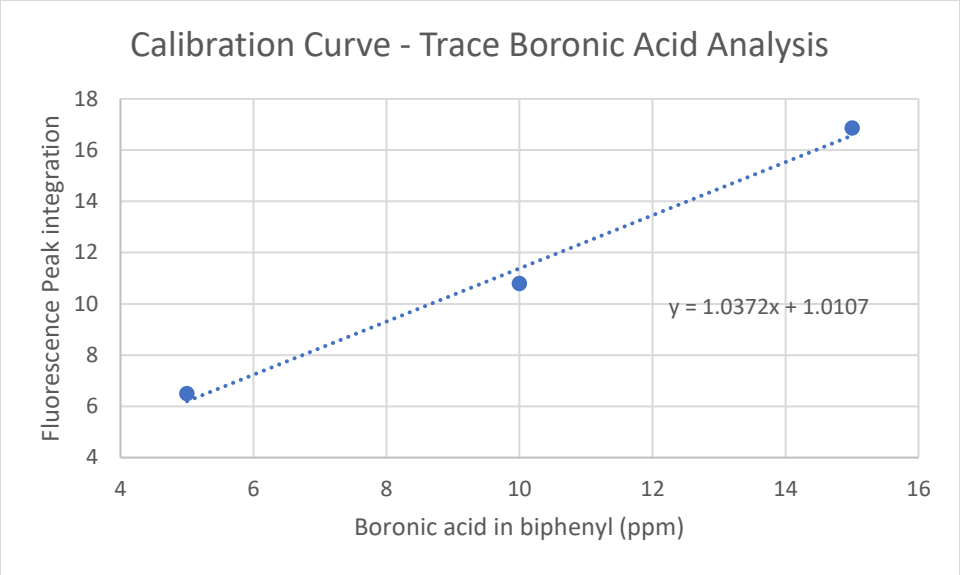

Figure 2-17. Calibration curve, with trendline equation, for three standard reaction samples of different boronic acid concentration. Fluorescence peak areas were determined from HPLC chromatograms.

In this proof of concept, the calibration range extends below 10 ppm, satisfying the analytical requirements for sensitivity. The unknown sample, with 10 ppm boronic acid, gave a signal area y = 10.8349, corresponding to a concentration of 9.5 ppm, or a 5% error margin, which is reasonable for a single replicate test. Future work would need to assess a range of substrates and assess the robustness and scope of the method.

2.4 Conclusions

Chapter 2 described the synthesis, structure, photophysical properties, and applications of a new luminescent polyaromatic boronic scaffold (DNKs). Preliminary synthetic methodology was developed to produce DNKs with differing phenyl and naphthyl substitution patterns in low to moderate yields across two steps. Out of a library of compounds, three DNKs were selected for

detailed characterisation and study. X-ray crystallographic study of two DNKs with ortho substitution, **2-14** and **2-15**, revealed notable structural differences between these compounds and phenyl-Bdan **2-3**, including markedly shortened C–N bonds and an elongated B–N bond adjacent to the carbonyl, which participated in an intramolecular hydrogen bond. Photophysical data was subsequently collected in solution and the solid state, revealing blue-shifted, narrowed, and intense emissions for DNKs in contrast to **2-3** and diamine **2-4.** Solvatochromic shifts were also smaller for DNKs compared to Bdan **2-3**, inviting computational study on the electronic structure of the species. DNK **2-5** exhibited an extremely high quantum yield of 89% in toluene, and along with fluorinated **2-15**, exhibited red-shifted emission (460 nm and 507 nm, respectively) compared to DNK **2-14** (442 nm). However, the large Stokes shifts of **2-15** and **2-5** may originate from different electronic mechanisms, as the former DNK exhibits strong solvatochromism. Though solid-state quantum yields are moderate, DNK **2-15** was found to exhibit AIE, with the exact mechanism of this effect not yet understood. Finally, some applications were developed using **2-5.** A simple 2-input 2-output model system suggests the DNK compounds have potential as a flexible, customizable molecular logic platform with various choices for input and output. Additionally, a system for the detection of trace boronic acid contaminants at the level of 5-15 ppm could be useful to pharmaceutical companies concerned with difficult to detect, mutagenic synthetic intermediates in drug samples. Further work will examine more DNK class members to understand structure-property relationships and take advantage of their varied photochemical properties for diverse applications.

2.5 Experimental

2.5.1 General information

Unless otherwise indicated, all reactions were performed under a nitrogen atmosphere using glassware that was dried for at least 24 hours in an oven (300 °C). All reagents were purchased from SigmaAldrich, Combi-Blocks or Alfa Aesar and used as received. Solvents for anhydrous reactions, such as toluene, were used directly from an MBraun Solvent Purification System, except ethanol. Ethanol was prepared for use by allowing nitrogen to bubble through it for one hour. Thin layer chromatography (TLC) was performed on Merck Silica Gel 60 F254 plates and visualized with UV light and curcumin or vanillin stain. Flash chromatography was performed with ultra-pure silica gel 230-400 mesh. Nuclear magnetic resonance (NMR) spectra were recorded on Agilent/Varian INOVA-400 and INOVA700 MHz instruments. The residual solvent protons (^{1}H) of $CDCl_3$ (7.26 ppm), acetone-d_6 (2.05 ppm), and D_2O (4.79 ppm) were used as internal standards, and the carbon signal (^{13}C) of $CDCl_3$ (77.06 ppm) and acetone-d_6 (29.84 and 206.26 ppm) were used as internal standards in their respective spectra. VnmrJ software was used to analyze the NMR data. The following abbreviations are used in reporting NMR data: s, singlet; d, doublet; t, triplet; app t, apparent triplet; q, quartet; dd, doublet of doublets; ddd, doublet of doublet of doublets; dddd, doublet of doublet of doublet of doublets; dhept, doublet of heptet; td, triplet of doublet; m, multiplet; comp m, complex multiplet. In ^{13}C NMR spectroscopy, the quaternary carbon bound to the boron atom is often missing due to the quadrupolar relaxation of boron. This effect was observed in each boronic acid or boronic ester compound. Infrared spectra (performed on a Nicolet Magna-IR 750 instrument equipped with a Nic-Plan microscope) were recorded by the University of Alberta Analytical and Instrumentation Laboratory. High-resolution mass spectra were recorded

by the University of Alberta Mass Spectrometry Services Laboratory using I weave - 30 electron impact (EI) and electrospray ionization (ESI) techniques. UV-Visible spectroscopy was performed on an Agilent 8453 Cary 5000 instrument in a quartz cuvette with a path length of 1 cm. Fluorometry data was collected on a Horiba-PTI QM-8075-11 spectrofluorometer in a quartz cuvette with a path length of 1 cm. The absolute fluorescence quantum yield was measured with an integrating sphere on the same spectrofluorometer. For quantum yield measurements, solutions were degassed with nitrogen and solid samples were under argon atmosphere in a sealed capillary tube. Due to purification issues, not all ^{13}C NMR spectra and melting point data were obtained.

2.5.2 Chemical synthesis and characterisation

General Procedure A for the Acylation of Aryl-Bdans

To a 20 mL pear shaped flask equipped with a stir bar was added aryl-Bdan (1 mmol), which was purged with nitrogen gas before adding THF (3 mL) and cooling to –78 °C. *n*-Butyllithium in hexanes (2.0 M, 2 mmol) was added dropwise over 3 minutes, then the mixture was left to stir for 90 minutes, maintaining the cooling bath. To a separate 20 mL round bottom flask with a stir bar under nitrogen, the acyl chloride (2 mmol) was added followed by THF (6 mL) and the flask was cooled to –78 °C. The aryl-Bdan mixture was added dropwise by syringe over 3 minutes. After holding at this temperature for ten minutes, the flask was allowed to warm to room temperature over one hour, upon which 5 mL of a solution of aqueous ammonium chloride were added to stop the reaction. The crude mixture was diluted with brine (50 mL) and extracted with dichloromethane (3 × 75 mL). The collected organic extracts were combined, dried with

anhydrous sodium sulfate, filtered, concentrated *in vacuo* and purified by flash chromatography with a hexanes:ethyl acetate gradient (40:1 – 7:1).

General Procedure B for the Acylation of Aryl-Bdans

To a 10 mL pear shaped flask equipped with a stir bar was added aryl-Bdan (0.50 mmol), which was purged with nitrogen gas before adding THF (3 mL) followed by DBU (130 mg, 0.90 mmol) at room temperature. The mixture was allowed to stir for 45 minutes before adding the acyl halide or anhydride (1.0 mmol) directly. After several hours the reaction mixture was concentrated *in vacuo* and purified by flash chromatography with a hexanes:ethyl acetate gradient (40:1 – 7:1).

Synthesis and Characterisation of Diamine **2-4**

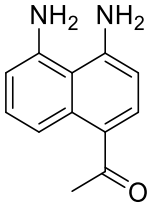

Diamine **2-4** was synthesized by a modified version of the Sugasawa reaction.[8] To a 10 mL pear-shaped flask was added 1,8-diaminonaphthalene (150 mg, 1.0 mmol) and a stir bar. After purging with nitrogen gas, toluene (3 mL) was added and the mixture was stirred at room temperature until homogenous. A three-necked 20 mL round bottom flask was equipped with a reflux condenser and stir bar, purged with nitrogen gas, and charged with boron trichloride in DCM (1.1 mL, 1.0 M) before cooling to 0 °C. The contents of the pear-shaped flask were added dropwise over 3 minutes to the three-necked flask, followed by acetonitrile (0.1 mL, 2 mmol)

and solid aluminum trichloride (150 mg, 1.1 mmol). The reaction was allowed to warm to room temperature over 45 minutes before heating to 100 °C for 15 hours, upon which the reaction was cooled to 0 °C and quenched by the addition of 2 M HCl (6 mL). The mixture was again heated to 95 °C for 45 minutes before diluting with DCM (75 mL) and water (75 mL). The organic layer was drained and the aqueous phase extracted once again (75 mL) before basifying the aqueous phase to ~pH 9 with saturated aqueous sodium hydroxide and extracting again with DCM (2 × 75 mL). The collected organic extracts were dried with anhydrous sodium sulfate, filtered, concentrated *in vacuo* and purified by flash column chromatography (4:1 hexanes:ethyl acetate or toluene:ethyl acetate) to afford a flaky, yellow-orange solid.

Melting point: 112-113 °C.

^{1}H NMR (498 MHz, acetonitrile-d_3) δ 8.58 (dd, *J* = 8.5, 1.2 Hz, 1 H), 7.89 (d, *J* = 8.5 Hz, 1 H), 7.28 (dd, *J* = 8.5, 8.5 Hz, 1 H), 6.77 (dd, *J* = 8.5, 1.2 Hz, 1 H), 6.53 (d, *J* = 8.5 Hz, 1 H), 2.56 (s, 3 H). N$\underline{H_2}$ not observed.

^{13}C NMR (176 MHz, acetonitrile-d_3) δ 198.4, 151.7, 145.2, 135.1, 133.8, 128.4, 122.4, 118.0, 115.5, 113.5, 106.7, 28.5.

IR (cast film, cm^{-1}): 3423, 3330, 3329, 3039, 2924, 2853, 1630, 1575, 1521, 1463, 1360, 1249, 1167.

HRMS (ESI) for $(M + H)^+$: calcd. for $C_{12}H_{12}N_2O$: 201.1022; found: 201.1030.

Synthesis and Characterisation of DNK **2-5**

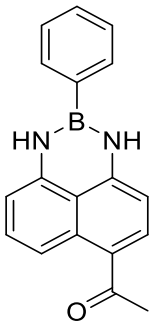

Diamine **2-4** (12 mg, 60 µmol) and phenylboronic acid (14 mg, 120 µmol) were added to a 5 mL round bottom flask with a stir bar. THF (0.3 mL) was added and the mixture was allowed to stir at room temperature for two hours, after which magnesium sulfate (5 mg) was added directly to the flask. After 3 more hours of stirring the mixture was filtered and the collected organic filtrates were concentrated *in vacuo* before purification by flash chromatography (toluene:ethyl acetate 4:1), affording a light green powder (19 mg, 88%).

Melting point: 180-181 °C.

^{1}H NMR (400 MHz, acetonitrile-d_3) δ 8.51 (d, *J* = 9.0 Hz, 1 H), 7.96 (d, *J* = 9.0 Hz, 1 H), 7.82 (dd, *J* = 7.8, 1.2 Hz, 2 H), 7.52-7.46 (m, 4 H), 7.37-7.34 (m, 2 H), 6.78 (d, *J* = 9.0 Hz, 1 H), 6.61 (d, *J* = 9.0 Hz, 1 H), 2.56 (s, 3 H).

^{13}C NMR (176 MHz, acetonitrile-d_3) δ 198.1, 147.5, 141.8, 135.4, 134.3, 132.3, 130.4, 130.1, 128.0, 122.8, 119.1, 116.2, 107.6, 104.9, 28.2.

^{11}B NMR (128 MHz, acetone-d_6) δ 28.9.

IR (cast film, cm^{-1}): 3359, 2944, 2860, 1738, 1592, 1488, 1415, 1247.

HRMS (EI) for $C_{18}H_{15}{}^{11}BN_2O$ calcd.: 286.1278; found: 286.1278.

Synthesis and Characterisation of DNK **2-7**

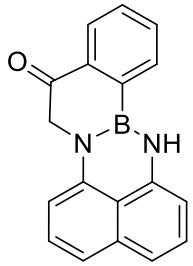

The bromination procedure was adapted from an unpublished protocol developed by Dr. Michele Boghi. To a 20 mL round bottom flask was added a stir bar, 2-acetylphenylboronic acid (210 mg, 1.2 mmol), *N*-bromosuccinimide (330 mg, 1.3 mmol), and *p*-toluenesulfonic acid (29 mg, 0.18 mmol), followed by acetonitrile (6 mL). The flask was equipped with a reflux condenser and heated to 85 °C open to air for 6 h, after which the mixture was allowed to cool, diluted with dichloromethane (25 mL) and washed with saturated ammonium chloride. The organic layer was drained, the aqueous phase was extracted with dichloromethane (3 × 75 mL) and the combined organic extracts were treated with sodium sulfate before filtration and concentration *in vacuo*. The crude mixture was added to a three-necked round bottom flask with 1,8-diaminonaphthalene (206 mg, 1.30 mmol) and a stir bar before affixing a Dean-Stark apparatus and purging the solids with nitrogen gas. Toluene (12 mL) was added to the flask and it was heated to 100 °C for 15 h before removing from heat and concentrating the mixture *in vacuo*. The crude product was purified by flash chromatography to afford an orange solid (15 mg, 5%).

^{1}H NMR (400 MHz, acetone-d_6) δ 8.27 (s, 1 H), 8.22 (d, J = 7.5 Hz, 1 H), 8.15 (d, J = 7.5 Hz, 1 H), 7.81-7.76 (m, 1 H), 7.72-7.68 (m, 1 H), 7.29 (dd, J = 7.5, 7.5 Hz, 1 H), 7.24-7.711 (m, 3 H), 6.78 (d, J = 7.5 Hz, 1 H), 6.58 (d, J = 7.5 Hz, 1 H), 4.21 (s, 2 H).

^{11}B NMR (160 MHz, acetone-d_6) δ 26.8.

HRMS (EI) for $C_{18}H_{13}ON_2{}^{11}B$: calcd.: 284.1121; found: 284.1122.

Synthesis and Characterisation of DNK **2-8**

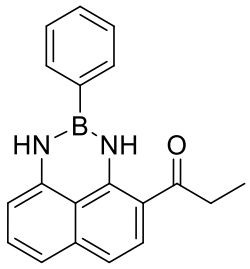

General procedure A was applied, with propanoyl chloride as the acyl chloride and phenyl-Bdan as the aryl-Bdan, to afford a green oil (47 mg, 24%).

^{1}H NMR (700 MHz, acetone-d_6) δ 11.95 (s, 1 H), 8.49 (s, 1 H), 7.95-7.89 (m, 2 H), 7.71-7.68 (m, 1 H), 7.55-7.46 (m, 3 H), 7.38 (dd, *J* = 8.0, 8.0 Hz, 1 H), 7.10 (d, *J* = 8.0, 1 H), 6.97 (d, *J* = 8.5 Hz, 1 H), 6.91 (d, *J* = 8.0 Hz, 1 H), 3.04 (q, 7.5 Hz, 2 H), 1.20 (t, *J* = 7.5 Hz, 3 H).

^{11}B NMR (160 MHz, acetone-d_6) δ 28.9.

HRMS (EI) for $C_{19}H_{17}ON_2{}^{11}B$: calcd.: 300.1434; found: 300.1435.

Synthesis and Characterisation of DNK **2-9**

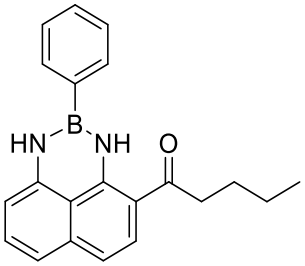

General procedure A was used, with valeryl chloride as the acyl chloride and phenyl-Bdan as the aryl-Bdan to afford a green crystalline solid (76 mg, 41%).

^{1}H NMR (700 MHz, acetone-d_6) δ 11.99 (s, 1 H), 8.51 (s, 1 H), 7.96-7.88 (m, 2 H), 7.71 (d, *J* = 9.0 Hz, 1 H), 7.53-7.47 (m, 3 H), 7.39 (dd, *J* = 8.5, 8.5 Hz, 1 H), 7.11 (d, *J* = 8.5 Hz, 1 H), 6.98 (d, *J* = 9.0 Hz, 1 H), 6.92 (d, *J* = 8.5 Hz, 1 H), 3.02 (t, *J* = 7.5 Hz, 2 H), 1.74 (quint., *J* = 7.5, 7.5 Hz, 2 H), 1.45 (sext., *J* = 7.5, 7.5 Hz, 2 H), 0.97 (t, *J* = 7.5 Hz, 3 H).

^{13}C NMR (100 MHz, acetone-d_6) δ 202.8, 149.1, 144.6, 138.9, 133.1, 131.8, 131.4, 129.1, 128.6, 119.9, 118.1, 117.2, 111.1, 109.7, 39.8, 27.9, 23.3, 14.4.

^{11}B NMR (160 MHz, acetone-d_6) δ 28.9.

IR (cast film, cm^{-1}): 3356, 3238, 3053, 2957, 2932, 2870, 1622, 1578, 1536, 1454, 1433, 1210.

HRMS (EI) for $C_{21}H_{21}N_2{}^{11}BO$: calcd.: 328.1747; found: 328.1735.

Synthesis and Characterisation of DNK **2-10**

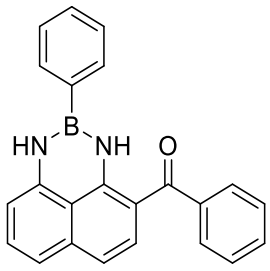

General procedure B was used, with benzoyl chloride as the acyl halide and phenyl-Bdan as the aryl-Bdan, to afford a dark green solid (9 mg, 6%).

^{1}H NMR (400 MHz, acetone-d_6) δ 8.67 (s, 1 H), 8.18 (d, *J* = 8.0 Hz, 1 H), 7.98-7.93 (m, 2 H), 7.68-7.59 (m, 4 H), 7.35 (d, *J* = 9.0 Hz, 2 H), 7.19-7.13 (m, 3 H), 7.01-6.95 (m, 3 H).

Note: one of the N-H protons was not observed.

^{11}B NMR (128 MHz, acetone-d_6) δ 29.0.

HRMS (EI) for $C_{23}H_{17}N_2{}^{11}BO$: calcd.: 348.1434; found: 348.1437.

Synthesis and Characterisation of DNK **2-11**

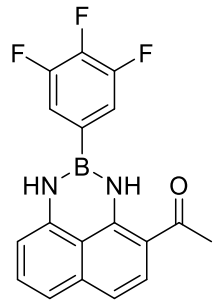

General procedure A was used, with acetyl chloride as the acyl chloride and 3,4,5-trifluoro-phenyl-Bdan as the aryl-Bdan, to afford a bright green solid (24 mg, 25%).

^{1}H NMR (400 MHz, acetone-d_6) δ 11.82 (s, 1 H), 8.58 (s, 1 H), 7.68 (d, *J* = 9.0 Hz, 1 H), 7.60 (t, *J* = 7.5 Hz, 2 H), 7.41 (dd, *J* = 7.5 Hz, 1 H), 7.15 (d, *J* = 9.0 Hz, 1 H), 7.02 (d, *J* = 9.0 Hz, 1 H), 6.88 (d, *J* = 7.5 Hz, 1 H), 2.62 (s, 3 H).

^{13}C NMR (176 MHz, acetone-d_6) δ 200.8, 152.1 (ddd, *J* = 252, 10, 4 Hz), 141.7 (dt, *J* = 252, 15 Hz), 148.4, 143.1, 138.9, 131.9, 129.2, 119.8, 118.6, 117.6, 117.1 (dd, *J* = 15, 4 Hz), 111.7, 109.9, 28.3.

^{11}B NMR (128 MHz, acetone-d_6) δ 27.8.

^{19}F NMR (376 MHz, acetone-d_6) δ –136.9, –160.4.

HRMS (EI) for $C_{18}H_{12}{}^{11}BN_2OF_3$: calcd.: 340.0995; found: 340.0991.

Synthesis and Characterisation of DNK **2-12**

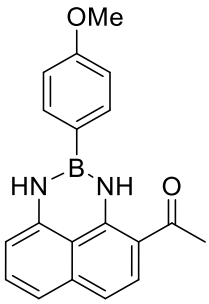

General procedure A was used, with acetyl chloride as the acyl chloride and 4-MeO-phenyl-Bdan as the aryl-Bdan, to afford a bright green solid (58 mg, 39%).

^{1}H NMR (700 MHz, acetone-d_6) δ 11.87 (s, 1 H), 8.46 (s, 1 H), 7.87 (d, *J* = 8.5 Hz, 2 H), 7.67 (d, *J* = 8.5 Hz, 1 H), 7.39 (dd, *J* = 8.5, 8.5 Hz, 1 H), 7.11 (d, *J* = 8.5 Hz, 1 H), 7.06 (d, *J* = 8.5 Hz, 2 H), 6.78 (d, *J* = 8.5 Hz, 1 H), 6.91 (d, *J* = 8.5 Hz, 1 H), 3.86 (s, 3 H), 2.62 (s, 3 H).

^{13}C NMR (176 MHz, acetone-d_6) δ 200.4, 162.9, 149.2, 144.7, 139.0, 134.8, 131.8, 129.3, 119.5, 117.9, 117.0, 114.7, 111.3, 109.6, 55.5, 28.3.

^{11}B NMR (128 MHz, acetone-d_6) δ 28.6.

IR (cast film, cm^{-1}): 3359, 3421, 3006, 2960, 1708, 1620, 1605, 1578, 1487, 1435, 1364, 1284, 1241, 1206, 1083.

HRMS (EI) for $C_{19}H_{17}{}^{11}BN_2O_2$: calcd.: 316.1383; found: 316.1384.

Synthesis and Characterisation of DNK **2-13**

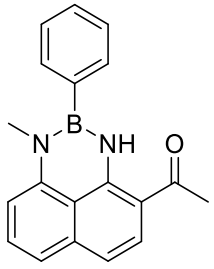

N-methyl-1,8-diaminonaphthalene was prepared according to a published procedure.[27] This compound was used in place of 1,8-diaminonaphthalene in a typical Suginome DAN protection without modification of conditions or equivalents[4] to afford N-methyl-phenyl-Bdan. Upon this aryl-Bdan, general procedure A was used, with acetyl chloride as the acyl chloride, to afford a green solid (21 mg, 25%).

^{1}H NMR (400 MHz, acetone-d_6) δ 7.77-7.70 (m, 3 H), 7.56 (dd, *J* = 8.0, 8.0 Hz, 1 H), 7.53-7.46 (m, 3 H), 7.27 (d, *J* = 8.0 Hz, 1 H), 7.10 (d, *J* = 8.0 Hz, 1 H), 6.89 (d, *J* = 8.0 Hz, 1 H), 3.29 (s, 3 H), 2.59 (s, 3 H).

^{11}B NMR (160 MHz, acetone-d_6) δ 30.7.

HRMS (EI) for $C_{19}H_{17}{}^{11}BN_2O$: calcd.: 300.1434; found: 300.1436.

Synthesis and Characterisation of DNK **2-14**

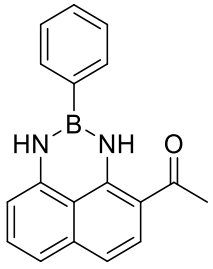

General procedure A was used, with acetyl chloride as the acyl chloride and phenyl-Bdan as the aryl-Bdan, to afford a yellow solid (84 mg, 23%).

^{1}H NMR (400 MHz, acetone-d_6) δ 11.90 (s, 1 H), 8.54 (s, 1 H), 7.93-7.89 (m, 2 H), 7.68 (d, *J* = 9.0 Hz, 1 H), 7.53-7.46 (m, 3 H), 7.40 (dd, *J* = 8.0, 8.0 Hz, 1 H), 7.12 (d, *J* = 8.0 Hz, 1 H), 7.00 (d, *J* = 9.0 Hz, 1 H), 6.93 (d, *J* = 8.0 Hz, 1 H), 2.61 (s, 3 H).

^{13}C NMR (176 MHz, acetone-d_6) δ 200.5, 149.1, 144.6, 139.0, 133.2, 131.9, 131.5, 129.4, 129.1, 119.8, 118.2, 117.2, 111.5, 109.8, 28.4.

^{11}B NMR (160 MHz, acetone-d_6) δ 28.9.

IR (cast film, cm^{-1}): 3341, 3240, 3049, 2924, 2853, 1720, 1618, 1576, 1535, 1483, 1433, 1364, 1282, 1242, 1207, 1151, 1090.

HRMS (EI) for $C_{18}H_{15}{}^{11}BN_2O$: calcd.: 286.1278; found: 286.1280.

Melting point: 152-153 °C.

Synthesis and Characterisation of DNK **2-15**

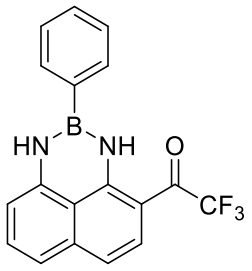

General procedure B was used, with trifluoroacetic anhydride as the acyl anhydride and phenyl-Bdan as the aryl-Bdan, to afford a bright yellow solid (133 mg, 65%).

Melting point: 151-152 °C.

^{1}H NMR (498 MHz, acetone-d_6) δ 11.70 (s, 1 H), 9.14 (s, 1 H), 7.98-7.96 (m, 2 H), 7.62 (dd, *J* = 8.5, 8.5 Hz, 1 H), 7.58-7.52 (m, 4 H), 7.27 (d, *J* = 8.5 Hz, 1 H), 7.17 (d, *J* = 8.5 Hz, 1 H), 7.10 (d, *J* = 8.5 Hz, 1 H).

^{13}C NMR (176 MHz, acetone-d_6) δ 206.3, 179.0 (q, *J* = 32.6 Hz), 154.4, 144.8, 138.9, 134.1, 133.3, 132.0, 129.3, 126.3, 126.3, 118.9, 118.6, 111.8, 105.2.

^{11}B NMR (128 MHz, acetone-d_6) δ 28.9.

^{19}F NMR (376 MHz, acetone-d_6) δ –70.1.

IR (cast film, cm^{-1}): 3402, 3371, 3263, 3056, 3023, 1626, 1577, 1539, 1436, 1343, 1222, 1190, 1093.

HRMS (EI) for $C_{18}H_{12}{}^{11}BN_2OF_3$ calcd.: 340.0995; found: 340.0997.

Synthesis and Characterisation of DNK **2-16**

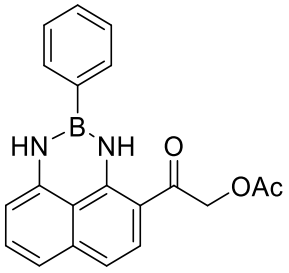

General procedure A was used, with acetoxyacetyl chloride as the acyl chloride and phenyl-Bdan as the aryl-Bdan, to afford a yellow solid (71 mg, 49%).

^{1}H NMR (700 MHz, acetone-d_6) δ 11.64 (s, 1 H), 8.65 (s, 1 H), 7.94-7.89 (m, 2 H), 7.63 (d, *J* = 9.0 Hz, 1 H), 7.55-7.48 (m, 3 H), 7.46 (dd, *J* = 8.5, 8.5 Hz, 1 H), 7.17 (d, *J* = 8.5 Hz, 1 H), 7.04 (d, *J* = 9.0 Hz, 1 H), 6.99 (d, *J* = 8.5 Hz, 1 H), 5.45 (s, 2 H), 2.19 (s, 3 H).

^{13}C NMR (176 MHz, acetone-d_6) δ 201.82, 193.8, 170.6, 149.6, 144.5, 138.9, 133.1, 132.3, 131.6, 129.1, 126.6, 118.3, 117.6, 110.2, 108.7, 66.8, 20.6.

^{11}B NMR (128 MHz, acetone-d_6) δ 28.8.

IR (cast film, cm^{-1}): 3365, 3255, 3025, 2931, 1730, 1626, 1604, 1575, 1435, 1201, 1091.

HRMS (EI) for $C_{20}H_{17}O_3N_2{}^{11}B$: calcd.: 344.1332; found: 344.1340.

2.5.3 Demonstrating evaluation of trace boronic acid contamination in pharmaceutical samples

Solid “cakes” comprised of 5, 10, and 15 molar ppm boronic acid:biphenyl were prepared by dissolving aliquots of a stock boronic acid solution in solutions of biphenyl, then concentrating *in*

vacuo and mixing the solid thoroughly. Without any anhydrous or anoxic precautions, three standard (5, 10, and 15 ppm boronic acid) and one "unknown" (10 ppm) reactions were prepared by weighing 2.5 mg each into separate 5 mL round bottom flasks equipped with stir bars. Diamine **2-4** was added (0.7 mg each) along with 0.1 mL acetonitrile. The flasks were sealed and allowed to heat at 40 °C for 3 hours, upon which the reaction mixture was diluted tenfold with acetonitrile. The mixture was subjected to HPLC using a C18 column and eluted at 11.8 min with 0.1% formic acid in water/acetonitrile, detected with 410 nm excitation and emission set to 485 nm.

2.6 References

(1) Wang, X.-Y.; Yao, X.; Narita, A.; Müllen, K. Heteroatom-Doped Nanographenes with Structural Precision. *Acc. Chem. Res.* **2019**, *52* (9), 2491–2505. https://doi.org/10.1021/acs.accounts.9b00322.

(2) Bosdet, M. J. D.; Piers, W. E. B-N as a C-C Substitute in Aromatic Systems. *Can. J. Chem.* **2009**, *87* (1), 8–29. https://doi.org/10.1139/v08-110.

(3) Hall, D. G. *Boronic Acids. Preparation and Applications in Organic Synthesis, Medicine and Materials*, 2nd Completely Revised ed.; Hall, D. G., Ed.; Wiley-VCH: Weinheim, Germany, 2011.

(4) Noguchi, H.; Hojo, K.; Suginome, M. Boron-Masking Strategy for the Selective Synthesis of Oligoarenes via Iterative Suzuki−Miyaura Coupling. *J. Am. Chem. Soc.* **2007**, *129* (4), 758–759. https://doi.org/10.1021/ja067975p.

(5) Weber, L. Recent Developments in the Chemistry of 1,3,2-Diazaborolines-(2,3-Dihydro-1H-1,3,2-Diazaboroles). *Coord. Chem. Rev.* **2008**, *252* (1), 1–31. https://doi.org/10.1016/j.ccr.2007.02.014.

(6) Weber, L.; Böhling, L. The Role of 2,3-Dihydro-1-H-1,3,2-Diazaboroles in Luminescent Molecules. *Coord. Chem. Rev.* **2015**, *284*, 236–275. https://doi.org/10.1016/j.ccr.2014.09.022.

(7) Wan, W.-M.; Tian, D.; Jing, Y.-N.; Zhang, X.-Y.; Wu, W.; Ren, H.; Bao, H.-L. NBN-Doped Conjugated Polycyclic Aromatic Hydrocarbons as an AIEgen Class for Extremely Sensitive Detection of Explosives. *Angew. Chem.* **2018**, *130* (47), 15736–15742. https://doi.org/10.1002/ange.201809844.

(8) Sugasawa, T.; Toyoda, T.; Adachi, M.; Sasakura, K. Aminohaloborane in Organic Synthesis. 1. Specific Ortho Substitution Reaction of Anilines. *J. Am. Chem. Soc.* **1978**, *100* (15), 4842–4852. https://doi.org/10.1021/ja00483a034.

(9) Prakash, G. K. S.; Paknia, F.; Narayan, A.; Mathew, T.; Olah, G. A. Synthesis of Perimidine and 1,5-Benzodiazepine Derivatives Using Tamed Brønsted Acid, BF3–H2O. *J. Fluor. Chem.* **2013**, *152*, 99–105. https://doi.org/10.1016/j.jfluchem.2013.03.023.
(10) Cox, P. J.; Kechagias, D.; Kelly, O. Conformations of Substituted Benzophenones. *Acta Crystallogr. B* **2008**, *64* (2), 206–216. https://doi.org/10.1107/S0108768108000232.
(11) Strongin, R. M.; Sibrian-Vazquez, M.; Wang, L.; Escobedo, C. J. O.; Lowry, M. A. Molecular Probes for Detection and Imaging of Pancreatic Cancer. WO2017205350 (A1), November 30, 2017.
(12) Slabber, C. A.; Grimmer, C.; Akerman, M. P.; Robinson, R. S. 2-Phenyl-naphtho-[1,8-de][1,3,2]Diaza-borinane. *Acta Crystallogr. Sect. E Struct. Rep. Online* **2011**, *67* (8), o1995–o1995. https://doi.org/10.1107/S1600536811026985.
(13) Valeur, B. *Molecular Fluorescence: Principles and Applications*; Wiley-VCH, 2001.
(14) Meng, S.; Caprasecca, S.; Guido, C. A.; Jurinovich, S.; Mennucci, B. Negative Solvatochromism of Push–Pull Biphenyl Compounds: A Theoretical Study. *Theor. Chem. Acc.* **2015**, *134* (12), 150. https://doi.org/10.1007/s00214-015-1754-z.
(15) Chen, Y.; Lam, J. W. Y.; Kwok, R. T. K.; Liu, B.; Tang, B. Z. Aggregation-Induced Emission: Fundamental Understanding and Future Developments. *Mater. Horiz.* **2019**, *6* (3), 428–433. https://doi.org/10.1039/C8MH01331D.
(16) Zhu, C.; Kwok, R. T. K.; Lam, J. W. Y.; Tang, B. Z. Aggregation-Induced Emission: A Trailblazing Journey to the Field of Biomedicine. *ACS Appl. Bio Mater.* **2018**, *1* (6), 1768–1786. https://doi.org/10.1021/acsabm.8b00600.
(17) Mei, J.; Hong, Y.; Lam, J. W. Y.; Qin, A.; Tang, Y.; Tang, B. Z. Aggregation-Induced Emission: The Whole Is More Brilliant than the Parts. *Adv. Mater.* **2014**, *26* (31), 5429–5479. https://doi.org/10.1002/adma.201401356.
(18) Jaeger, R.; Blalock, T. *Microelectronic Circuit Design*, 4th ed.; McGraw-Hill: New York, 2011.
(19) de Silva, P. A.; Gunaratne, N. H. Q.; McCoy, C. P. A Molecular Photoionic AND Gate Based on Fluorescent Signalling. *Nature* **1993**, *364* (6432), 42–44. https://doi.org/10.1038/364042a0.
(20) Erbas-Cakmak, S.; Kolemen, S.; Sedgwick, A. C.; Gunnlaugsson, T.; James, T. D.; Yoon, J.; Akkaya, E. U. Molecular Logic Gates: The Past, Present and Future. *Chem. Soc. Rev.* **2018**, *47* (7), 2228–2248. https://doi.org/10.1039/C7CS00491E.
(21) Andréasson, J.; Pischel, U. Molecules for Security Measures: From Keypad Locks to Advanced Communication Protocols. *Chem. Soc. Rev.* **2018**, *47* (7), 2266–2279. https://doi.org/10.1039/C7CS00287D.
(22) Schmulbach, C. D. The Acetonitrile-Aluminium Chloride System. *J. Inorg. Nucl. Chem.* **1964**, *26* (5), 745–749. https://doi.org/10.1016/0022-1902(64)80318-3.
(23) Richardson, D.; Alger, T. D. Proton Magnetic Resonance Studies of Aluminum(III) and Gallium(III) in Methanol and Ethanol. Determination of Solvation Number and Exchange Rate. *J. Phys. Chem.* **1975**, *79* (16), 1733–1739. https://doi.org/10.1021/j100583a026.
(24) Hansen, M. M.; Jolly, R. A.; Linder, R. J. Boronic Acids and Derivatives—Probing the Structure–Activity Relationships for Mutagenicity. **2015**. https://doi.org/10.1021/acs.oprd.5b00150.
(25) O'Donovan, M. R.; Mee, C. D.; Fenner, S.; Teasdale, A.; Phillips, D. H. Boronic Acids—A Novel Class of Bacterial Mutagen. *Mutat. Res. Toxicol. Environ. Mutagen.* **2011**, *724* (1), 1–6. https://doi.org/10.1016/j.mrgentox.2011.05.006.

(26) Boström, J.; Brown, D. G.; Young, R. J.; Keserü, G. M. Expanding the Medicinal Chemistry Synthetic Toolbox. *Nat. Rev. Drug Discov.* **2018**, *17* (10), 709–727. https://doi.org/10.1038/nrd.2018.116.
(27) Brancatelli, G.; Drommi, D.; Feminò, G.; Saporita, M.; Bottari, G.; Faraone, F. Basicity and Bulkiness Effects of 1,8-Diaminonaphthalene, 8-Aminoquinoline and Their Alkylated Derivatives on the Different Efficiencies of H5-C5H5 and H5-C5Me5 Ruthenium Precatalysts in Allylic Etherification Reactions. *New J. Chem.* **2010**, *34* (12), 2853–2860. https://doi.org/10.1039/C0NJ00338G.

The formation of novel B–N polyaromatic molecules: borylated enamines

3.1 Introduction

Graphene, when first isolated and characterised in 2004, was shown to possess fascinating mechanical, magnetic, optical, and electronic properties.[1] Reflecting the significance of this work, the two researchers responsible for its isolation were awarded the Nobel Prize six years later,[2] triggering an explosion of intellectual activity across disciplines ranging from physics to medicine.[3] Of particular interest is the control of properties through structural modification. One popular method is the introduction of heteroatoms, such as boron, sulfur, nitrogen, and oxygen, into structures.[4] Additionally, when graphene is confined to the nanoscale, giving nanographenes, its properties are markedly altered, enabling application in LEDs, batteries, molecular-scale wires, biosensing, cell imaging, targeted drug delivery, and more.[5,6] This size confinement, in which graphene fragments essentially resemble polyaromatic hydrocarbons (PAHs), makes nanographenes relevant to the field of organic chemistry and its classical experimental strategies. Compared to other scientific disciplines, organic chemistry offers advantages to the production and study of nanographenes. Study of PAHs and their manipulation has a long tradition,[7] and these techniques are often transferrable. Unlike materials chemistry or engineering, which tends to produce a modal distribution of structural shapes and sizes, experimental organic chemistry offers an atomic-level precision in the control over structure,[8] which is necessary to produce materials for refined or small-scale applications.[9] As it stands, there is a strong need for novel structures and

efficient synthetic methodology to produce them, and cues can be taken from existing work in heterocyclic, heteroaromatic, and aromatic chemistry.[10]

With respect to boron in aromatics, Dewar and coworkers reported foundational studies in the 1950s and 1960s.[11] They applied the B–N bond as a replacement for C=C bonds in aromatic hydrocarbons, launching the field of azaborine chemistry that has received contributions from Liu, Ashe, Piers, Lin, Molander, and many other distinguished boron chemists.[12–14] Their work demonstrates that B–N replacement is an effective strategy for enriching the chemical space of aromatics. Though the B–N and C=C moieties are isoelectronic and isosteric, the B–N replacement can significantly alter the photophysical, aromatic and electronic properties of an aromatic molecule, diversifying its applications.[14] Azaborines have also found use in synthetic methodology as optoelectronic materials,[13] ligands,[15] or synthetic intermediates.[16] Recently, azaborines have even shown promise as drug candidates.[17]

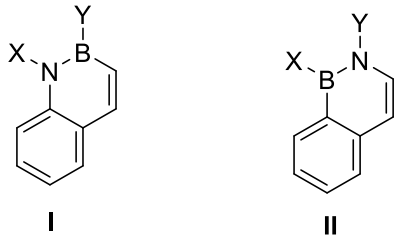

Figure 3-1. Naphthoid azaborine isomers.

Naphthalene is one of the simplest hydrocarbons on which to apply this strategy, and almost all the isomers have been discussed in the literature, computationally or experimentally.[18] By far, the most popular 1,2-azaborine analogue has been the anilino species **I** (Figure 3-1)**.**[13] Until recently, its isomer **II**, with the boron and nitrogen reversed in position, had not been synthesized. In 2015, Cui and coworkers used classic BBr_3 C-H borylation, a somewhat harsh methodology, to produce species with halide or carbon substitution on the boron (Scheme 3-1a).[19] Very recently,

in 2019, Groziak and coworkers reported the reaction of commercially available o-formylphenylboronic acid with 1,3-aminoketones to produce hemiboronates (Scheme 3-1b).[20]

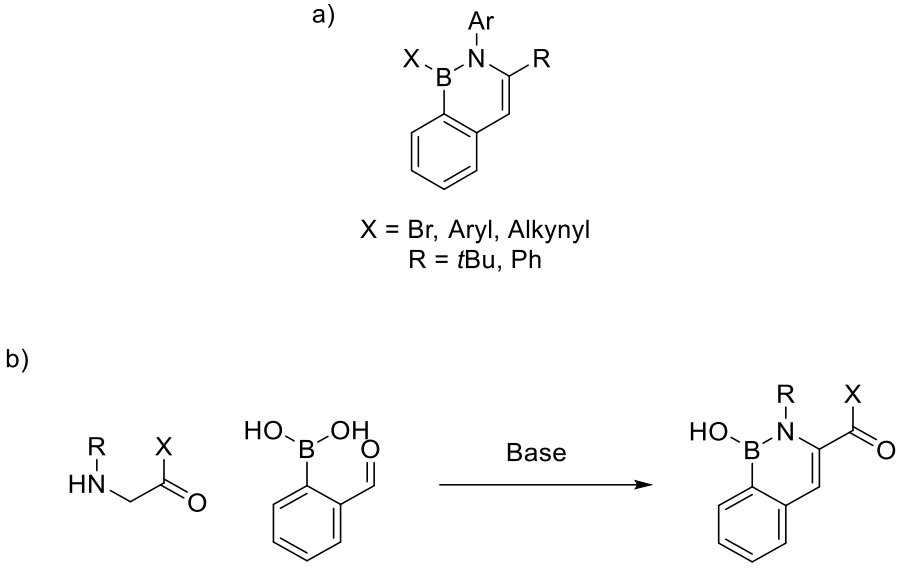

Scheme 3-1. a) The borazaronaphthalene structures produced by Cui and coworkers. b) The boronic acid and the aminocarbonyl module used by Groziak and coworkers to produce hemiboronate borazaronaphthalene.

Cui's method suffers from the use of harsh reagents like *n*-butyllithium and boron tribromide and results in borinate and boron halide species, which tend to be more unstable than boronic structures.[21] Though Groziak's work is the first to produce boronic structures, it requires strong base, heat, and specific α-amino carbonyls. An attractive contribution to this body of research could combine mild reaction conditions and a set of widely-accessible amine modules to produce a diverse library.

3.2 Objectives

In our work, the underexplored borazaronaphthyl isomer **II** was envisioned as a product of an enamine cyclisation and an esterification of a boronic acid with a benzylic ketone moiety (Figure 3-2). In this novel synthetic strategy, the boronic acid is a platform for condensation with easily-accessible and cheap amine modules, generating a diverse library of new structures with aromatic isosterism. These compounds can be screened for properties relevant to optoelectronic or medicinal applications.

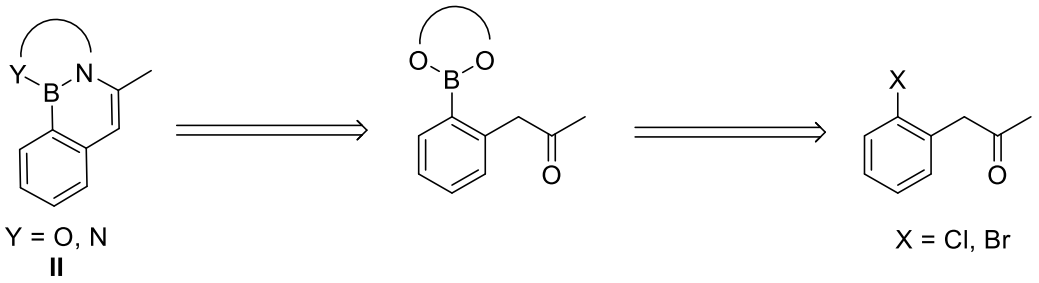

Figure 3-2. The enamine disconnection envisioned for isomer **II** and the proposed synthetic strategy.

Of particular interest is the 1,8-diaminonaphthalene (DAN) adduct as a polycycle with potential for useful properties in materials chemistry (Figure 3-3). It also represents a model compound towards the eventual synthesis of larger, nanographene-like molecules.

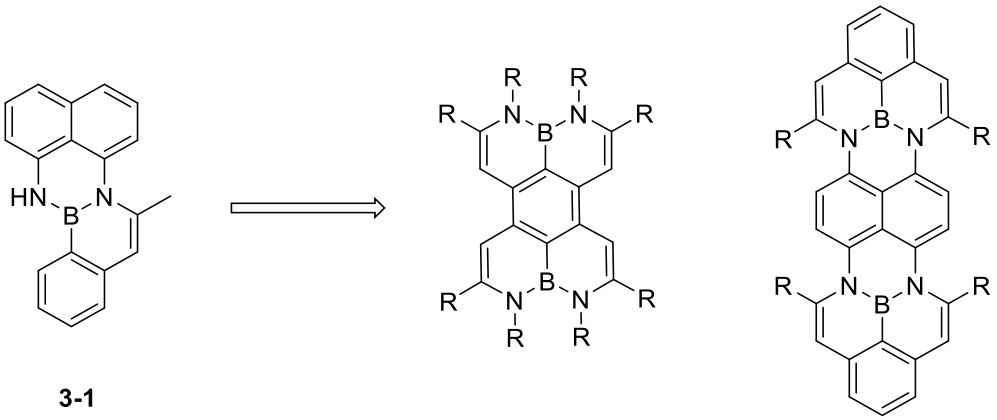

3-1

Figure 3-3. Enamine **3-1** can act as a model compound towards the design of large, symmetrical nanographene structures.

3.3 Results and discussion

3.3.1 Boronic acids: synthesis and properties

3.3.1.1 Phenylacetone-*o*-boronic acid

As the DAN adduct was of primary interest for its potential in materials chemistry, we began with a strategy that might furnish it directly. Following a report from Buchwald and coworkers[22] on the palladium-catalyzed installation of benzyl ketones onto aryl systems, we attempted this method on the aryl-Bdan species **3-2**, prepared according to Suginome's classic DAN protection protocol[23] (Scheme 3-2). While attractive for its simplicity, the volatility of the ketone source and the high reaction temperature made the odds of success more remote. Though acetone was added in excess and the vial was sealed to avoid evaporation, the reaction was unsuccessful and yielded a mixture of several unidentified products.

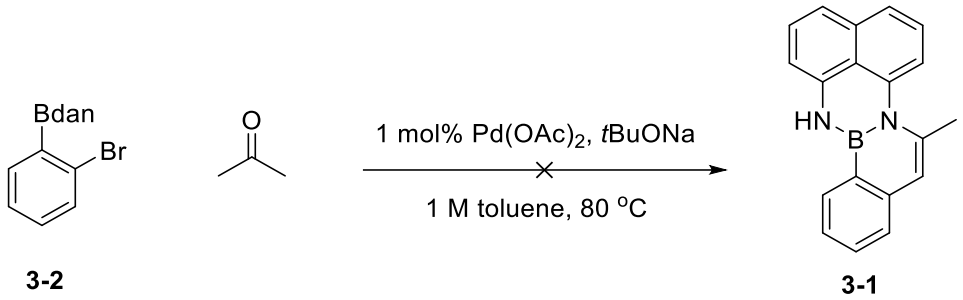

3-2 **3-1**

Scheme 3-2. Buchwald's α-ketone arylation in pursuit of **3-1.**

Concurrently, a modified Miyaura borylation (Scheme 3-3) called for an unusual, unsymmetric Bpin-Bdan reagent instead of the classical B_2pin_2.[24] The diboron reagent **3-3** was prepared, according to patent literature,[25] in the manner of a transesterification of B_2pin_2 with a stoichiometric equivalent of base. The unsymmetric borylation reaction gave several products, but characterisation revealed the desired DAN-enamine **3-1** was obtained in trace yield (<5%).

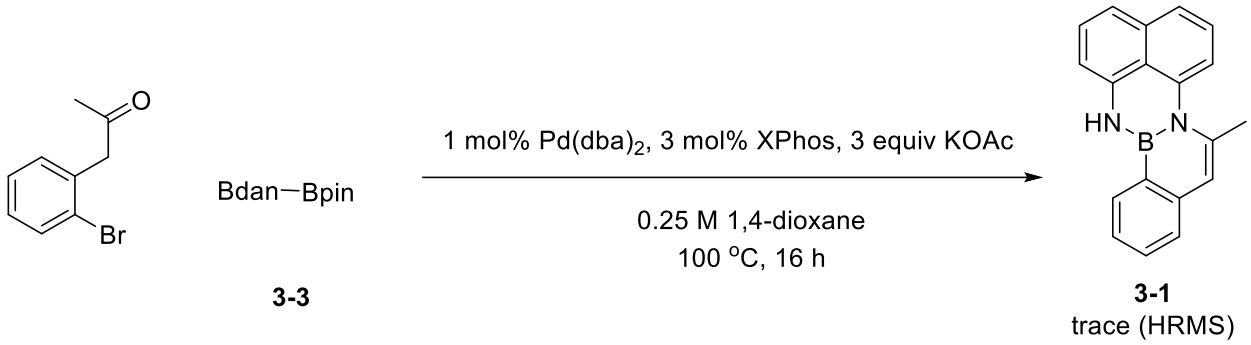

3-3

3-1
trace (HRMS)

Scheme 3-3. Modified Miyaura borylation with an unsymmetric diboron reagent.

This result suggested, encouragingly, that the desired DAN adduct could be formed and the cyclization from the ketone could occur spontaneously in heated solvent. However, it also revealed that the synthetic strategy was unworkable, perhaps in part due to the water formed as condensation proceeded. Following this result, we opted to simplify our strategy and seek to first make and isolate the boronic ketone building block (R = carbon fragment, Figure 3-4), which was

the foundation of the enamine disconnection. While the carboxylic acid, amide, and ester were known in the literature, this type of arylboronic acid derivative was not described.

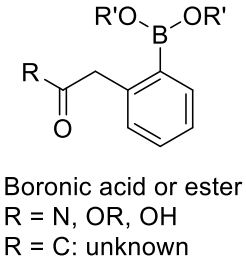

Figure 3-4. Boronic acids with a homobenzylic carbonyl. While amides and carboxylic acids are known, ketones are not.

The only comparable compound was reported by Sheppard and coworkers.[26] They isolated a similar species, a cyclic boron enolate **3-4**, but only to prove it was an intermediate in their gold-catalyzed reaction with alkyne precursors (Scheme 3-4).

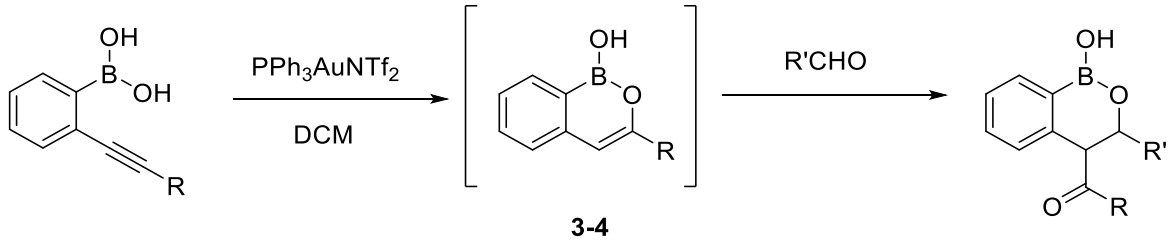

Scheme 3-4. Sheppard's gold-catalyzed alkyne cyclization of boronic acids proceeds through a cyclic enolate, which is not generally isolated. This intermediate underwent *in situ* aldol reaction to furnish synthetically relevant hemiboronate intermediates.

The most obvious approach to synthesize a simple homobenzylic ketone boronate such as **3-5**, classical Miyaura borylation (Scheme 3-5), failed to give any of the desired product. Previous work from our group has informed that the synthesis of ortho-substituted arylboronic esters is frequently not straightforward and general. Inspecting the substrate and conditions, the base was

suspected to present a problem. Though exact pKas are not available, in the presence of 3 equivalents of base, it could be that at least some of the substrate would exist in the conjugated enol form, as the benzylic proton could have reasonably high acidity. If this enolization occurred with even 5% of the substrate, that could be enough to present a significant interaction with the catalyst: the oxygen might act as a nucleophile and interact unproductively with the palladium species, such as forming a chelate.

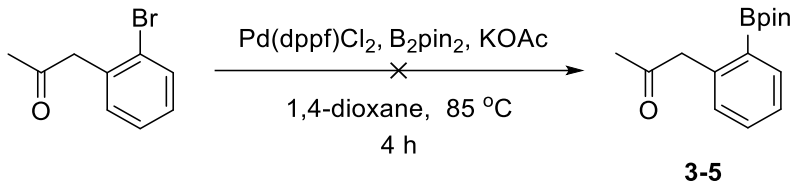

Scheme 3-5. Typical Miyaura borylation conditions, repeated several times, failed to give any of the desired product.

To test this hypothesis, base-free Miyaura borylation conditions were sought. Yamamoto and coworkers had developed a protocol,[27] and though significant alterations in the reaction setup prevented us from drawing concrete conclusions about our base hypothesis, the reaction furnished the desired product in moderate yield (Scheme 3-6).

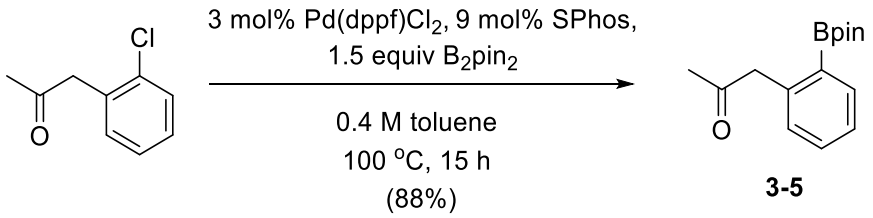

Scheme 3-6. Yamamoto's base-free Miyaura borylation conditions. Catalyst was modified from the original procedure.

Interestingly, reactions run with the catalyst described in the original work, $Pd(dba)_2$, did not yield the desired product. This could be explained in terms of the ligands on $Pd(dppf)Cl_2$. In the original paper, the authors reported that the presence of a chlorine atom on the palladium is essential because, in lieu of base, it interacts strongly with the Lewis-acidic diboron reagent to activate it.[27,28] Further, the addition of LiCl as a chloride source in sluggish reactions with aryl bromides or triflates dramatically accelerated the reaction rate. Therefore, the catalyst substitution could be thought of as an additional chloride source, or 'preactivation' for boryl transfer. A less simplistic explanation would take into consideration the equilibrium between SPhos and the other ligands, as presumably dba is more easily displaced than dppf.

The isolation of **3-5** marked the first synthesis of a new boronic ester building block. However, removing the pinacol ester motif presented difficulties. Attempts to transesterify with DAN, in neutral, basic, and acidic conditions, gave the N,N-ketal. Removing pinacol via oxidation with sodium periodate to release acetone[29] or via an intermediate potassium trifluoroborate[30,31] both gave decomposition, possibly due to the kinetic stability of the resulting boronic acid to these reagents.

Instead, Molander's modified protocol of the Miyaura borylation[32] was attempted to synthesize the boronic acid directly and avoid the problem of pinacol deprotection (Scheme 3-7). The methodology is unusual in its use of coarsely-degassed ethanol as the solvent, and as the boron source decomposes to boric acid during aqueous workup, the common problem of B_2pin_2 and pinacol contamination is avoided. Gratifyingly, the product **3-6** was furnished in apparently high yield without use of protecting groups for the ketone moiety: in fact, borylation of the acetal protected[33] chloride resulted in lower yields for this step (about 50%). The reaction could be scaled up to 4 mmol (~600 mg).

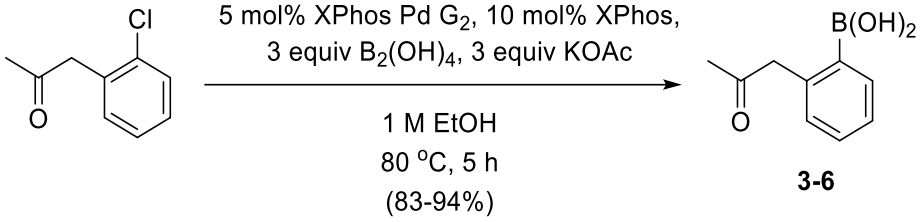

Scheme 3-7. Molander's modifications of the Miyaura borylation worked efficiently.

The product could be subjected to column chromatography. The material isolated was a tan-coloured, pungently sweet-smelling oil with a complex ^{1}H NMR spectrum, even with addition of a drop of D_2O for the purpose of hydrolyzing boronic anhydrides in equilibrium. Several observations, such as the apparent volatility and colour change over days, suggested it may have poor kinetic stability to water and ambient conditions, making characterisation of the pure material impossible: indeed, in the original work, Molander and coworkers captured the boronic acids as esters *in situ.* Recalling Sheppard's work on boron enolates, it's possible that the compound exists in an equilibrium of keto-enol forms. Unlike typical arylboronic acids, the compound showed little to no streaking along the silica in thin layer chromatography and it presented as a strongly purple-fluorescing spot, suggesting the π delocalization seen in the enol polycycle form. A sharp singlet consistent with an enol can be observed in the region of 6 ppm on its ^{1}H NMR spectrum, but the keto-enol forms could not be detected by mass spectroscopy. Moving forward, the successful synthesis of these simple homobenzylic boronic acids inspired further work towards more complex boronate species.

3.3.1.2 2,6-Diacetonephenylboronic acid

Cursory efforts were made towards an ortho diketone of type **3-7** (Figure 3-5). One proposed route applied *p*-cresol (Figure 3-6).

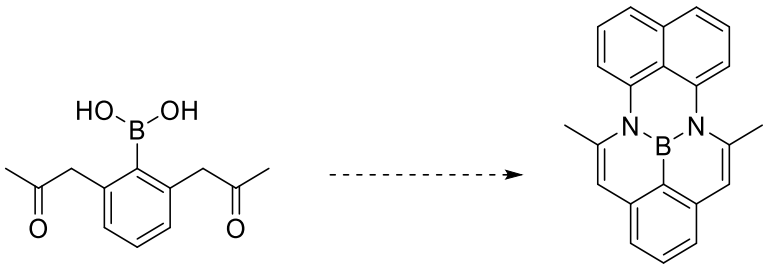

3-7

Figure 3-5. An ortho diketone **3-7** was proposed, towards a perylene-like, NBN cored structure.

By blocking the para site on the phenol ring, a Claisen rearrangement strategy could place allyl fragments on one or both ortho sites.[34] Then, the alcohol could be masked by a triflate and subjected to Miyaura borylation. Finally, the vinyl units could be transformed into the desired ketone groups. However, though the prenylation reaction was attempted several times with different bases and halides, it mostly gave starting material (Scheme 3-8).

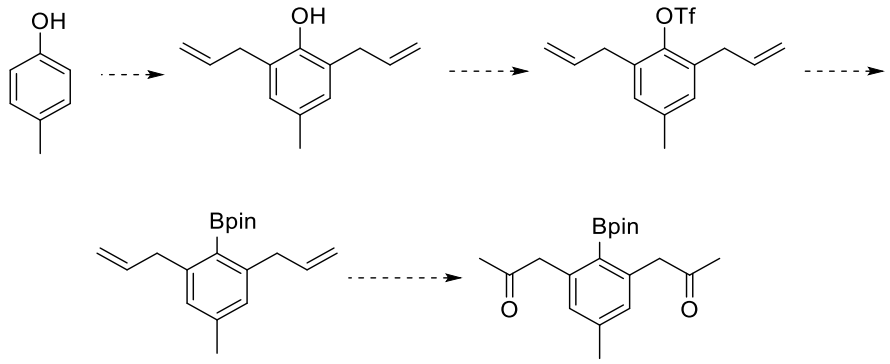

Figure 3-6. A synthetic strategy towards a compound of similar structure to **3-7.**

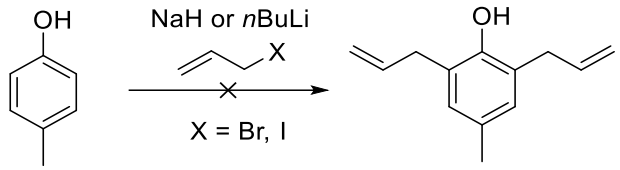

3-8

Scheme 3-8. Failed ortho prenylation of *p*-cresol.

A modified procedure from Hartwig and coworkers was also attempted.[35] In this work, chlorine was used as an ortho directing group for arylborylation reactions. Here, the electrophile was exchanged for an allylic halide to give a mono- or di-allylated arene (Scheme 3-9).

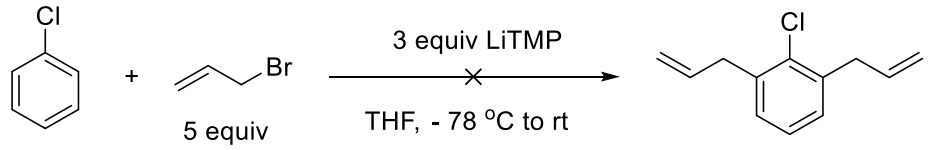

Scheme 3-9. A modification of Hartwig's electrophilic ortho-directed borylation.

The reaction was not successful and seemed to return a significant quantity of starting material. Due to other priorities, no further work was undertaken towards these targets.

3.3.1.3 Acetophenone-*o*-boronic acid

A boronic acid **3-9** with different ketone substitution was proposed, along with a potential polycyclic condensation product (Figure 3-7). Compound **3-10,** an attractive target on its own, could eventually be used as a substrate for the Scholl reaction,[36] a C-C bond forming reaction that would annulate the pendant phenyl ring to the naphthyl system and thereby expand conjugation. The requisite boronic acid **3-9** could be reached by applying a chlorinated precursor in the Molander borylation, previously demonstrated to be effective in Scheme 3-7. However, the

chlorinated precursor **3-12** was not commercially available, and reported methods to synthesize it were sparsely described or low-yielding. A few different strategies were devised and attempted.

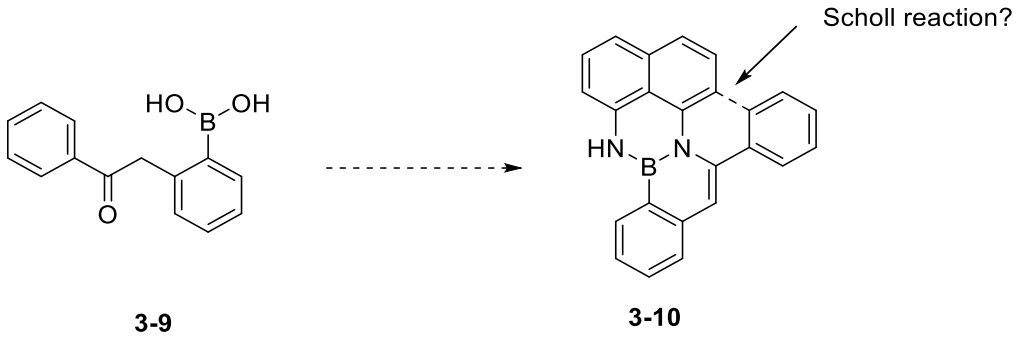

Figure 3-7. A phenyl ketone and a possible polycyclic condensation target.

First, a low yielding, but operationally simple, method using phenyllithium had been reported in conjunction with the phenylacetic acid derivative[37] (Scheme 3-10). In this approach, TMS-Cl would trap the alkoxide and transform it into an effective leaving group, yielding the desired ketone upon workup. Regrettably, this reaction yielded mostly biphenyl. Supposing metal-halogen exchange could be a competing mechanism, we substituted phenylmagnesium bromide, but this modification gave a similar outcome.

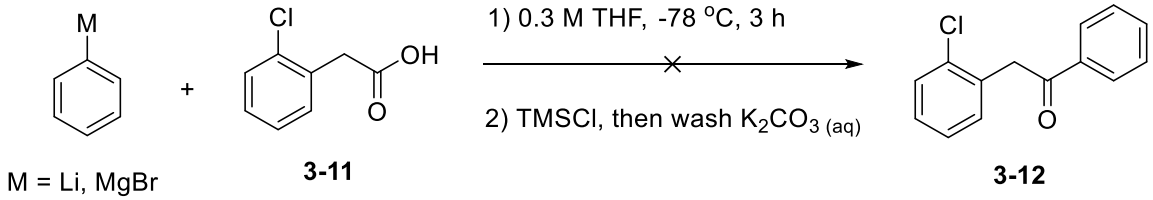

Scheme 3-10. Reaction at the carboxyl site would trap the alkoxide *in situ* with trimethylsilane, forming an effective leaving group during workup.

Taillefer and coworkers reported a transition metal free, radical mediated reaction for forming aryl ketones using potassium *tert*-butoxide[38] (Scheme 3-11). Using this method, the

product appeared to be formed, but in low quantities and mixed with considerable quantity of starting material. Seeking a more efficient method, a palladium-catalyzed method was applied, which was developed by Buchwald and coworkers and used similar starting materials (Scheme 3-12).

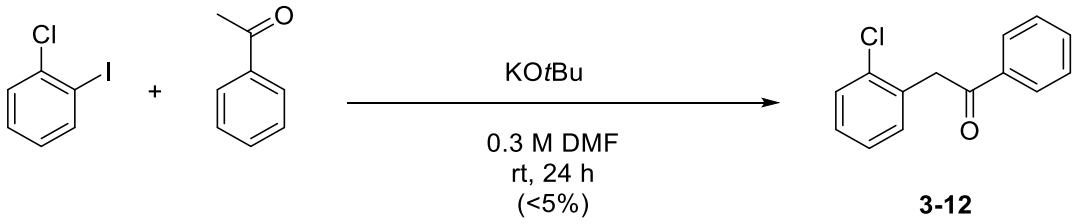

Scheme 3-11. Taillefer's radical-mediated alpha-arylation.

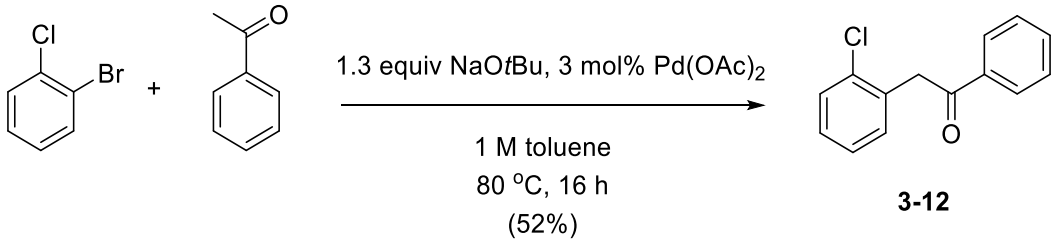

Scheme 3-12. Buchwald's palladium-catalyzed method.

Though the reaction proceeded, it presented some operational difficulties that rendered it unattractive. The desired product had a similar R_f as acetophenone, and it streaked down the silica during column chromatography, making effective separation difficult. Further, increased catalyst loading or use of excess arylbromide to consume the acetophenone was ineffectual.

Desirous of a cleaner, more effective method, efforts turned to the synthesis of the Weinreb amide. Two disconnections were simultaneously pursued, with different arenes as the Weinreb amide source.

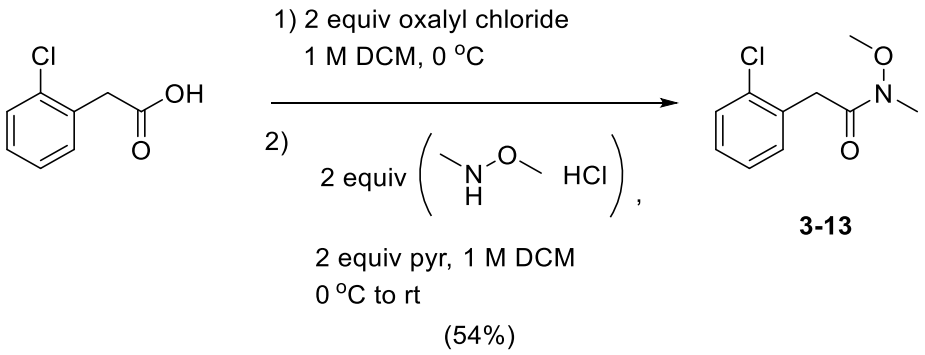

Scheme 3-13. Preparation of Weinreb amide from the carboxylic acid.

Combining two classical preparation methods, the carboxylic acid is transformed to the acyl chloride,[39] then the amide,[40] in a one-pot reaction, giving about 54% yield across both steps (Scheme 3-13). Excess oxalyl chloride could be removed using rotary evaporation cycles, adding toluene to redissolve the viscous crude and improve evaporation. The yield was also improved by leaving the hydroxylamine hydrochloride *in vacuo* for several hours, as this solid is hygroscopic and water could destroy the acyl chloride intermediate. Reaction with Grignard reagent furnished the desired product (Scheme 3-14), albeit in low yield.

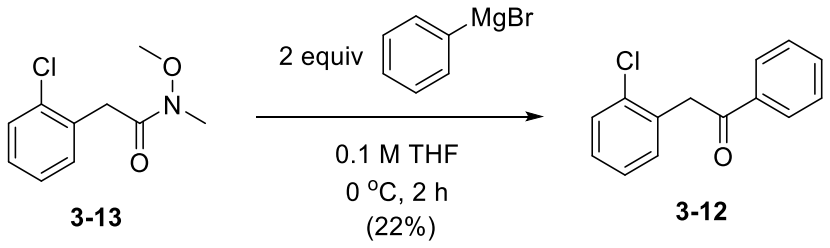

Scheme 3-14. Grignard reaction with Weinreb amide **3-13.**

The simpler Weinreb amide could also be produced according to established procedure.[41,42] Following a unique procedure developed by researchers at Merck,[43] Scheme 3-15 uses citric acid to decarboxylate the product during workup.

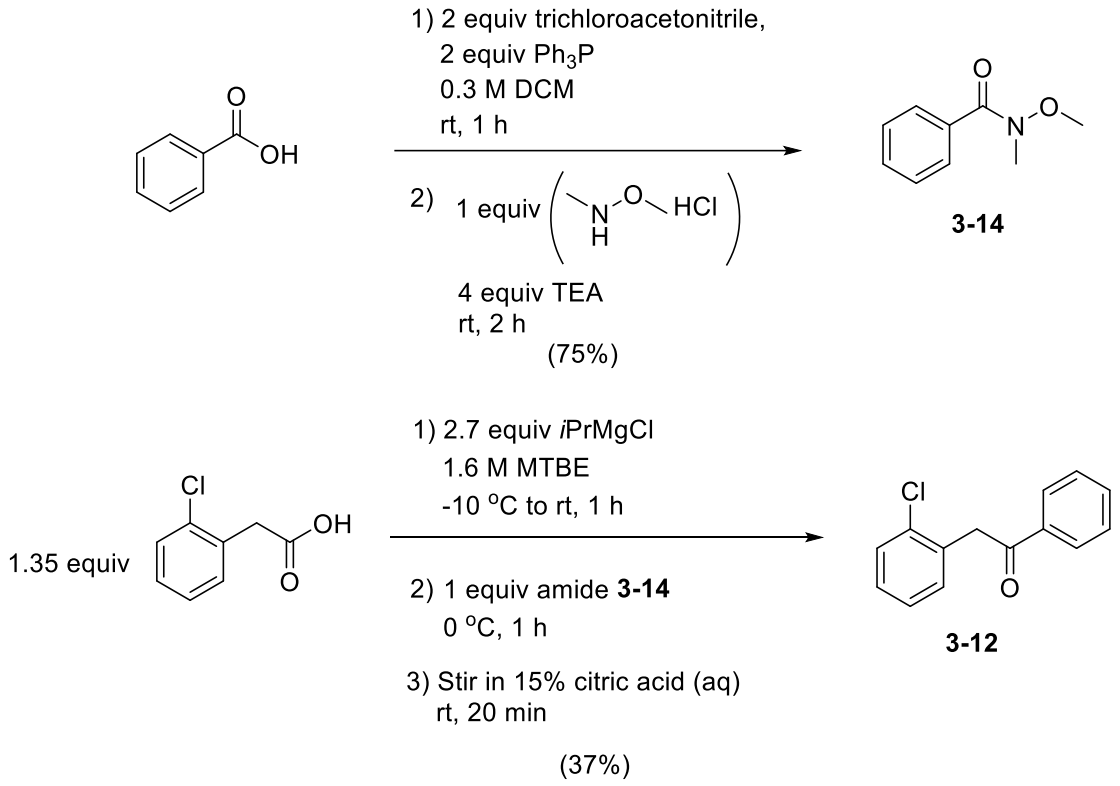

Scheme 3-15. Synthesis of the Weinreb amide for application in Merck's decarboxylative ketone synthesis.

Though optimization of these sequences was not undertaken, this work served to establish viable routes towards the synthesis of the necessary chloride precursor. Some of this material was applied in the Molander borylation (Scheme 3-16).

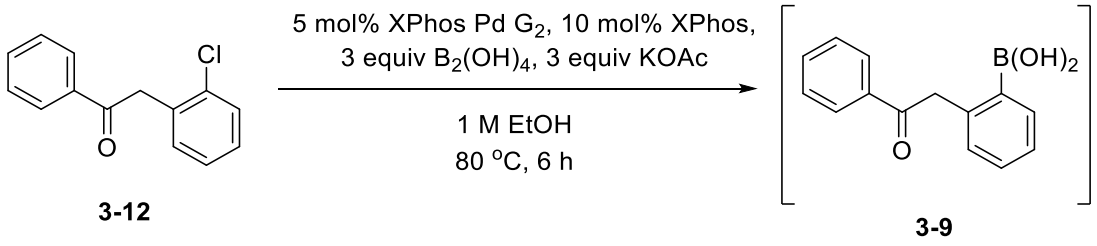

Scheme 3-16. Molander borylation to produce the phenyl ketone **3-9** (not isolated).

After workup, TLC analysis suggested that protodeboronated material was a major side product. However, consistent with the appearance of boronic acid **3-6** described earlier, a round

spot that tested positive for the curcumin stain TLC assay[44] appeared to correspond to the desired product. Given concerns about the kinetic stability of the boronic acid on silica, the crude mixture from this test reaction was taken directly to the next step, described in Section 3.3.2.7.

3.3.2 Naphthalene B–N isosteres via the condensation reaction

Having obtained the desired boronic acid **3-6**, it was subjected to condensation reaction with a variety of amines to get a sense of the generality of this building block (Figure 3-8).

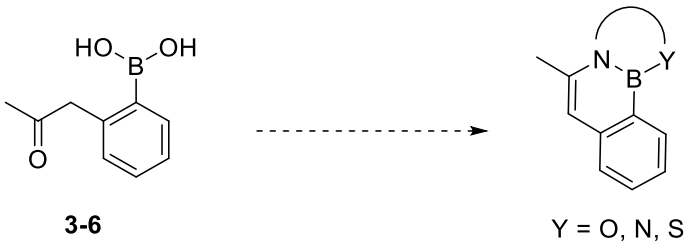

Figure 3-8. The template for formation of heteroatom adducts with boronic acid **3-6.**

The common feature of these modules is the presence of a primary amine, which would translate into a tertiary enamine after a multiple condensation reaction yielding three equivalents of water as biproduct. The nature of this amine was to be determined: alkyl and aryl mono- and di-amines; 1,2- and 1,3- substitutions of diamino or aminoalcohols; and amino acids were investigated. Various conditions could afford the desired adducts, ranging from refluxing toluene in a Dean-Stark apparatus for several hours to simple mix-and-stir conditions with no anhydrous precautions for less than an hour. However, the boronic acid was observed to be relatively unstable, which likely contributes to low yields in hot, acidic, or basic conditions. Helpful in identification of the products was the diagnostic alkene proton in ^{1}H NMR, a sharp singlet below 7 ppm,

consistent with literature values for similar structures.[19,26] The variety of structures synthesized, and their properties, where applicable, will be discussed by subsection. Furthermore, fluorometry results will be discussed together.

A note should be included regarding the kinetic stability of these compounds. When the DAN adduct was left in chloroform overnight for NMR studies, significant decomposition occurred, possibly due to moisture and acidity in the solvent. Similarly, phenyl-Bdan compounds often exhibit a gradual colour change in chlorinated solvents, including dichloromethane. As a precaution, exposure to chlorinated solvents is avoided whenever possible for all enamine adducts.

3.3.2.1 Aryl diamines and aminophenol

Conditions for adduct formation were designed in analogy to Suginome's protocol for the DAN protection of a boronic acid, with refluxing toluene in a Dean-Stark apparatus for several hours. Though recent work suggests that DAN protection may proceed even at room temperature in THF free of anhydrous precautions,[45] this unoptimized reaction afforded enough of the desired product **3-1**, a forest-green solid, for characterisation, at an 8% yield. Attempts to use 15 mol% acid or base as an additive resulted in worse yields, presumably due to instability of the boronic acid.

While the same Dean-Stark procedure was used to generate the 1,2-diaminobenzene adduct **3-15**, the yield was higher, 28%, across two steps (Figure 3-9). The favourable thermodynamic formation of these adducts with boronic acid is well known and generally attributed to the geometry of the diamine and the stability of the five membered ring.[21] Further, Huckel aromaticity

could be invoked for these systems, as the seven-electron count of Bdan makes this ring system antiaromatic, a model supported by recent NICS computations.[45]

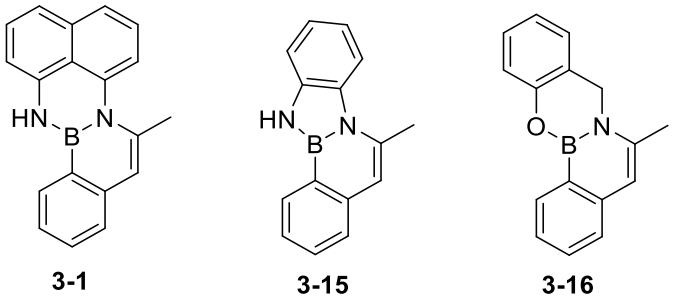

Figure 3-9. Aryl amine and aminophenol adducts of boronic acid **3-6**.

In contrast, adduct **3-16** could be produced in a yield intermediate to **3-1** and **3-15**, at about 14%. It is possible the introduction of an sp^3 centre to the ring relieves angle strain. Though adduct **3-16** was not studied in detail, its ^{11}B NMR chemical shift was a surprisingly high value of 30.4 ppm, similar to 29.4 ppm for **3-1** and in contrast to 26.8 ppm for five-membered boronate **3-15**. This result suggests that, outside of aromaticity arguments, ring geometry could affect the electronic localization around the boron atom.

3.3.2.2 Monoamines

Generally, reactions using a Dean-Stark apparatus and involving aryl or alkylamines gave mixtures of hemiboronates and the anhydrides (Scheme 3-17). Mix-and-stir reaction conditions were also attempted with alkylamines, and these experiments demonstrated that hemiboronates form in a matter of minutes. If these mixtures were heated gently (<50 °C), significant conversion to the boronic anhydrides was observed.

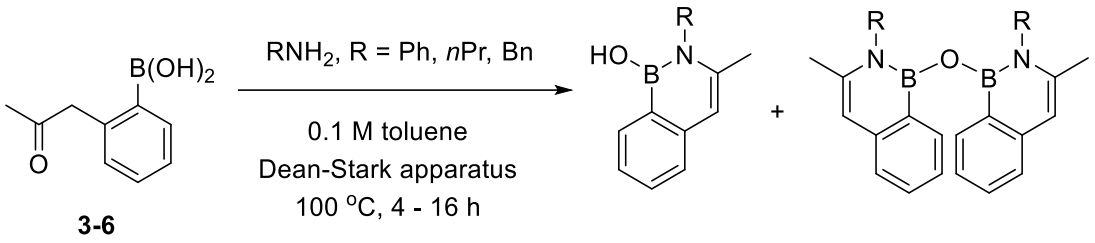

Scheme 3-17. Condensation of monoamines gives a mixture of hemiboronic acids and anhydrides.

The anhydrides (Figure 3-10) were kinetically stable enough to detect via NMR and HRMS spectroscopies, though they appeared to be moisture sensitive. The hemiboronates could be subjected to column chromatography and observed via NMR, but particularly in the case of the n-propylamine adduct, the products appeared unstable, making the characterisation of the pure material difficult.

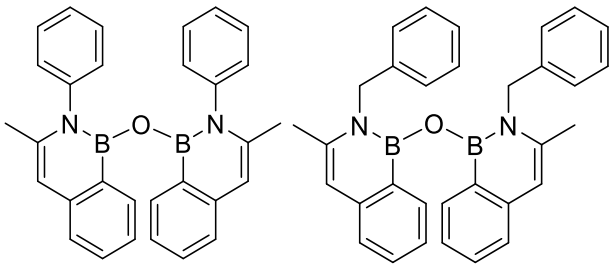

Figure 3-10. The anhydrides isolated and fully characterised.

3.3.2.3 1,3-Aminopropanol

Though not as pharmaceutically important as 1,2-aminoalcohols, the 1,3-aminoalcohol motif is found in some biologically relevant compounds, such as the sialic acid family. 1,3-aminoalcohols are also important as ligands and reagents in asymmetric synthesis.[46] Therefore,

condensation with the simplest 1,3-aminoalcohol, 1,3-aminopropanol, was attempted in Dean-Stark conditions overnight. The yield was 12%, but the product was easy to purify by column chromatography and obtain as a white, crystalline solid (Figure 3-11).

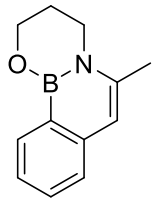

3-19

Figure 3-11. The aminopropanol adduct of boronic acid **3-6.**

Some attempts were made to improve the yield of the reaction across two steps. First, conditions were screened for the condensation reaction with the isolated boronic acid (Table 3-1). Evidently, heat and acid have a detrimental effect on the reaction, while removal of water is relatively unimportant.

Table 3-1. Screening for improved condensation reaction conditions

Entry	**0.1 M solvent**	**Temperature**	**Additive**	**Yield (2 steps, %)**
1	Toluene	110 ºC (Dean-Stark)	0.5 equiv PPTS	4
2	Toluene	rt	Molecular sieves	11
3	DCM	rt	-	10
4	Toluene	rt	-	10
5	Toluene	rt to 110 ºC	-	7

Next, it was proposed to directly 'capture' the boronic acid in adduct form following Miyaura borylation (Table 3-2). As the adduct is an easy-to-handle, stable solid, this could also become an attractive protecting group or a solution for the long term storage of the boronic acid.

Table 3-2. Modifications to Molander borylation procedure allowing in situ adduct formation

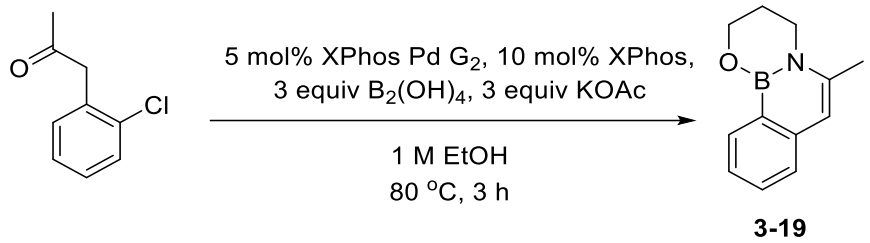

3-19

Entry	Modification	Yield (%)
1	Replace KOAc with aminopropanol, a base.	0
2	In addition to KOAc, add one equivalent of aminopropanol to trap the boronic acid as it forms.	0
3	When TLC indicates the borylation reaction is complete, add excess aminopropanol, let stir 1-3 h, then filter through Celite with no aqueous workup. Concentrate this solution and purify by column chromatography.	25

In entries 1 and 2, it appeared that aminopropanol degraded the catalyst quickly after addition. The improved yield of entry 3 compared to the results of Table 3-1 suggests decomposition of the boronic acid could be a significant factor in low yields for the condensation reactions.

Considering its attractive properties, the adduct **3-19** was selected as a representative member of this class of compounds for further characterisation. Recently, the Hall group has begun creating a standard operating procedure (SOP) delineating data to be collected for the comprehensive characterisation of any new boron heterocycle. The objective of this document is to generate a data set that will describe the physical organic chemistry of the compound and inform potential applications.

3.3.1.3.1 Basic properties and stability

The adduct **3-19** was found to be highly soluble in most common organic solvents, including DMSO, dichloromethane, ethyl acetate, acetone, chloroform, methanol, and diethyl ether; it was not water soluble. ^{1}H, ^{13}C and ^{11}B NMR spectra of adduct **3-19** were collected in both deuterated acetone and methanol. In addition, a long-term study was conducted on three samples to examine the kinetic stability of the adduct over time in storage conditions that resemble those used by pharmaceutical companies (Table 3-3).

Table 3-3. Long-term studies on kinetic stability of **3-19** to ambient conditions

Entry	Sample description	Testing	Decomposition
1	5 mg of sample dissolved in slightly moist (~1-2 drop D_2O) deuterated DMSO, stored bench top in an NMR tube and protected from light.	Tested directly via ^{1}H and ^{11}B NMR spectroscopy after 6 h, then 24 hr, then one week, then every month after.	6 months
2	5 mg of sample dissolved in slightly moist (~1-2 drop D_2O) deuterated DMSO, stored in the freezer in an NMR tube and protected from light.	Tested directly via ^{1}H and ^{11}B NMR spectroscopy after 6 h, then 24 hr, then one week, then every month after.	>8 months
3	5 mg of sample stored as a solid in a glass vial, not protected from light.	Dissolved in deuterated acetone, then tested directly via ^{1}H and ^{11}B NMR spectroscopy after 6 h, then 24 hr, then one week, then every month after. Following NMR testing the sample is dried exhaustively and returned to glass vial.	5 months
4	5 mg of sample stored as a solid in a glass vial, not protected from light.	Dissolved in deuterated acetone, then tested directly via ^{1}H and ^{11}B NMR spectroscopy at 8 months.	>8 months

Entry 1 showed decomposition after 6 months. Entry 3 showed decomposition after 5 months, but this is thought to be an artifact of the sample collection itself: an identical sample, stored for 8 months but not exposed to any solvent, was tested and showed no trace of decomposition (entry 4). At the time of writing (8 months), decomposition is not detectable for entry 2.

An experiment was also performed to assess kinetic stability to flash silica chromatography. A standardized chromatography setup is designed with a ratio of 100 mL silica to 1 g compound, and a solvent system (without special drying or purification) that gives an R_f value of 0.3. To this end, 12:1 hexanes:ethyl acetate was chosen as the solvent system and 6.68 mL silica were prepared. 60.8 mg of pure material were weighed and subjected to column chromatography. Following this procedure, 87% of the material was recovered, indicating the adduct has reasonable stability to the conditions of silica gel chromatography.

3.3.1.3.2 Crystal structure

To provide data on the electronic character and possible aromaticity of the enamine system, a single crystal of sufficient quality for X-ray crystallographic study was obtained by slow evaporation of acetone. As seen in the profile orientation in Figure 3-12, the molecule is planar excepting the methylene bridge (C4–C5–C6). The B–N bond is statistically similar (1.437 Å) to typical 1,2-azaborines (1.42 Å).[19] The C1–C12 bond length is 1.439 Å, longer than the corresponding bond in naphthalene at 1.42 Å, though the N–C2 bond is shortened, at 1.396 Å (1.42 Å in naphthalene). The B–C bond length of 1.539 Å is shorter than in phenylboronic acid (1.568 Å).[21] As the boronic acid in the latter species is slightly in π conjugation with the phenyl ring, this

data suggests that the boron atom in adduct **3-19** has greater double bond character and π delocalization.

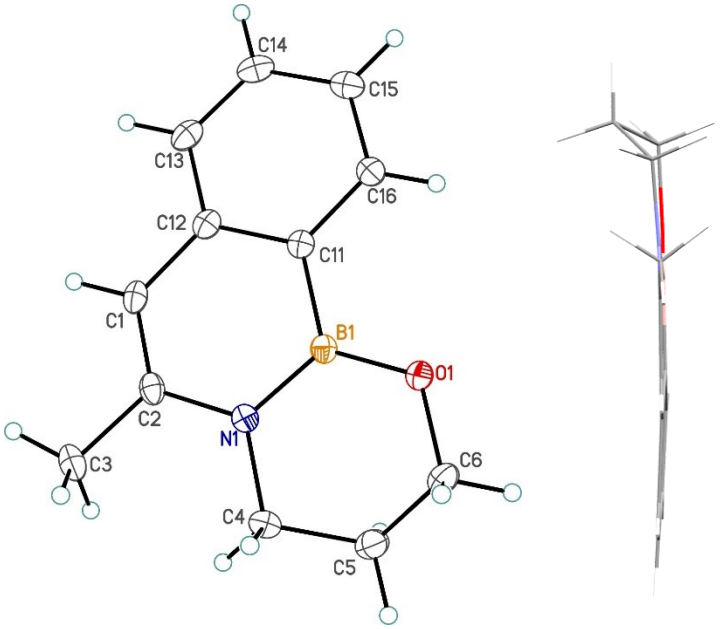

Figure 3-12. ORTEP drawing of **3-19** with a model of the molecule in profile to portray its planarity.

The bond lengths can be compared with an acyclic boron enamine[47] (Figure 3-13) described in the literature. The C–N bond is 1.417 Å, elongated compared to the C_{sp2}–N bond in the adduct **3-19** (1.396 Å), suggesting that the adduct has a measure of aromaticity in this ring system. However, the adduct's C1–C2 bond (1.356 Å) is statistically similar to the acyclic enamine C=C bond (1.347 Å). The B–N bond does not invite close comparison as it is a borinic derivative (9-BBN), but it is 1.399 Å in length, consistent with the more electron-poor boron seen in these species.

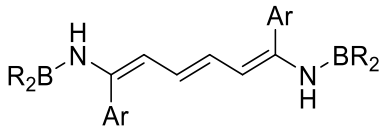

Figure 3-13. The acyclic boron enamine comparator (BR_2 = BBN).

3.3.1.3.3 pKa Titration via NMR spectroscopy

To quantify the Lewis acidity of a boronic acid or ester, pKa titration may be performed using boron NMR chemical shift to indicate the relative concentrations of the Lewis acid and its tetrahedral conjugate base[48] (Figure 3-14).

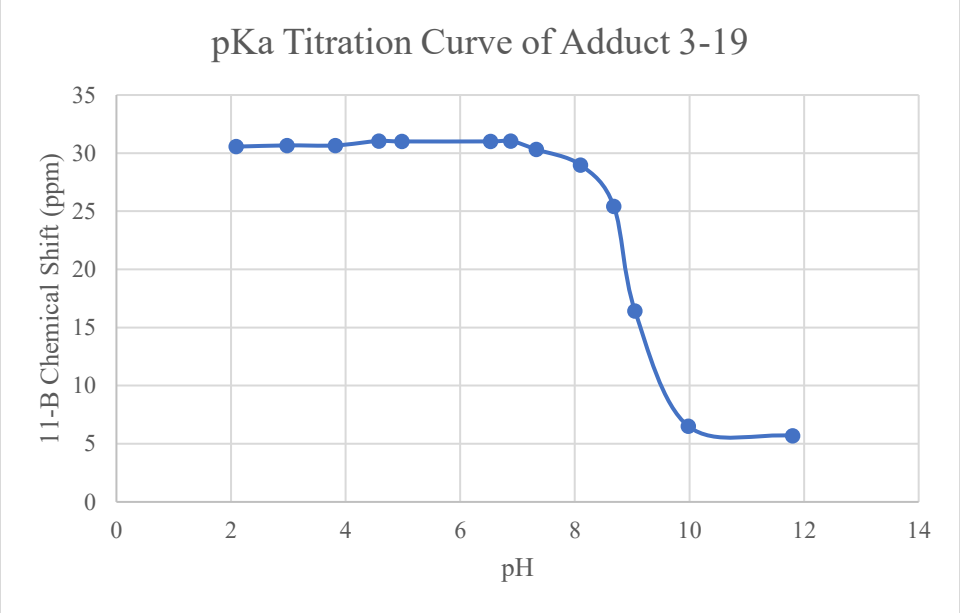

Figure 3-14. pKa titration of **3-19** was performed in aqueous solutions (with a small amount of DMSO) of varied pH.

With a value of about 9.0, the adduct has a pKa similar to boric acid and phenylboronic acid. This value is unusually high for a cyclic arylboronic ester[21] and could be attributed to the geometric stability of the adduct or possible aromatic character of the B–N ring, which would be disrupted by the coordination of a hydroxide ion at boron. Tetrahedral coordination could also create unfavourable 1,3-diaxial interactions between the hydroxide and the propanolamine ring system.

3.3.1.3.4 Biological assays

The adduct **3-19** was submitted to our collaborators at the not-for-profit initiative, Community for Open Antimicrobial Drug Discovery (CO–ADD), at the University of Queensland in Australia. The organization seeks to identify new compounds to address the growing global problem of drug-resistant infections. Preliminary screening assesses inhibition against 7 microbial strains, including methicillin-resistant *S. aureus* (MRSA), *E. coli*, *C. albicans*, and *K. pneumoniae*. Though it had weak or negligible response to most of these microbes, the assay showed that adduct **3-19** has good activity against MRSA, and at similar levels (92% growth inhibition at 32 μg/mL) compared to the commercially-available boronic heterocycle drug scaffold benzoxaborole.[49] The compound will be subjected to further dose response studies to assess its viability towards medical application.

3.3.2.4 1,2-Aminoalcohols and amino acids

The 1,2-aminoalcohol motif is present in a wide variety of biologically relevant molecules, including natural products, medicines, and nucleosides.[50] Successful formation of an adduct between the boronic acid **3-6** and these aminoalcohol motifs could make the boroenamine adducts a relevant module for biomedical applications, including bioconjugation. To use a more specific example, with amino acids, efficient condensation and enamine cyclization could allow the boronic acid to form a tight adduct with a protein or peptide fragment. Tighter, chelate-like bonding could resolve the lability that sometimes hampers the application of boronic acids as protein tags.

Several amino acids were selected for testing in a variety of conditions (Table 3-4). Simple models suggested that, in some cases such as serine and glutamic acid, the p_z orbital of boron may be accessible for interaction with the lone electron pairs of the R substituent. This could lead to a stabilizing, trichelating interaction analogous to the MIDA protecting group;[51] alternately, pyramidalization of the boron atom could modify the geometry of the boronate ring and relieve strain that might otherwise preclude adduct formation.

Table 3-4. Screening for conditions to form amino acid adducts with boronic acid **3-6**

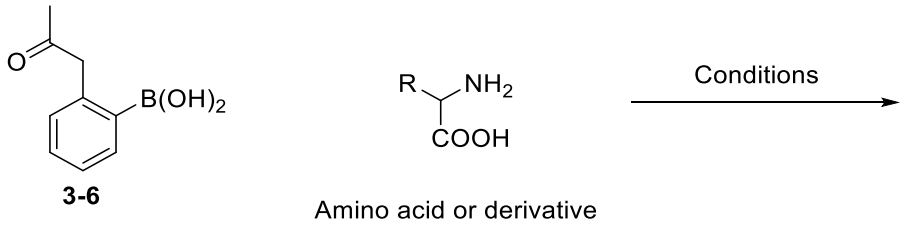

Entry	Amino Acid	Conditions	Result
1	Glycine, R = H	0.5 equiv DIPEA, 0.3 M DCM, rt	Failed
2	beta-Alanine	0.5 equiv DIPEA, 0.3 M DCM, rt	Failed
3	L-Glutamate-HCl, R = EtCOOH	1.5 equiv DIPEA, 0.3 M DCM, rt	Failed
4	Glycine, R = H	0.1 M toluene, reflux, Dean-Stark	Failed
5	beta-Alanine	0.1 M toluene, reflux, Dean-Stark	Failed
6	beta-Alanine	1 equiv DIPEA, DCM/MeOH, rt 24hr	Failed
7	Cysteine, R = CH_2SH	1 equiv DIPEA, DCM/MeOH, rt 24hr	Failed
8	Cysteine ethyl ester HCl	1 equiv DIPEA, DCM/MeOH, rt 24hr	Failed
9	Cysteine ethyl ester HCl	0.1 M toluene, reflux, Dean-Stark	Failed
10	Cysteine ethyl ester HCl	Dean Stark, 1 equiv TEA	Failed
11	beta-Alanine	Phosphate buffer/methanol cosolvent	Failed
12	Glycine, R = H	Phosphate buffer/methanol cosolvent	Failed
13	Cysteine ethyl ester HCl	Phosphate buffer/methanol cosolvent	Failed
14	L-Glutamate-HCl, R = EtCOOH	Phosphate buffer/methanol cosolvent	Failed
15	L-Serine, R = CH_2OH	0.3 M THF, 50 °C, 16 h	Failed

At moderate pH, amino acids generally exist as zwitterions, which deactivates the stronger nucleophile, the amine. The addition of a base was used to address this problem. However, entries

1-4, plus a control experiment in the absence of amino acid, suggested that base rapidly converts the boronic acid **3-6** into another, unknown form. Attempts to isolate the species caused its rapid reversion. Supposing that, in this form, the boronic acid **3-6** might be deactivated, protic solvent (entries 5-8) and buffered systems (entries 11-14) were attempted to no avail.

Generally, five-membered cyclic boronic esters are less thermodynamically stable than six-membered homologs. For these enamines, simple models suggested ring strain could be a factor in preventing product formation. The altered hybridization of the ring atoms in amino acid adducts, compared to the five-membered ring **3-15**, could justify why formation of the former was not facile.

3.3.2.5 Cysteine and sulfur adducts

Following studies on amino acids, sulfur adducts were proposed as interesting targets. While the structural similarity of these adducts to thiophenes could make them interesting for photophysical applications, the capacity of boronic acid **3-6** to condense with thiols could also be relevant for medicinal or biomedical application, such as selective tagging of amino acids or cysteine side chains.

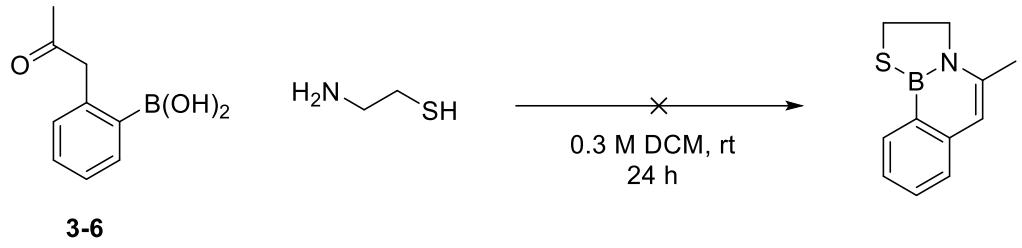

3-6

Scheme 3-18. Attempt to synthesize a boronic thioester from **3-6.**

Surprisingly few aminothiols are commercially available or easy to synthesize. Following the work with cysteine, a 1,2-thiolamine was mixed with the boronic acid and monitored over 24 hours, without formation of any adduct (Scheme 3-18).

3.3.2.6 BINAM adduct

In interest of creating a chiral compound for the library of boroenamines, a condensation reaction with BINAM racemate **3-20** was attempted in Dean-Stark condensation conditions (Scheme 3-19). The product could not be obtained. As seen in Chapter 2, the formation of a boronic acid-BINAM adduct is not facile, possibly due to geometric stability of the product.

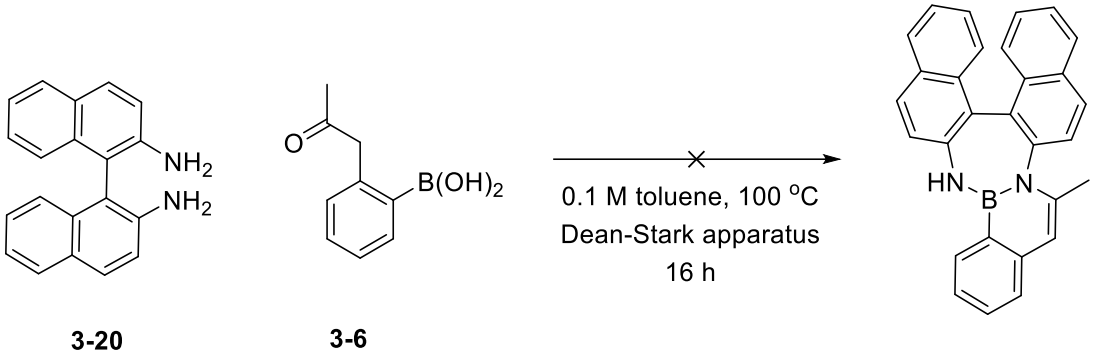

3-20 **3-6**

Scheme 3-19. Ring strain in this unusual 7-membered cyclic boronate could be why the desired condensation product was not observed.

3.3.2.7 DAN and boronic acid **3-9**

The crude boronic acid **3-9** was subjected to a condensation reaction under Dean-Stark condensation conditions (Scheme 3-20). Flash chromatography afforded ~5 mg of material that

was difficult to separate from the chloride precursor to the boronic acid, **3-12** (Scheme 3-16). Though the material was too impure and in small quantity to get clear ^{13}C and ^{1}H NMR spectra, ^{1}B NMR and HRMS data were consistent with the desired product. Similar to enamine **3-1**, the boron NMR peak appears at 34.7 ppm in $CDCl_3$, while the base peak in HRMS (EI) is 344.1483 (calculated for $C_{24}H_{17}{}^{11}BN_2$: 344.1485).

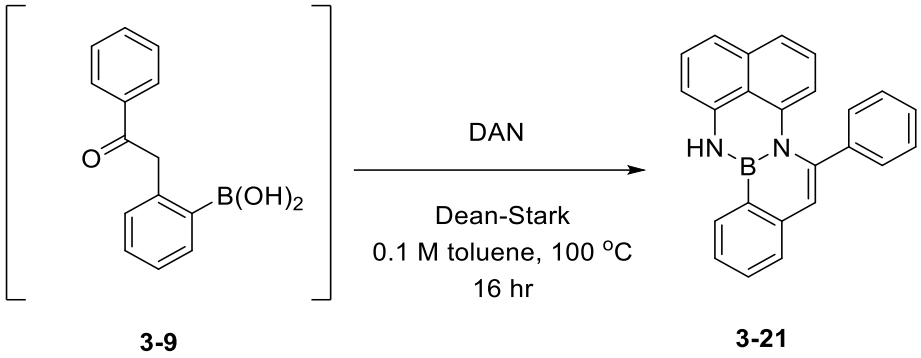

3-9 **3-21**

Scheme 3-20. The attempted condensation reaction of **3-9**.

3.3.2.8 Fluorometry of the adducts

Given their polyaromatic structures and the potential for B-N arenes in materials chemistry, preliminary UV-vis spectroscopy and fluorometry data were collected in acetonitrile for four of these class members at 15 μM concentration (Table 3-5). Phenyl-Bdan data is included for comparison.

Table 3-5. Qualitative absorption and fluorescence emission data for four boroenamines in acetonitrile

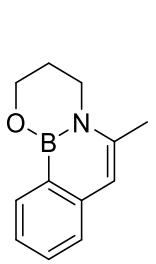

3-19

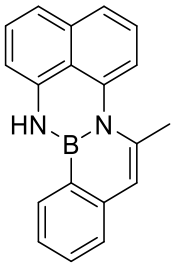

3-1

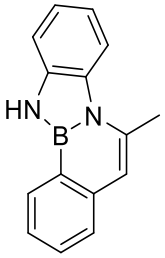

3-15

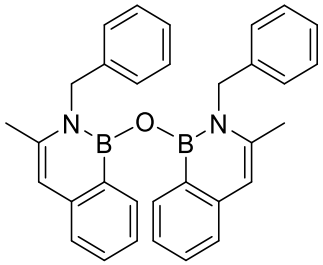

3-18

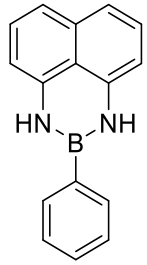

Phenyl Bdan

Compound	**λ_{abs} (nm)**	**λ_{em} (nm)**	**Stokes Shift (cm^{-1})**
3-19	287	378	8390
3-1	352	465	6900
3-15	325	366	3450
3-18	322	370	4030
Phenyl-Bdan	328	510	10900

Evidently, the nature of the XBN ring has a significant effect on the fluorescence properties of the boroenamines, with the most extensive conjugation in **3-1** giving the most red-shifted emission. Adduct **3-1**, which differs from phenyl-Bdan in its greater ring annulation and lowered flexibility, has blue-shifted emission and a smaller Stokes shift, possibly relating to a change in dipole moment or decreased capacity for conformational relaxation. Interestingly, the boroenamine with the smallest structure and least extended conjugation has the largest Stokes shift, which is often attributed to a large excited state dipole. Comparing adduct **3-19** with 1-methoxynaphthalene (Figure 3-15), the UV-visible absorption spectrum of the carbon analogue has a marked red shift in the lowest energy absorption band (375 nm[52] versus 287 nm for **3-19**). However, in this same report, excitation of 1-methoxynaphthalene at 280 nm resulted in fluorescence emission of 375 nm, which is very similar to **3-19.** The absorption and emission wavelengths of adduct **3-15** appear similar to non-annulated phenyl-1,3-2-diazaboroline[45,53,54]

compounds, but to effectively compare with literature data, quantum yields and fluorescence spectra in different solvents would need to be collected. Electronic communication, such as conjugation, through the B–O–B bond in anhydride **3-18** could be expected to significantly impact the emission wavelengths, but the single emission wavelength and its similarity to **3-19** suggests that fluorescence phenomena may be restricted within a single subunit of the dimer. The anilino-anhydride **3-17** appeared to fluoresce under UV light and likely merits investigation.

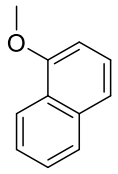

Figure 3-15. 1-methoxynaphthalene, a comparator for adduct **3-19**.

Cui and coworkers also collected fluorometry data on similar structures (Figure 3-16).[19] Close comparison is prohibited by their use of *n*-hexane as a solvent and the different substitution patterns on the borazaronaphthalene ring core, though emission wavelengths were generally above 400 nm. Compounds with an additional π substituent on boron showed a second red shifted emission peak corresponding to a conformation allowing π-π interaction. Quantum yields for the two compounds measured were low (11%).

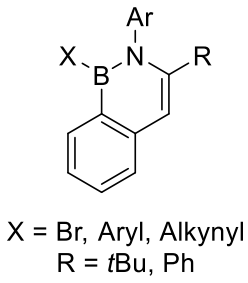

Figure 3-16. Hemiborinic structures studied fluorometrically by Cui and coworkers.

3.4 Conclusion

Chapter 3 first describes the synthesis of novel boronic acid derivatives as inherently useful synthetic building blocks, but particularly as platforms for double ester-enamine condensation reactions towards a small library of adducts with a core that is isosteric and isoelectronic to naphthalene. From a synthetic standpoint, non-classical borylation methods were necessary to produce previously unknown boronates **3-5, 3-6** and **3-9**. Enamine adducts could be formed by reaction with various alkyl or aryl amines and aminoalcohols, though notable failures include 1,2-aminoalcohols, aminosulfur compounds and amino acids. Adduct **3-19** was chosen as a representative compound for thorough characterization. Screening suggests that it is effective against methicillin-resistant *S. aureus*, inviting further biological study to assess its medicinal potential. Its pKa of 9 was similar to free arylboronic acids and higher than typical arylboronic cyclic esters, which could be due to partial aromatic character of the B–N containing ring. X-ray crystallographic studies revealed a highly planar structure with unusually short C–N and C–B bonds within the enamine ring, which supported the interpretation of increased π delocalization. A small screening array with this compound also suggested that *in situ* trapping of the unstable boronic acid **3-6** can improve yields and may be a more effective strategy for condensation with amines. Basic fluorometry data was collected for a few class members, which suggests fluorescence may be general for these species. The qualitative fluorescence is unique compared to naphthalenes and non-enamine phenyl-Bdan, which calls for further investigation and the collection of quantum yields. Looking forward, this small library of compounds based on a novel B–N scaffold can be subjected to systematic screening for biological, optoelectronic, and even methodological or catalytic applications.

3.5 Experimental

3.5.1 General information

Unless otherwise indicated, all reactions were performed under a nitrogen atmosphere using glassware that was dried for at least 24 hours in an oven (300 °C). All reagents were purchased from SigmaAldrich, Combi-Blocks or Alfa Aesar and used as received. Solvents for anhydrous reactions, such as toluene, were used directly from an MBraun Solvent Purification System, except ethanol. Ethanol was prepared for use by allowing nitrogen to bubble through it for one hour. Thin layer chromatography (TLC) was performed on Merck Silica Gel 60 F254 plates and visualized with UV light and curcumin stain. Flash chromatography was performed with ultra-pure silica gel 230-400 mesh. Nuclear magnetic resonance (NMR) spectra were recorded on Agilent/Varian INOVA-400 and INOVA700 MHz instruments. The residual solvent protons (1 H) of $CDCl_3$ (7.26 ppm), Acetone-d_6 (2.05 ppm), and D_2O (4.79 ppm) were used as internal standards, and the carbon signal (^{13}C) of $CDCl_3$ (77.06 ppm) and acetone-d6 (29.84 and 206.26 ppm) were used as internal standards in their respective spectra. VnmrJ software was used to analyze the NMR data. The following abbreviations are used in reporting NMR data: s, singlet; d, doublet; t, triplet; app t, apparent triplet; q, quartet; dd, doublet of doublets; ddd, doublet of doublet of doublets; dddd, doublet of doublet of doublet of doublets; dhept, doublet of heptlet; td, triplet of doublet; m, multiplet; comp m, complex multiplet. In ^{13}C NMR spectroscopy, the quaternary carbon bound to the boron atom is often missing due to the quadrupolar relaxation of boron. This effect was observed in each boronic acid or boronic ester compound. Infrared spectra (performed on a Nicolet Magna-IR 750 instrument equipped with a Nic-Plan microscope) were recorded by the University of Alberta Analytical and Instrumentation Laboratory. High-resolution mass spectra were recorded

by the University of Alberta Mass Spectrometry Services Laboratory using I weave - 30 electron impact (EI) techniques. UV-Visible spectroscopy was performed on an Agilent 8453 Cary 5000 instrument in a quartz cuvette with a path length of 1 cm. Fluorometry data was collected on a Horiba-PTI QM-8075-11 spectrofluorometer in a quartz cuvette with a path length of 1 cm.

3.5.2 Chemical synthesis and characterisation

Boronic acid **3-6** was prepared according to a literature procedure[32] and the crude material was purified by flash chromatography, using a hexanes:ethyl acetate gradient from 40:1 to 15:1. The resulting material was a translucent beige oil with a strong, sweet odor. The unfunctionalized boronic acid could not be characterized as a pure material, likely due to stability issues.

General Procedure A for Condensation Reaction in Dean-Stark Apparatus

A three-necked, 20 mL round bottom flask was equipped with a stir bar and a Dean-Stark apparatus, then charged with boronic acid **3-6** (1 equiv), amine (1.1 equiv), and freshly distilled toluene (0.01 M). The mixture was stirred for 16 h at 100 °C, following which it was concentrated *in vacuo.* The crude material was subjected to flash column chromatography with an eluent gradient of hexanes:ethyl acetate (40:1 to 20:1).

General Procedure B for Condensation Reaction in Mix-and-Stir Conditions

Without any anhydrous precautions, and under ambient air, a 20 mL round bottom flask equipped with a stir bar was charged with boronic acid **3-6** (1 equiv), amine, (1.1 equiv), and solvent (0.3 M). The mixture was stirred for 6 h then concentrated *in vacuo*. The crude material was purified by flash column chromatography with an eluent gradient of hexanes:ethyl acetate (40:1 to 20:1).

Synthesis and Characterisation of Adduct **3-1**

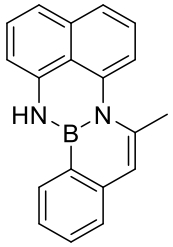

General procedure A was followed with 1,8-diaminonaphthalene as the amine to afford a dark green, tarry solid (25.7 mg, 8% yield).

^{1}H NMR (498 MHz, $CDCl_3$) δ 7.82 (d, *J* = 7.9 Hz, 1 H), 7.53 (dd, *J* = 7.9, 7.9 Hz, 1 H), 7.39 (d, *J* = 7.9 Hz, 1 H), 7.33-7.23 (m, 4 H), 7.18 (d, *J* = 7.9 Hz, 1 H), 6.91 (dd, *J* = 7.9, 2.3 Hz, 1 H), 6.60 (d, *J* = 7.9 Hz, 1 H), 6.43 (br s, 1 H), 6.31 (s, 1 H), 2.53 (s, 3 H).

^{13}C NMR (176 MHz, $CDCl_3$) δ 141.2, 139.3, 138.0, 137.3, 136.1, 131.1, 129.8, 127.1, 126.3, 125.4, 124.4, 122.0, 121,0, 117.7, 114.2, 113.7, 106.6, 22.2.

^{11}B NMR (128 MHz, $CDCl_3$) δ 29.4.

IR (cast film, cm^{-1}): 3381, 3059, 3004, 2962, 2926, 2855, 1713, 1623, 1590, 1411, 1362, 1221.

HRMS (EI) for $C_{19}H_{15}N_2{}^{11}B$: calcd.:282.1328; found: 282.1325.

Synthesis and Characterisation of Boronic Ester **3-5**

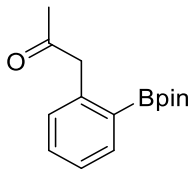

Boronic ester **3-5** was prepared by a modified version of a published procedure[27]. To an oven-dried 10 mL round bottom flask was added B_2pin_2 (370 mg, 1.5 mmol), SPhos (33 mg, 0.09 mmol) and Pd(dppf)Cl_2•DCM (26 mg, 0.03 mmol). These solids were purged with nitrogen gas before adding toluene (3 mL) and stirring at room temperature for 10 minutes, after which 2'-chloroacetophenone (190 mg, 1.1 mmol) was added and the flask was heated to 100 °C. The solution was allowed to stir at this temperature 16 h, then brought to room temperature and filtered through Celite with ethyl acetate. The filtrate was concentrated *in vacuo* and purified by flash chromatography with hexanes:ethyl acetate (40:1 to 20:1) to afford the title compound as a colourless solid (263 mg, 88%).

^{1}H NMR (400 MHz, $CDCl_3$) δ 7.44-7.39 (m, 1 H), 7.29-7.21 (m, 3 H), 3.86 (s, 2 H), 2.23 (s, 3 H), 1.27 (s, 12 H).

^{11}B NMR (128 MHz, $CDCl_3$) δ 30.5.

Synthesis and Characterisation of Adduct **3-15**

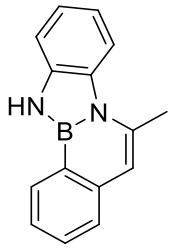

General procedure A was followed with 1,2-phenylenediamine as the amine to afford a light yellow powder (48.1 mg, 28% yield).

^{1}H NMR (400 MHz, $CDCl_3$) δ 8.06 (d, *J* = 8.1 Hz, 1 H), 7.88 (d, *J* = 8.1 Hz, 1 H), 7.65-7.58 (m, 2 H), 7.43-7.35 (m, 2 H), 7.14 (dd, *J* = 8.1, 8.1 Hz, 1 H), 7.18-7.06 (m, 2 H), 6.47 (s, 1 H), 2.97 (s, 3 H).

^{13}C NMR (176 MHz, $CDCl_3$) δ 141.2, 137.5, 137.5, 133.4, 131.1, 129.8, 126.2, 123.9, 121.6, 118.8, 114.4, 112.2, 110.1, 27.0, 22.9.

^{11}B NMR (128 MHz, $CDCl_3$) δ 26.8.

IR (cast film, cm^{-1}): 3432, 3053, 3004, 2958, 2924, 1713, 1626, 1541, 1483, 1472, 1426, 1386, 1361, 1271, 1221.

HRMS (EI) for $C_{15}H_{13}N_2{}^{11}B$: calcd.: 232.1172; found: 232.1175.

Synthesis and Characterisation of Adduct **3-16**

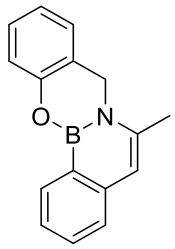

General procedure A was followed with 2-(aminomethyl)phenol as the amine to afford an orange solid (23.2 mg, 14% yield).

^{1}H NMR (498 MHz, acetone-d_6) δ 7.93 (d, *J* = 7.5 Hz, 1 H), 7.52 (dd, *J* = 7.5, 7.5 Hz, 1 H), 7.44-7.39 (m, 1 H), 7.37-7.31 (m, 2 H), 7.29-7.23 (m, 2 H), 7.13 (dd, *J* = 7.5, 7.5 Hz, 1 H), 6.40 (s, 1 H), 5.00 (s, 2 H), 2.54 (s, 3 H).

^{13}C NMR (176 MHz, acetone-d_6) δ 143.6, 138.3, 137.1, 132.2, 132.0, 129.7, 129.1, 127.0, 126.3, 125.1, 124.0, 121.4, 112.8, 65.0, 21.3.

^{11}B NMR (160 MHz, acetone-d_6) δ 30.4.

IR (cast film, cm^{-1}): 3323, 3061, 2960, 2927, 2852, 1711, 1669, 1594, 1453, 1362, 1235, 1091.

HRMS (EI) for $C_{16}H_{14}N^{11}BO$: calcd.: 247.1169; found: 247.1170.

Synthesis and Characterisation of Adduct **3-17**

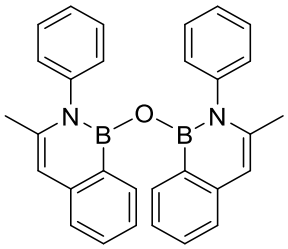

General procedure A was followed with aniline as the amine to afford a deep orange solid (27.6 mg, 11% yield).

^{1}H NMR (498 MHz, $CDCl_3$) δ 7.70 (d, *J* = 8.0 Hz, 1 H), 7.50 (dd, *J* = 8.0, 8.0 Hz, 1 H), 7.44 (d, *J* = 8.0 Hz, 1 H), 7.31-7.26 (m, 1 H), 7.25-7.19 (m, 2 H), 7.13-7.06 (m, 2 H), 6.59 (d, *J* = 8.0 Hz, 1 H), 6.256 (s, 1 H), 1.949 (s, 3 H).

^{13}C NMR (176 MHz, $CDCl_3$) δ 143.4, 142.5, 140.8, 132.6, 130.5, 128.9, 128.6, 128.4, 128.4, 126.3, 125.0, 123.4, 106.0, 21.9.

^{11}B NMR (160 MHz, $CDCl_3$) δ 28.1.

IR (cast film, cm^{-1}): 3049, 3013, 2987, 2921, 2853, 1711, 1628, 1596, 1493, 1475, 1375, 1296, 1235.

HRMS (EI) for $C_{30}H_{26}N_2{}^{11}B_2O$: calcd.: 452.2231; found: 452.2234.

Synthesis and Characterisation of Adduct **3-18**

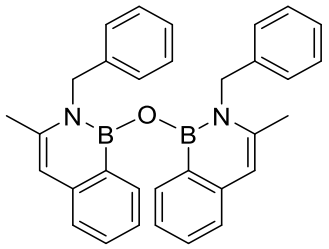

General procedure A was followed with benzylamine as the amine to afford a white powder (6.0 mg, 4% yield).

^{1}H NMR (498 MHz, $CDCl_3$) δ 7.65 (d, *J* = 7.7 Hz, 1 H), 7.49-7.43 (m, 2 H), 7.17-7.10 (m, 3 H), 7.06-7.02 (m, 1 H), 6.97 (d, *J* = 7.7 Hz, 1 H), 6.30 (s, 1 H), 5.00-4.94 (m, 1 H), 4.86-4.81 (m, 1 H), 2.25 (s, 3 H).

^{13}C NMR (176 MHz, $CDCl_3$) δ 143.5, 142.7, 141.7, 140.0, 132.6, 130.4, 128.3, 126.4, 125.8, 125.0, 123.2, 107.2, 47.6, 29.7, 20.7.

^{11}B NMR (128 MHz, $CDCl_3$) δ 28.7.

IR (cast film, cm^{-1}): 2957, 2925, 2853, 1718, 1666, 1619, 1451, 1393, 1360, 1292, 1262, 1070, 1028.

HRMS (EI) for $C_{32}H_{30}N_2{}^{11}B_2O$: calcd.: 480.2544; found: 480.2551.

Synthesis and Characterisation of Adduct **3-19**

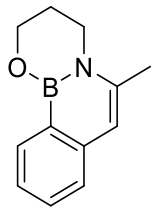

To an oven-dried 10 mL round bottom flask equipped with a stir bar were added XPhos Pd G_2 (4 mg, 5.0 μmol), $B_2(OH)_4$ (0.270 g, 3.0 mmol), KOAc (0.295 g, 3.0 mmol) and XPhos (5 mg, 10 μmol). These solids were purged with nitrogen gas before adding degassed ethanol (1 mL) and heating to 60 °C. The mixture was left to stir for 15 minutes to ensure it formed a smooth slurry before adding 2'-chloroacetophenone (0.169 g, 1.0 mmol). After 6 h, the flask was removed from heat and 1 mL of 1,3-propanolamine was added. After stirring for 3 h, the solution was diluted with ethyl acetate and filtered through Celite. This filtrate was concentrated *in vacuo* and purified by flash chromatography (30:1 hexanes:ethyl acetate) to afford the title compound as a white crystalline solid (49.8 mg, 25%).

^{1}H NMR (400 MHz, acetone-d_6) δ 7.87 (d, *J* = 7.7 Hz, 1 H), 7.40 (dd, *J* = 7.7, 7.7 Hz, 1 H), 7.29 (d, *J* = 7.7 Hz, 1 H), 7.14 (dd, *J* = 7.7, 7.7 Hz, 1 H), 6.07 (s, 1 H), 4.11 (t, *J* = 5.6, 2 H), 3.74 (t, *J* = 5.6 Hz, 2 H), 2.27 (s, 3 H), 2.14-2.07 (m, 2 H).

^{13}C NMR (177 MHz, acetone-d_6) δ 143.7, 142.0, 131.7, 130.7, 125.5, 123.6, 106.1, 62.6, 43.1, 27.4, 19.9.

^{11}B NMR (128 MHz, acetone-d_6) δ 28.3.

IR (cast film, cm^{-1}): 3042, 2961, 2933, 2882, 1620, 1547, 1483, 1436, 1424, 1411, 1299, 1286, 1293, 1168.

HRMS (EI) for $C_{12}H_{14}NO^{11}B$: calcd.: 199.1169; found: 199.1165.

3.5.3 NMR pKa titration of **3-19**

A phosphate buffer solution was prepared by dissolving 690 mg of NaH_2PO_4 in 5 mL of D_2O and diluting to 50 mL with H_2O in a volumetric flask. In a second flask, 0.25 mmol of the adduct was dissolved in the minimum quantity of deuterated DMSO. Gentle heating was required to dissolve. At room temperature, this solution was diluted to 25 mL with the buffer solution. The solution was separated into twelve vials, and using a pH probe and solutions of HCl and NaOH, these vials were adjusted to a range of pH values between 2 and 12. Using the D_2O solvent signal as the internal standard, the boron peak chemical shifts were recorded. These values were plotted against pH with the equivalence point defined as the pKa of the adduct.

3.5.4 CO–ADD Microbe screening assays

All screening was performed in two replicates, with two separate plates created and incubated at the same time.

Antibacterial Data Collection

Inhibition of bacterial growth was determined measuring absorbance at 600 nm (OD600), using a Tecan M1000 Pro monochromator plate reader. The percentage of growth inhibition was calculated for each well, using the negative control (media only) and positive control (bacteria without inhibitors) on the same plate as references.

Antifungal Data Collection

Growth inhibition of *C. albicans* was determined measuring absorbance at 530 nm (OD530), while the growth inhibition of *C. neoformans* was determined measuring the difference in absorbance between 600 and 570 nm (OD600-570), after the addition of resazurin (0.001% final concentration) and incubation at 35 °C for additional 2 h. The absorbance was measured using a Biotek Synergy HTX plate reader. The percentage of growth inhibition was calculated for each well, using the negative control (media only) and positive control (bacteria without inhibitors) on the same plate as references.

Inhibition

Percentage growth inhibition of an individual sample is calculated based on negative controls (media only) and positive controls (bacterial/fungal media without inhibitors). Please note negative inhibition values indicate that the growth rate (or OD600) is higher compared to the negative control (Bacteria/fungi only, set to 0% inhibition). The growth rates for all bacteria and fungi has a variation of -/+ 10%, which is within the reported normal distribution of bacterial/fungal growth. Any significant variation (or outliers/hits) is identified by the modified Z-Score, and actives are selected by a combination of inhibition value and Z-Score.

3.6 References

(1) Novoselov, K. S.; Geim, A. K.; Morozov, S. V.; Jiang, D.; Zhang, Y.; Dubonos, S. V.; Grigorieva, I. V.; Firsov, A. A. Electric Field Effect in Atomically Thin Carbon Films. *Science* **2004**, *306* (5696), 666–669. https://doi.org/10.1126/science.1102896.

(2) The Nobel Prize in Physics 2010 https://www.nobelprize.org/prizes/physics/2010/press-release/ (accessed Dec 9, 2019).

(3) Coroş, M.; Pogăcean, F.; Măgeruşan, L.; Socaci, C.; Pruneanu, S. A Brief Overview on Synthesis and Applications of Graphene and Graphene-Based Nanomaterials. *Front. Mater. Sci.* **2019**, *13* (1), 23–32. https://doi.org/10.1007/s11706-019-0452-5.

(4) Wang, X.-Y.; Yao, X.; Narita, A.; Müllen, K. Heteroatom-Doped Nanographenes with Structural Precision. *Acc. Chem. Res.* **2019**, *52* (9), 2491–2505. https://doi.org/10.1021/acs.accounts.9b00322.

(5) Narita, A.; Wang, X.-Y.; Feng, X.; Müllen, K. New Advances in Nanographene Chemistry. *Chem. Soc. Rev.* **2015**, *44* (18), 6616–6643. https://doi.org/10.1039/C5CS00183H.

(6) Lin, H.-A.; Sato, Y.; Segawa, Y.; Nishihara, T.; Sugimoto, N.; Scott, L. T.; Higashiyama, T.; Itami, K. A Water-Soluble Warped Nanographene: Synthesis and Applications for Photoinduced Cell Death. *Angew. Chem. Int. Ed.* **2018**, *57* (11), 2874–2878. https://doi.org/10.1002/anie.201713387.

(7) Schleyer, P. von R. Introduction: Aromaticity. *Chem. Rev.* **2001**, *101* (5), 1115–1118. https://doi.org/10.1021/cr0103221.

(8) Tour, J. M. Top-Down versus Bottom-Up Fabrication of Graphene-Based Electronics. *Chem. Mater.* **2014**, *26* (1), 163–171. https://doi.org/10.1021/cm402179h.

(9) Cortizo-Lacalle, D.; Mora-Fuentes, J. P.; Strutyński, K.; Saeki, A.; Melle-Franco, M.; Mateo-Alonso, A. Monodisperse N-Doped Graphene Nanoribbons Reaching 7.7 Nanometers in Length. *Angew. Chem. Int. Ed.* **2018**, *57* (3), 703–708. https://doi.org/10.1002/anie.201710467.

(10) Wei, H.; Liu, Y.; Gopalakrishna, T. Y.; Phan, H.; Huang, X.; Bao, L.; Guo, J.; Zhou, J.; Luo, S.; Wu, J.; et al. B–N–B Bond Embedded Phenalenyl and Its Anions. *J. Am. Chem. Soc.* **2017**, *139* (44), 15760–15767. https://doi.org/10.1021/jacs.7b07375.

(11) Dewar, M. J. S.; Kubba, V. P.; Pettit, R. 624. New Heteroaromatic Compounds. Part I. 9-Aza-10-Boraphenanthrene. *J. Chem. Soc. Resumed* **1958**, No. 0, 3073–3076. https://doi.org/10.1039/JR9580003073.

(12) Bosdet, M. J. D.; Piers, W. E. B-N as a C-C Substitute in Aromatic Systems. *Can. J. Chem.* **2009**, *87* (1), 8–29. https://doi.org/10.1139/v08-110.

(13) Campbell, P. G.; Marwitz, A. J. V.; Liu, S.-Y. Recent Advances in Azaborine Chemistry. *Angew. Chem. Int. Ed.* **2012**, *51* (25), 6074–6092. https://doi.org/10.1002/anie.201200063.

(14) Giustra, Z. X.; Liu, S.-Y. The State of the Art in Azaborine Chemistry: New Synthetic Methods and Applications. *J. Am. Chem. Soc.* **2018**, *140* (4), 1184–1194. https://doi.org/10.1021/jacs.7b09446.

(15) Pan, J.; Kampf, J. W.; Ashe, A. J. The Ligand Properties of 2-Vinyl-1,2-Azaboratabenzene. *J. Organomet. Chem.* **2009**, *694* (7), 1036–1040. https://doi.org/10.1016/j.jorganchem.2008.10.043.

(16) Giustra, Z. X.; Yang, X.; Chen, M.; Bettinger, H. F.; Liu, S.-Y. Accessing 1,2-Substituted Cyclobutanes through 1,2-Azaborine Photoisomerization. *Angew. Chem. Int. Ed. n/a* (n/a). https://doi.org/10.1002/anie.201912132.
(17) Zhao, P.; Nettleton, D. O.; Karki, R. G.; Zécri, F. J.; Liu, S.-Y. Medicinal Chemistry Profiling of Monocyclic 1,2-Azaborines. *ChemMedChem* **2017**, *12* (5), 358–361. https://doi.org/10.1002/cmdc.201700047.
(18) Stojanović, M.; Baranac-Stojanović, M. Mono BN-Substituted Analogues of Naphthalene: A Theoretical Analysis of the Effect of BN Position on Stability, Aromaticity and Frontier Orbital Energies. *New J. Chem.* **2018**, *42* (15), 12968–12976. https://doi.org/10.1039/C8NJ01529E.
(19) Liu, X.; Wu, P.; Li, J.; Cui, C. Synthesis of 1,2-Borazaronaphthalenes from Imines by Base-Promoted Borylation of C–H Bond. *J. Org. Chem.* **2015**, *80* (8), 3737–3744. https://doi.org/10.1021/jo5029437.
(20) de Lescure, L. R.; Jesse, T.; Groziak, M. P.; Powers, X. B.; Olmstead, M. M. Polycyclic Aromatic Heterocycles with a Benzo[c][1,2]Azaborinine Core. *J. Heterocycl. Chem.* **2019**, *56* (10), 2960–2965. https://doi.org/10.1002/jhet.3651.
(21) Hall, D. G. *Boronic Acids. Preparation and Applications in Organic Synthesis, Medicine and Materials*, 2nd Completely Revised ed.; Hall, D. G., Ed.; Wiley-VCH: Weinheim, Germany, 2011.
(22) Fox, J. M.; Huang, X.; Chieffi, A.; Buchwald, S. L. Highly Active and Selective Catalysts for the Formation of α-Aryl Ketones. *J. Am. Chem. Soc.* **2000**, *122* (7), 1360–1370. https://doi.org/10.1021/ja993912d.
(23) Noguchi, H.; Hojo, K.; Suginome, M. Boron-Masking Strategy for the Selective Synthesis of Oligoarenes via Iterative Suzuki−Miyaura Coupling. *J. Am. Chem. Soc.* **2007**, *129* (4), 758–759. https://doi.org/10.1021/ja067975p.
(24) Xu, L.; Li, P. Direct Introduction of a Naphthalene-1,8-Diamino Boryl [B(Dan)] Group by a Pd-Catalysed Selective Boryl Transfer Reaction. *Chem. Commun.* **2015**, *51* (26), 5656–5659. https://doi.org/10.1039/C5CC00231A.
(25) Ding, S.; Zhao, Y.; Ma, Q.; Tian, S.; Liu, J.; Yu, F. New Method for Preparing Asymmetric Boron Reagent Bpin-Bdan. CN106946916 (A), July 14, 2017.
(26) Körner, C.; Starkov, P.; Sheppard, T. D. An Alternative Approach to Aldol Reactions: Gold-Catalyzed Formation of Boron Enolates from Alkynes. *J. Am. Chem. Soc.* **2010**, *132* (17), 5968–5969. https://doi.org/10.1021/ja102129c.
(27) Yamamoto, Y.; Matsubara, H.; Yorimitsu, H.; Osuka, A. Base-Free Palladium-Catalyzed Borylation of Aryl Chlorides with Diborons. *ChemCatChem* **2016**, *8* (14), 2317–2320. https://doi.org/10.1002/cctc.201600456.
(28) Yamamoto, Y.; Matsubara, H.; Murakami, K.; Yorimitsu, H.; Osuka, A. Activator-Free Palladium-Catalyzed Silylation of Aryl Chlorides with Silylsilatranes. *Chem. – Asian J.* **2015**, *10* (1), 219–224. https://doi.org/10.1002/asia.201402595.
(29) Coutts, S. J.; Adams, J.; Krolikowski, D.; Snow, R. J. Two Efficient Methods for the Cleavage of Pinanediol Boronate Esters Yielding the Free Boronic Acids. *Tetrahedron Lett.* **1994**, *35* (29), 5109–5112. https://doi.org/10.1016/S0040-4039(00)77040-7.
(30) Yuen, A. K. L.; Hutton, C. A. Deprotection of Pinacolyl Boronate Esters via Hydrolysis of Intermediate Potassium Trifluoroborates. *Tetrahedron Lett.* **2005**, *46* (46), 7899–7903. https://doi.org/10.1016/j.tetlet.2005.09.101.

(31) Bagutski, V.; Ros, A.; Aggarwal, V. K. Improved Method for the Conversion of Pinacolboronic Esters into Trifluoroborate Salts: Facile Synthesis of Chiral Secondary and Tertiary Trifluoroborates. *Tetrahedron* **2009**, *65* (48), 9956–9960. https://doi.org/10.1016/j.tet.2009.10.002.
(32) Molander, G. A.; Trice, S. L. J.; Kennedy, S. M.; Dreher, S. D.; Tudge, M. T. Scope of the Palladium-Catalyzed Aryl Borylation Utilizing Bis-Boronic Acid. *J. Am. Chem. Soc.* **2012**, *134* (28), 11667–11673. https://doi.org/10.1021/ja303181m.
(33) Dong, J.-L.; Yu, L.-S.-H.; Xie, J.-W. A Simple and Versatile Method for the Formation of Acetals/Ketals Using Trace Conventional Acids. *ACS Omega* **2018**, *3* (5), 4974–4985. https://doi.org/10.1021/acsomega.8b00159.
(34) Patra, T.; Bag, S.; Kancherla, R.; Mondal, A.; Dey, A.; Pimparkar, S.; Agasti, S.; Modak, A.; Maiti, D. Palladium-Catalyzed Directed Para C−H Functionalization of Phenols. *Angew. Chem. Int. Ed.* **2016**, *55* (27), 7751–7755. https://doi.org/10.1002/anie.201601999.
(35) Kristensen, J.; Lysén, M.; Vedsø, P.; Begtrup, M. Synthesis of Ortho Substituted Arylboronic Esters by in Situ Trapping of Unstable Lithio Intermediates. *Org. Lett.* **2001**, *3* (10), 1435–1437. https://doi.org/10.1021/ol015598+.
(36) King, B. T.; Kroulík, J.; Robertson, C. R.; Rempala, P.; Hilton, C. L.; Korinek, J. D.; Gortari, L. M. Controlling the Scholl Reaction. *J. Org. Chem.* **2007**, *72* (7), 2279–2288. https://doi.org/10.1021/jo061515x.
(37) J. Cooper, D.; N. Owen, L. Cytotoxic Compounds. Part VII. α-Aryl-α-Halogenoacetophenones, Their Enol Acetates, and Some Related Compounds. *J. Chem. Soc. C Org.* **1966**, *0* (0), 533–540. https://doi.org/10.1039/J39660000533.
(38) Pichette Drapeau, M.; Fabre, I.; Grimaud, L.; Ciofini, I.; Ollevier, T.; Taillefer, M. Transition-Metal-Free α-Arylation of Enolizable Aryl Ketones and Mechanistic Evidence for a Radical Process. *Angew. Chem. Int. Ed Engl.* **2015**, *54* (36), 10587–10591. https://doi.org/10.1002/anie.201502332.
(39) Srinivasan, R.; Pheng Tan, L.; Wu, H.; Yang, P.-Y.; A. Kalesh, K.; Q. Yao, S. High-Throughput Synthesis of Azide Libraries Suitable for Direct "Click" Chemistry and in Situ Screening. *Org. Biomol. Chem.* **2009**, *7* (9), 1821–1828. https://doi.org/10.1039/B902338K.
(40) Nahm, S.; Weinreb, S. M. N-Methoxy-n-Methylamides as Effective Acylating Agents. *Tetrahedron Lett.* **1981**, *22* (39), 3815–3818. https://doi.org/10.1016/S0040-4039(01)91316-4.
(41) Kim, J. G.; Jang, D. A Convenient One-Pot Method for the Synthesis of N-Methoxy-N-Methyl Amides from Carboxylic Acids. *Bull. Korean Chem. Soc.* **2010**, *31* (1), 171–173. https://doi.org/10.5012/bkcs.2010.31.01.171.
(42) Jammula, S. R.; Anna, V. R.; Tatina, S.; Krishna, T.; Sreenivas, B. Y.; Pal, M. A New Strategy for Accessing (S)-1-(Furan-2-Yl)Pent-4-En-1-Ol: A Key Precursor of Ipomoeassin Family of Compounds and C1–C15 Domain of Halichondrins. *Tetrahedron Lett.* **2016**, *57* (35), 3924–3928. https://doi.org/10.1016/j.tetlet.2016.07.059.
(43) Zacuto, M. J.; Dunn, R. F.; Figus, M. One-Step Synthesis of 1-Chloro-3-Arylacetone Derivatives from Arylacetic Acids. *J. Org. Chem.* **2014**, *79* (18), 8917–8925. https://doi.org/10.1021/jo5016486.
(44) Lawrence, K.; Flower, S. E.; Kociok-Kohn, G.; Frost, C. G.; James, T. D. A Simple and Effective Colorimetric Technique for the Detection of Boronic Acids and Their

Derivatives. *Anal. Methods* **2012**, *4* (8), 2215–2217. https://doi.org/10.1039/C2AY25346A.
(45) Wan, W.-M.; Tian, D.; Jing, Y.-N.; Zhang, X.-Y.; Wu, W.; Ren, H.; Bao, H.-L. NBN-Doped Conjugated Polycyclic Aromatic Hydrocarbons as an AIEgen Class for Extremely Sensitive Detection of Explosives. *Angew. Chem.* **2018**, *130* (47), 15736–15742. https://doi.org/10.1002/ange.201809844.
(46) Lait, S. M.; Rankic, D. A.; Keay, B. A. 1,3-Aminoalcohols and Their Derivatives in Asymmetric Organic Synthesis. *Chem. Rev.* **2007**, *107* (3), 767–796. https://doi.org/10.1021/cr050065q.
(47) Erker, G.; Wingbermühle, D.; Grehl, M.; Fröhlich, R. Borylation of a Stable Primary Enamine. *Chem. Ber.* **1994**, *127* (7), 1331–1332. https://doi.org/10.1002/cber.19941270725.
(48) Aguilera-Sáez, L. M.; Belmonte-Sánchez, J. R.; Romero-González, R.; Vidal, J. L. M.; Arrebola, F. J.; Frenich, A. G.; Fernández, I. Pushing the Frontiers: Boron-11 NMR as a Method for Quantitative Boron Analysis and Its Application to Determine Boric Acid in Commercial Biocides. *Analyst* **2018**, *143* (19), 4707–4714. https://doi.org/10.1039/C8AN00505B.
(49) Nocentini, A.; Supuran, C. T.; Winum, J.-Y. Benzoxaborole Compounds for Therapeutic Uses: A Patent Review (2010- 2018). *Expert Opin. Ther. Pat.* **2018**, *28* (6), 493–504. https://doi.org/10.1080/13543776.2018.1473379.
(50) Ager, D. J.; Prakash, I.; Schaad, D. R. 1,2-Amino Alcohols and Their Heterocyclic Derivatives as Chiral Auxiliaries in Asymmetric Synthesis. *Chem. Rev.* **1996**, *96* (2), 835–876. https://doi.org/10.1021/cr9500038.
(51) Mancilla, T.; Contreras, R.; Wrackmeyer, B. New Bicyclic Organylboronic Esters Derived from Iminodiacetic Acids. *J. Organomet. Chem.* **1986**, *307* (1), 1–6. https://doi.org/10.1016/0022-328X(86)80169-3.
(52) Bardhan, M.; Misra, T.; Chowdhury, J.; Ganguly, T. Comparative Studies by Using Spectroscopic Tools on the Charge Transfer (CT) Band of a Novel Synthesized Short-Chain Dyad in Isotropic Media and in a Gel (P123). *Chem. Phys. Lett.* **2009**, *481* (1), 142–148. https://doi.org/10.1016/j.cplett.2009.09.054.
(53) Weber, L. Recent Developments in the Chemistry of 1,3,2-Diazaborolines-(2,3-Dihydro-1H-1,3,2-Diazaboroles). *Coord. Chem. Rev.* **2008**, *252* (1), 1–31. https://doi.org/10.1016/j.ccr.2007.02.014.
(54) Weber, L.; Böhling, L. The Role of 2,3-Dihydro-1-H-1,3,2-Diazaboroles in Luminescent Molecules. *Coord. Chem. Rev.* **2015**, *284*, 236–275. https://doi.org/10.1016/j.ccr.2014.09.022.

Conclusions and future directions

4.1 Summary and research proposals

Heterocyclic research bridges between many subdisciplines of chemistry, as the fundamental properties of the compounds can be translated into diverse applications. Small boronate molecules intended for medicinal chemistry can demonstrate exciting optoelectronic properties and vice versa. In this work, the synthesis and properties of new XBN heterocyclic systems are disclosed, and whenever possible, small prototypic libraries are assessed for applications in analytical, medicinal, and optoelectronic areas.

Chapter 1 comprehensively surveys the literature of tricoordinate arylboron species exhibiting luminescence and attempts to critically assess and contextualize the role of the boron atom and XBY motif in the electronic properties of these fascinating compounds. Chapter 2 describes the synthesis, structure, properties, and applications of a new NBN fluorophore scaffold, termed diazaborolyl-naphthyl-ketones (DNKs). Two synthetic protocols are applied to produce a variety of compounds with rich luminescent properties, including AIE, solvatochromism, high quantum yields, and solid state luminescence, with a marked digression from the luminescence properties of comparator compounds. Proofs of concept are demonstrated for DNK application in molecular logic gates and the sensing of trace boronic acids (<10 ppm) in pharmaceutical samples.

Chapter 3 describes the synthesis of novel boronic acid derivatives as platforms for double ester-enamine condensation reactions towards a library of adducts with a core that is isosteric and isoelectronic to naphthalene. From a synthetic standpoint, non-classical borylation methods are

necessary to produce previously unknown aryl boronates. Boroenamine adducts could be formed by reaction with many alkyl or aryl amines and aminoalcohols, though notable failures include 1,2-aminoalcohols, aminosulfur compounds and amino acids. Class members exhibited fluorescent and antibacterial properties.

Following completion of this thesis, a few possible research directions for the projects are proposed. For the fluorescent DNKs in Chapter 2, a subsequent phase of this project would more comprehensively characterise the photophysical behaviour of various class members to study structure-property relationships (Figure 4-1). More diverse derivatives should be generated to cover greater chemical space. It is likely that substitution on the naphthyl ring or ketone group makes a more significant difference to behaviour than changing substituents on the phenyl ring, so a good starting point would be to create methodology to control naphthyl substitution. Additionally, other para-ketones could be produced by substituting different nitriles in the Sugasawa reaction.

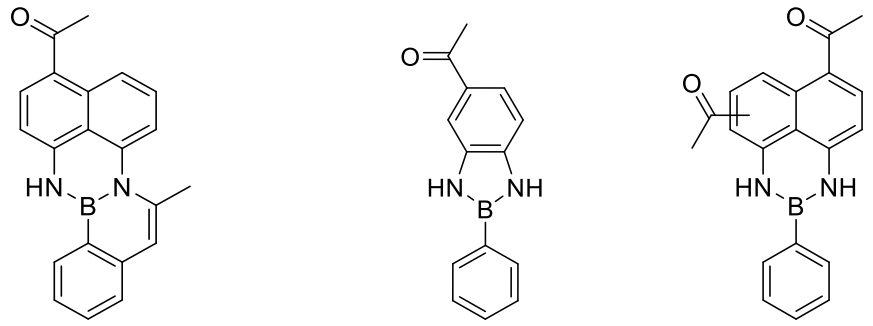

Figure 4-1. A few proposed DNK analogues.

The diamine **2-4** (Figure 4-2) may be a promising candidate for bioconjugation chemistry. There is a body of work on unnatural amino acids with boronic acid substituents and their incorporation into proteins, for therapeutic applications or fundamental research.[7–9] The mild

conditions of adduct formation may allow site-selective protein labelling via the *in situ* formation of a fluorescent DNK marker. To begin, condensation reaction rates between diamine **2-3** and arylboronic acids could be investigated in neutral buffer or mixed organic/aqueous solvent systems.

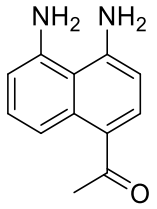

Figure 4-2. The diamine **2-4.**

A few other features of DNKs may make them attractive for biological applications. The excitation wavelengths (~400 nm) are within range of those useful for near-infrared two-photon microscopy, a technique that offers less tissue damage, superior tissue penetration, and greater spatial resolution compared to confocal microscopy.[10] Additionally, aggregation-induced emission has a special relationship to biomedical chemistry, as it has allowed new processes for the monitoring and manipulation of biochemical species at the molecular, cellular, and animal level.[11]

In Chapter 3, one boroenamine was generated with an endocyclic methylene carbon. As such, it may be an attractive substrate for cation pool electrochemistry (Figure 4-3).[1–3] The stability (and properties) of the iminium salt itself are inherently interesting, but it may be a useful intermediate to generate substitution at the benzylic position.

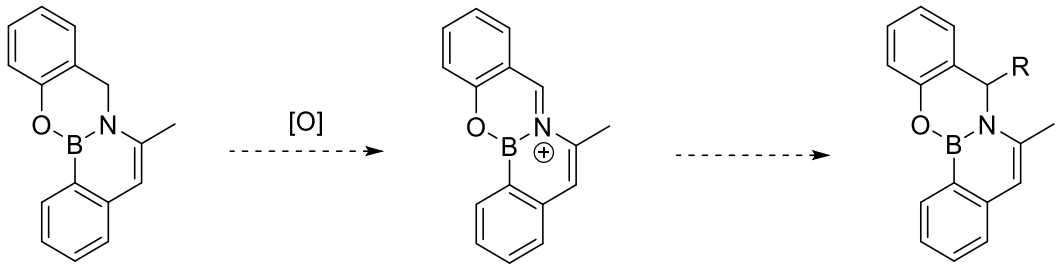

Figure 4-3. The cation resulting from anodic oxidation would be stabilized by connection to the nitrogen, an electron-rich arene, and the formation of a formally aromatic ring.

Alternately, considering that boronic acid **3-6** easily formed boronic anhydrides when treated with primary amines (Section 3.3.2.2), rigidified 'dimer' species are proposed (Figure 4-4). Steric repulsion between the B-phenyl rings will give axially chiral structures. To the author's knowledge, there are no accounts in the literature of helicenes with BNB-edged bay regions. The effect of these heteroatoms (and their edge placement) on the electronic structure, torsion angle, and enantiomerization barrier of helicenes is worthy of investigation. The distortion of the B–N unit may also affect its electronic properties.

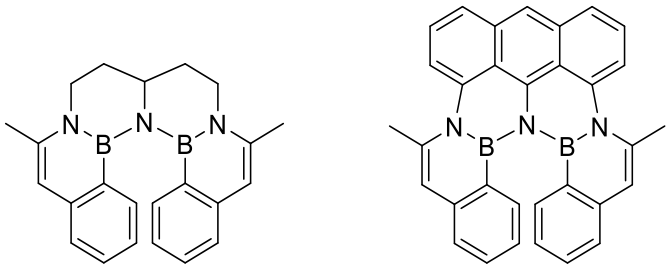

Figure 4-4. In contrast to the boronic anhydrides, these dimeric species should show improved stability to hydrolysis and decreased conformational flexibility.

Depending on the ease of adduct formation, and the optical behaviour of the adduct, this could be a model system for a biogenic polyamine sensor (assuming the adduct formed easily *in situ* and was luminescent). The aliphatic polyamine adduct may be significantly easier to form than

the aryl one, as electron-rich aliphatic amines were observed to form condensates with the boronic acid **3-6** within minutes. The corresponding trialkylamine has also been described in the literature in multi-step syntheses.[4,5] The arylated adduct has more extensive conjugation, and the application of an anthracene scaffold may confer attractive photophysical properties,[6] but the triaminated anthracene unit is not described in the literature.

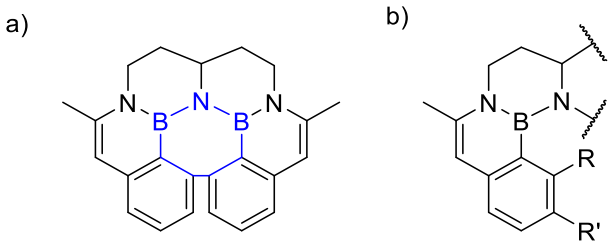

Figure 4-5. a) Scholl reaction may lead to ring annulation; the formally aromatic core ring is shown in blue. b) R or R' = Me, *t*Bu. Substitution in the R' position may make for an easier borylation (and condensation) reaction target.

A Scholl reaction could be attempted on either species to see if it is possible to form a BNB seven-membered core ring with formal Hückel aromaticity (Figure 4-5a). Alternately, substituents may be placed on the B-phenyl ring to discourage optical racemization (Figure 4-5b). The difficulty of producing the boronic acid precursor must be counterbalanced with the improvement of the enantiomerization barrier; thus, a methyl substituent in the meta position may be a good strategy to attempt first. The chlorinated synthetic precursor to borylation is commercially available (Figure 4-6).

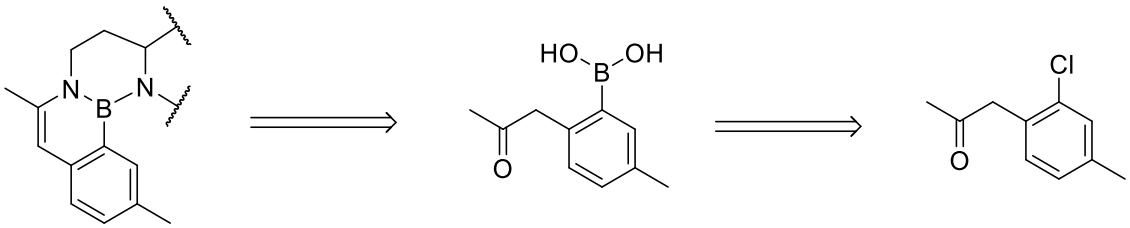

Figure 4-6. A retrosynthetic route to a dimer with a higher barrier to enantiomeric interconversion.

These rough proposals only hint at the rich, interdisciplinary potential of boronic heterocycles. Future developments of this research would be an addition to an exciting, rapidly-growing body of literature that reveals new facets in the time-honoured discipline of organoboron chemistry.

4.2 References

(1) Yoshida, J.; Suga, S.; Suzuki, S.; Kinomura, N.; Yamamoto, A.; Fujiwara, K. Direct Oxidative Carbon−Carbon Bond Formation Using the "Cation Pool" Method. 1. Generation of Iminium Cation Pools and Their Reaction with Carbon Nucleophiles. *J. Am. Chem. Soc.* **1999**, *121* (41), 9546–9549. https://doi.org/10.1021/ja9920112.

(2) Suga, S.; Suzuki, S.; Yoshida, J. Reduction of a "Cation Pool": A New Approach to Radical Mediated C−C Bond Formation. *J. Am. Chem. Soc.* **2002**, *124* (1), 30–31. https://doi.org/10.1021/ja0171759.

(3) Suga, S. Cation-Pool Method. In *Encyclopedia of Applied Electrochemistry*; Kreysa, G., Ota, K., Savinell, R. F., Eds.; Springer: New York, NY, 2014; pp 154–159. https://doi.org/10.1007/978-1-4419-6996-5_342.

(4) Weigert, F. J. Polyamines from Cyanobutadienes. *J. Org. Chem.* **1978**, *43* (4), 622–626. https://doi.org/10.1021/jo00398a021.

(5) Suissa, M. R.; Rømming, C.; Dale, J. Synthesis and Conformation Studies of a Dodecaazanonacyclotetratetracontane. *Chem. – Eur. J.* **1999**, *5* (10), 3055–3065. https://doi.org/10.1002/(SICI)1521-3765(19991001)5:10<3055::AID-CHEM3055>3.0.CO;2-N.

(6) Yang, D.-T.; Nakamura, T.; He, Z.; Wang, X.; Wakamiya, A.; Peng, T.; Wang, S. Doping Polycyclic Arenes with Nitrogen–Boron–Nitrogen (NBN) Units. *Org. Lett.* **2018**, *20* (21), 6741–6745. https://doi.org/10.1021/acs.orglett.8b02850.

(7) Brustad, E.; Bushey, M. L.; Lee, J. W.; Groff, D.; Liu, W.; Schultz, P. G. A Genetically Encoded Boronate Amino Acid. *Angew. Chem. Int. Ed Engl.* **2008**, *47* (43), 8220–8223. https://doi.org/10.1002/anie.200803240.

(8) António, J. P. M.; Russo, R.; Carvalho, C. P.; Cal, P. M. S. D.; Gois, P. M. P. Boronic Acids as Building Blocks for the Construction of Therapeutically Useful Bioconjugates. *Chem. Soc. Rev.* **2019**, *48* (13), 3513–3536. https://doi.org/10.1039/C9CS00184K.
(9) Akgun, B.; Hall, D. G. Boronic Acids as Bioorthogonal Probes for Site-Selective Labeling of Proteins. *Angew. Chem. Int. Ed.* **2018**, *57* (40), 13028–13044. https://doi.org/10.1002/anie.201712611.
(10) Svoboda, K.; Yasuda, R. Principles of Two-Photon Excitation Microscopy and Its Applications to Neuroscience. *Neuron* **2006**, *50* (6), 823–839. https://doi.org/10.1016/j.neuron.2006.05.019.
(11) Zhu, C.; Kwok, R. T. K.; Lam, J. W. Y.; Tang, B. Z. Aggregation-Induced Emission: A Trailblazing Journey to the Field of Biomedicine. *ACS Appl. Bio Mater.* **2018**, *1* (6), 1768–1786. https://doi.org/10.1021/acsabm.8b00600.

Bibliography

(1) Mellerup, S. K.; Wang, S. Boron-Doped Molecules for Optoelectronics. *Trends Chem.* **2019**, *1* (1), 77–89. https://doi.org/10.1016/j.trechm.2019.01.003.

(2) Wang, X.-Y.; Yao, X.; Narita, A.; Müllen, K. Heteroatom-Doped Nanographenes with Structural Precision. *Acc. Chem. Res.* **2019**, *52* (9), 2491–2505. https://doi.org/10.1021/acs.accounts.9b00322.

(3) Campbell, P. G.; Marwitz, A. J. V.; Liu, S.-Y. Recent Advances in Azaborine Chemistry. *Angew. Chem. Int. Ed.* **2012**, *51* (25), 6074–6092. https://doi.org/10.1002/anie.201200063.

(4) Bosdet, M. J. D.; Piers, W. E. B-N as a C-C Substitute in Aromatic Systems. *Can. J. Chem.* **2009**, *87* (1), 8–29. https://doi.org/10.1139/v08-110.

(5) Loudet, A.; Burgess, K. BODIPY Dyes and Their Derivatives: Syntheses and Spectroscopic Properties. *Chem. Rev.* **2007**, *107* (11), 4891–4932. https://doi.org/10.1021/cr078381n.

(6) Hall, D. G. *Boronic Acids. Preparation and Applications in Organic Synthesis, Medicine and Materials*, 2nd Completely Revised ed.; Hall, D. G., Ed.; Wiley-VCH: Weinheim, Germany, 2011.

(7) Weber, L.; Böhling, L. The Role of 2,3-Dihydro-1-H-1,3,2-Diazaboroles in Luminescent Molecules. *Coord. Chem. Rev.* **2015**, *284*, 236–275. https://doi.org/10.1016/j.ccr.2014.09.022.

(8) Barbon, S. M.; Reinkeluers, P. A.; Price, J. T.; Staroverov, V. N.; Gilroy, J. B. Structurally Tunable 3-Cyanoformazanate Boron Difluoride Dyes. *Chem. – Eur. J.* **2014**, *20* (36), 11340–11344. https://doi.org/10.1002/chem.201404297.

(9) Luo, H.-X.; Niu, Y.; Jin, X.; Cao, X.-P.; Yao, X.; Ye, X.-S. Indolo-Quinoline Boron Difluoride Dyes: Synthesis and Spectroscopic Properties. *Org. Biomol. Chem.* **2016**, *14* (18), 4185–4188. https://doi.org/10.1039/C6OB00623J.

(10) Kuno, S.; Kanamori, T.; Yijing, Z.; Ohtani, H.; Yuasa, H. Long Persistent Phosphorescence of Crystalline Phenylboronic Acid Derivatives: Photophysics and a Mechanistic Study. *ChemPhotoChem* **2017**, *1* (3), 102–106. https://doi.org/10.1002/cptc.201600031.

(11) Fang, G.; Wang, H.; Bian, Z.; Sun, J.; Liu, A.; Fang, H.; Liu, B.; Yao, Q.; Wu, Z. Recent Development of Boronic Acid-Based Fluorescent Sensors. *RSC Adv.* **2018**, *8* (51), 29400–29427. https://doi.org/10.1039/C8RA04503H.

(12) Weber, L. Recent Developments in the Chemistry of 1,3,2-Diazaborolines-(2,3-Dihydro-1H-1,3,2-Diazaboroles). *Coord. Chem. Rev.* **2008**, *252* (1), 1–31. https://doi.org/10.1016/j.ccr.2007.02.014.

(13) Weber, L.; Eickhoff, D.; Chrostowska, A.; Darrigan, C.; Stammler, H.-G.; Neumann, B. Synthesis, Structure, and Properties of Luminescent Diazaborole and Indole Systems. *Chem. Heterocycl. Compd.* **2017**, *53* (1), 54–65. https://doi.org/10.1007/s10593-017-2021-0.

(14) Stock, A.; Pohland, E. Borwasserstoffe, VIII. Zur Kenntnis Des B2H6 Und Des B5H11. *Berichte Dtsch. Chem. Ges. B Ser.* **1926**, *59* (9), 2210–2215. https://doi.org/10.1002/cber.19260590906.

(15) Dewar, M. J. S.; Kubba, V. P.; Pettit, R. 624. New Heteroaromatic Compounds. Part I. 9-Aza-10-Boraphenanthrene. *J. Chem. Soc. Resumed* **1958**, No. 0, 3073–3076. https://doi.org/10.1039/JR9580003073.

(16) Davies, K. M.; Dewar, M. J. S.; Rona, Peter. New Heteroaromatic Compounds. XXVI. Synthesis of Borazarenes. *J. Am. Chem. Soc.* **1967**, *89* (24), 6294–6297. https://doi.org/10.1021/ja01000a054.
(17) Islas, R.; Chamorro, E.; Robles, J.; Heine, T.; Santos, J. C.; Merino, G. Borazine: To Be or Not to Be Aromatic. *Struct. Chem.* **2007**, *18* (6), 833–839. https://doi.org/10.1007/s11224-007-9229-z.
(18) Narita, A.; Wang, X.-Y.; Feng, X.; Müllen, K. New Advances in Nanographene Chemistry. *Chem. Soc. Rev.* **2015**, *44* (18), 6616–6643. https://doi.org/10.1039/C5CS00183H.
(19) Wakamiya, A.; Ide, T.; Yamaguchi, S. Toward π-Conjugated Molecule Bundles: Synthesis of a Series of *B,B ‘* , *B ‘ ‘* -Trianthryl- *N,N ‘* , *N ‘ ‘* -Triarylborazines and the Bundle Effects on Their Properties. *J. Am. Chem. Soc.* **2005**, *127* (42), 14859–14866. https://doi.org/10.1021/ja0537171.
(20) Hoffmann, R.; Imamura, A.; Hehre, W. J. Benzynes, Dehydroconjugated Molecules, and the Interaction of Orbitals Separated by a Number of Intervening Sigma Bonds. *J. Am. Chem. Soc.* **1968**, *90* (6), 1499–1509. https://doi.org/10.1021/ja01008a018.
(21) Majewski, M. A.; Stępień, M. Bowls, Hoops, and Saddles: Synthetic Approaches to Curved Aromatic Molecules. *Angew. Chem. Int. Ed.* **2019**, *58* (1), 86–116. https://doi.org/10.1002/anie.201807004.
(22) Krieg, M.; Reicherter, F.; Haiss, P.; Ströbele, M.; Eichele, K.; Treanor, M.-J.; Schaub, R.; Bettinger, H. F. Construction of an Internally B3N3-Doped Nanographene Molecule. *Angew. Chem. Int. Ed.* **2015**, *54* (28), 8284–8286. https://doi.org/10.1002/anie.201412165.
(23) Dosso, J.; Tasseroul, J.; Fasano, F.; Marinelli, D.; Biot, N.; Fermi, A.; Bonifazi, D. Synthesis and Optoelectronic Properties of Hexa- *Peri* -Hexabenzoborazinocoronene. *Angew. Chem. Int. Ed.* **2017**, *56* (16), 4483–4487. https://doi.org/10.1002/anie.201700907.
(24) Biswas, S.; Müller, M.; Tönshoff, C.; Eichele, K.; Maichle-Mössmer, C.; Ruff, A.; Speiser, B.; Bettinger, H. F. The Overcrowded Borazine Derivative of Hexabenzotriphenylene Obtained through Dehydrohalogenation: The Overcrowded Borazine Derivative of Hexabenzotriphenylene. *Eur. J. Org. Chem.* **2012**, *2012* (24), 4634–4639. https://doi.org/10.1002/ejoc.201200322.
(25) Köster, R.; Hattori, S.; Morita, Y. 1,2:3,4:5,6-Tris-(2,2′ -Biphenylylene) Borazole a Trimer of 9,10-Azaboraphenanthrene. *Angew. Chem. Int. Ed. Engl.* **1965**, *4* (8), 695–695. https://doi.org/10.1002/anie.196506951.
(26) Fingerle, M.; Stocker, S.; Bettinger, H. F. New Synthesis of a Dibenzoperylene Motif Featuring a Doubly Boron–Nitrogen-Doped Bay Region. *Synthesis* **2019**, *51* (22), 4147–4152. https://doi.org/10.1055/s-0039-1690687.
(27) Numano, M.; Nagami, N.; Nakatsuka, S.; Katayama, T.; Nakajima, K.; Tatsumi, S.; Yasuda, N.; Hatakeyama, T. Synthesis of Boronate-Based Benzo[Fg]Tetracene and Benzo[Hi]Hexacene via Demethylative Direct Borylation. *Chem. – Eur. J.* **2016**, *22* (33), 11574–11577. https://doi.org/10.1002/chem.201602753.
(28) de Lescure, L. R.; Jesse, T.; Groziak, M. P.; Powers, X. B.; Olmstead, M. M. Polycyclic Aromatic Heterocycles with a Benzo[c][1,2]Azaborinine Core. *J. Heterocycl. Chem.* **2019**, *56* (10), 2960–2965. https://doi.org/10.1002/jhet.3651.
(29) Seixas de Melo, J.; Moura, A. P.; Melo, M. J. Photophysical and Spectroscopic Studies of Indigo Derivatives in Their Keto and Leuco Forms. *J. Phys. Chem. A* **2004**, *108* (34), 6975–6981. https://doi.org/10.1021/jp049076y.

(30) Ma, C.; Li, H.; Yang, Y.; Li, D.; Liu, Y. TD-DFT Study on Electron Transfer Mobility and Intramolecular Hydrogen Bond of Substituted Indigo Derivatives. *Chem. Phys. Lett.* **2015**, *638*, 72–77. https://doi.org/10.1016/j.cplett.2015.08.012.
(31) Yang, D.-T.; Nakamura, T.; He, Z.; Wang, X.; Wakamiya, A.; Peng, T.; Wang, S. Doping Polycyclic Arenes with Nitrogen–Boron–Nitrogen (NBN) Units. *Org. Lett.* **2018**, *20* (21), 6741–6745. https://doi.org/10.1021/acs.orglett.8b02850.
(32) King, B. T.; Kroulík, J.; Robertson, C. R.; Rempala, P.; Hilton, C. L.; Korinek, J. D.; Gortari, L. M. Controlling the Scholl Reaction. *J. Org. Chem.* **2007**, *72* (7), 2279–2288. https://doi.org/10.1021/jo061515x.
(33) Wan, W.-M.; Tian, D.; Jing, Y.-N.; Zhang, X.-Y.; Wu, W.; Ren, H.; Bao, H.-L. NBN-Doped Conjugated Polycyclic Aromatic Hydrocarbons as an AIEgen Class for Extremely Sensitive Detection of Explosives. *Angew. Chem.* **2018**, *130* (47), 15736–15742. https://doi.org/10.1002/ange.201809844.
(34) Noguchi, H.; Hojo, K.; Suginome, M. Boron-Masking Strategy for the Selective Synthesis of Oligoarenes via Iterative Suzuki−Miyaura Coupling. *J. Am. Chem. Soc.* **2007**, *129* (4), 758–759. https://doi.org/10.1021/ja067975p.
(35) Hong, Y.; Lam, J. W. Y.; Tang, B. Z. Aggregation-Induced Emission: Phenomenon, Mechanism and Applications. *Chem. Commun.* **2009**, No. 29, 4332–4353. https://doi.org/10.1039/B904665H.
(36) Mei, J.; Hong, Y.; Lam, J. W. Y.; Qin, A.; Tang, Y.; Tang, B. Z. Aggregation-Induced Emission: The Whole Is More Brilliant than the Parts. *Adv. Mater.* **2014**, *26* (31), 5429–5479. https://doi.org/10.1002/adma.201401356.
(37) Zhu, C.; Kwok, R. T. K.; Lam, J. W. Y.; Tang, B. Z. Aggregation-Induced Emission: A Trailblazing Journey to the Field of Biomedicine. *ACS Appl. Bio Mater.* **2018**, *1* (6), 1768–1786. https://doi.org/10.1021/acsabm.8b00600.
(38) Patil, S. S.; Muddapur, G. V.; Patil, N. R.; Melavanki, R. M.; Kusanur, R. A. Fluorescence Characteristics of Aryl Boronic Acid Derivate (PBA). *Spectrochim. Acta. A. Mol. Biomol. Spectrosc.* **2015**, *138*, 85–91. https://doi.org/10.1016/j.saa.2014.11.028.
(39) Crawford, A. G.; Dwyer, A. D.; Liu, Z.; Steffen, A.; Beeby, A.; Pålsson, L.-O.; Tozer, D. J.; Marder, T. B. Experimental and Theoretical Studies of the Photophysical Properties of 2- and 2,7-Functionalized Pyrene Derivatives. *J. Am. Chem. Soc.* **2011**, *133* (34), 13349–13362. https://doi.org/10.1021/ja2006862.
(40) Crawford, A. G.; Liu, Z.; Mkhalid, I. A. I.; Thibault, M.-H.; Schwarz, N.; Alcaraz, G.; Steffen, A.; Collings, J. C.; Batsanov, A. S.; Howard, J. A. K.; et al. Synthesis of 2- and 2,7-Functionalized Pyrene Derivatives: An Application of Selective C□H Borylation. *Chem. – Eur. J.* **2012**, *18* (16), 5022–5035. https://doi.org/10.1002/chem.201103774.
(41) Kato, K.; Lin, H.-A.; Kuwayama, M.; Nagase, M.; Segawa, Y.; Scott, L. T.; Itami, K. Two-Step Synthesis of a Red-Emissive Warped Nanographene Derivative via a Ten-Fold C–H Borylation. *Chem. Sci.* **2019**, *10* (39), 9038–9041. https://doi.org/10.1039/C9SC03061A.
(42) Lavis, L. D.; Raines, R. T. Bright Ideas for Chemical Biology. *ACS Chem. Biol.* **2008**, *3* (3), 142–155. https://doi.org/10.1021/cb700248m.
(43) Kutniewska, S. E.; Jarzembska, K. N.; Kamiński, R.; Stasyuk, A. J.; Gryko, D. T.; Cyrański, M. K. Structural, Energetic and Spectroscopic Studies of New Luminescent Complexes Based on 2-(2′-Hy-droxy-phenyl)-imidazo[1,2-a]Pyridines and 1,2-

Phenyl-ene-diboronic Acid. *Acta Crystallogr. Sect. B Struct. Sci. Cryst. Eng. Mater.* **2018**, *74* (6), 725–737. https://doi.org/10.1107/S2052520618015469.
(44) Soroka, Krystyna.; Vithanage, R. S.; Phillips, D. A.; Walker, Brian.; Dasgupta, P. K. Fluorescence Properties of Metal Complexes of 8-Hydroxyquinoline-5-Sulfonic Acid and Chromatographic Applications. *Anal. Chem.* **1987**, *59* (4), 629–636. https://doi.org/10.1021/ac00131a019.
(45) Sadu, V. S.; Bin, H.-R.; Lee, D.-M.; Lee, K.-I. One-Pot Synthesis of Four-Coordinate Boron(III) Complexes by the Ligand-Promoted Organic Group Migration between Boronic Acids. *Sci. Rep.* **2017**, *7*. https://doi.org/10.1038/s41598-017-00236-2.
(46) Wang, X.-Y.; Narita, A.; Zhang, W.; Feng, X.; Müllen, K. Synthesis of Stable Nanographenes with OBO-Doped Zigzag Edges Based on Tandem Demethylation-Electrophilic Borylation. *J. Am. Chem. Soc.* **2016**, *138* (29), 9021–9024. https://doi.org/10.1021/jacs.6b04092.
(47) Ajayakumar, M. R.; Fu, Y.; Ma, J.; Hennersdorf, F.; Komber, H.; Weigand, J. J.; Alfonsov, A.; Popov, A. A.; Berger, R.; Liu, J.; et al. Toward Full Zigzag-Edged Nanographenes: Peri-Tetracene and Its Corresponding Circumanthracene. *J. Am. Chem. Soc.* **2018**, *140* (20), 6240–6244. https://doi.org/10.1021/jacs.8b03711.
(48) Katayama, T.; Nakatsuka, S.; Hirai, H.; Yasuda, N.; Kumar, J.; Kawai, T.; Hatakeyama, T. Two-Step Synthesis of Boron-Fused Double Helicenes. *J. Am. Chem. Soc.* **2016**, *138* (16), 5210–5213. https://doi.org/10.1021/jacs.6b01674.
(49) Shoji, Y.; Ikabata, Y.; Wang, Q.; Nemoto, D.; Sakamoto, A.; Tanaka, N.; Seino, J.; Nakai, H.; Fukushima, T. Unveiling a New Aspect of Simple Arylboronic Esters: Long-Lived Room-Temperature Phosphorescence from Heavy-Atom-Free Molecules. *J. Am. Chem. Soc.* **2017**, *139* (7), 2728–2733. https://doi.org/10.1021/jacs.6b11984.
(50) Valeur, B. *Molecular Fluorescence: Principles and Applications*; Wiley-VCH, 2001.
(51) Wang, T.; Zhang, N.; Zhang, K.; Dai, J.; Bai, W.; Bai, R. Pyrene Boronic Acid Cyclic Ester: A New Fast Self-Recovering Mechanoluminescent Material at Room Temperature. *Chem. Commun.* **2016**, *52* (62), 9679–9682. https://doi.org/10.1039/C6CC03248F.
(52) Yang, J.; Ren, Z.; Xie, Z.; Liu, Y.; Wang, C.; Xie, Y.; Peng, Q.; Xu, B.; Tian, W.; Zhang, F.; et al. AIEgen with Fluorescence–Phosphorescence Dual Mechanoluminescence at Room Temperature. *Angew. Chem. Int. Ed.* **2017**, *56* (3), 880–884. https://doi.org/10.1002/anie.201610453.
(53) Srikun, D.; Miller, E. W.; Domaille, D. W.; Chang, C. J. An ICT-Based Approach to Ratiometric Fluorescence Imaging of Hydrogen Peroxide Produced in Living Cells. *J. Am. Chem. Soc.* **2008**, *130* (14), 4596–4597. https://doi.org/10.1021/ja711480f.
(54) Li, M.; Ge, H.; Arrowsmith, R. L.; Mirabello, V.; Botchway, S. W.; Zhu, W.; Pascu, S. I.; James, T. D. Ditopic Boronic Acid and Imine-Based Naphthalimide Fluorescence Sensor for Copper(II). *Chem Commun* **2014**, *50* (80), 11806–11809. https://doi.org/10.1039/C4CC03453H.
(55) Wang, S.-T.; Sie, Y.-W.; Wan, C.-F.; Wu, A.-T. A Reaction-Based Fluorescent Sensor for Detection of Cyanide in Aqueous Media. *J. Lumin.* **2016**, *173*, 25–29. https://doi.org/10.1016/j.jlumin.2015.12.041.
(56) Lampard, E. V.; Sedgwick, A. C.; Sun, X.; Filer, K. L.; Hewins, S. C.; Kim, G.; Yoon, J.; Bull, S. D.; James, T. D. Boronate-Based Fluorescence Probes for the Detection of Hydrogen Peroxide. *ChemistryOpen* **2018**, *7* (3), 262–265. https://doi.org/10.1002/open.201700189.

(57) Sugasawa, T.; Toyoda, T.; Adachi, M.; Sasakura, K. Aminohaloborane in Organic Synthesis. 1. Specific Ortho Substitution Reaction of Anilines. *J. Am. Chem. Soc.* **1978**, *100* (15), 4842–4852. https://doi.org/10.1021/ja00483a034.
(58) Prakash, G. K. S.; Paknia, F.; Narayan, A.; Mathew, T.; Olah, G. A. Synthesis of Perimidine and 1,5-Benzodiazepine Derivatives Using Tamed Brønsted Acid, BF3–H2O. *J. Fluor. Chem.* **2013**, *152*, 99–105. https://doi.org/10.1016/j.jfluchem.2013.03.023.
(59) Cox, P. J.; Kechagias, D.; Kelly, O. Conformations of Substituted Benzophenones. *Acta Crystallogr. B* **2008**, *64* (2), 206–216. https://doi.org/10.1107/S0108768108000232.
(60) Strongin, R. M.; Sibrian-Vazquez, M.; Wang, L.; Escobedo, C. J. O.; Lowry, M. A. Molecular Probes for Detection and Imaging of Pancreatic Cancer. WO2017205350 (A1), November 30, 2017.
(61) Slabber, C. A.; Grimmer, C.; Akerman, M. P.; Robinson, R. S. 2-Phenyl-naphtho-[1,8-de][1,3,2]Diaza-borinane. *Acta Crystallogr. Sect. E Struct. Rep. Online* **2011**, *67* (8), o1995–o1995. https://doi.org/10.1107/S1600536811026985.
(62) Meng, S.; Caprasecca, S.; Guido, C. A.; Jurinovich, S.; Mennucci, B. Negative Solvatochromism of Push–Pull Biphenyl Compounds: A Theoretical Study. *Theor. Chem. Acc.* **2015**, *134* (12), 150. https://doi.org/10.1007/s00214-015-1754-z.
(63) Chen, Y.; Lam, J. W. Y.; Kwok, R. T. K.; Liu, B.; Tang, B. Z. Aggregation-Induced Emission: Fundamental Understanding and Future Developments. *Mater. Horiz.* **2019**, *6* (3), 428–433. https://doi.org/10.1039/C8MH01331D.
(64) Jaeger, R.; Blalock, T. *Microelectronic Circuit Design*, 4th ed.; McGraw-Hill: New York, 2011.
(65) de Silva, P. A.; Gunaratne, N. H. Q.; McCoy, C. P. A Molecular Photoionic AND Gate Based on Fluorescent Signalling. *Nature* **1993**, *364* (6432), 42–44. https://doi.org/10.1038/364042a0.
(66) Erbas-Cakmak, S.; Kolemen, S.; Sedgwick, A. C.; Gunnlaugsson, T.; James, T. D.; Yoon, J.; Akkaya, E. U. Molecular Logic Gates: The Past, Present and Future. *Chem. Soc. Rev.* **2018**, *47* (7), 2228–2248. https://doi.org/10.1039/C7CS00491E.
(67) Andréasson, J.; Pischel, U. Molecules for Security Measures: From Keypad Locks to Advanced Communication Protocols. *Chem. Soc. Rev.* **2018**, *47* (7), 2266–2279. https://doi.org/10.1039/C7CS00287D.
(68) Schmulbach, C. D. The Acetonitrile-Aluminium Chloride System. *J. Inorg. Nucl. Chem.* **1964**, *26* (5), 745–749. https://doi.org/10.1016/0022-1902(64)80318-3.
(69) Richardson, D.; Alger, T. D. Proton Magnetic Resonance Studies of Aluminum(III) and Gallium(III) in Methanol and Ethanol. Determination of Solvation Number and Exchange Rate. *J. Phys. Chem.* **1975**, *79* (16), 1733–1739. https://doi.org/10.1021/j100583a026.
(70) Hansen, M. M.; Jolly, R. A.; Linder, R. J. Boronic Acids and Derivatives—Probing the Structure–Activity Relationships for Mutagenicity. **2015**. https://doi.org/10.1021/acs.oprd.5b00150.
(71) O'Donovan, M. R.; Mee, C. D.; Fenner, S.; Teasdale, A.; Phillips, D. H. Boronic Acids—A Novel Class of Bacterial Mutagen. *Mutat. Res. Toxicol. Environ. Mutagen.* **2011**, *724* (1), 1–6. https://doi.org/10.1016/j.mrgentox.2011.05.006.
(72) Boström, J.; Brown, D. G.; Young, R. J.; Keserü, G. M. Expanding the Medicinal Chemistry Synthetic Toolbox. *Nat. Rev. Drug Discov.* **2018**, *17* (10), 709–727. https://doi.org/10.1038/nrd.2018.116.

(73) Brancatelli, G.; Drommi, D.; Feminò, G.; Saporita, M.; Bottari, G.; Faraone, F. Basicity and Bulkiness Effects of 1,8-Diaminonaphthalene, 8-Aminoquinoline and Their Alkylated Derivatives on the Different Efficiencies of H5-C5H5 and H5-C5Me5 Ruthenium Precatalysts in Allylic Etherification Reactions. *New J. Chem.* **2010**, *34* (12), 2853–2860. https://doi.org/10.1039/C0NJ00338G.
(74) Novoselov, K. S.; Geim, A. K.; Morozov, S. V.; Jiang, D.; Zhang, Y.; Dubonos, S. V.; Grigorieva, I. V.; Firsov, A. A. Electric Field Effect in Atomically Thin Carbon Films. *Science* **2004**, *306* (5696), 666–669. https://doi.org/10.1126/science.1102896.
(75) The Nobel Prize in Physics 2010 https://www.nobelprize.org/prizes/physics/2010/press-release/ (accessed Dec 9, 2019).
(76) Coroş, M.; Pogăcean, F.; Măgeruşan, L.; Socaci, C.; Pruneanu, S. A Brief Overview on Synthesis and Applications of Graphene and Graphene-Based Nanomaterials. *Front. Mater. Sci.* **2019**, *13* (1), 23–32. https://doi.org/10.1007/s11706-019-0452-5.
(77) Lin, H.-A.; Sato, Y.; Segawa, Y.; Nishihara, T.; Sugimoto, N.; Scott, L. T.; Higashiyama, T.; Itami, K. A Water-Soluble Warped Nanographene: Synthesis and Applications for Photoinduced Cell Death. *Angew. Chem. Int. Ed.* **2018**, *57* (11), 2874–2878. https://doi.org/10.1002/anie.201713387.
(78) Schleyer, P. von R. Introduction: Aromaticity. *Chem. Rev.* **2001**, *101* (5), 1115–1118. https://doi.org/10.1021/cr0103221.
(79) Tour, J. M. Top-Down versus Bottom-Up Fabrication of Graphene-Based Electronics. *Chem. Mater.* **2014**, *26* (1), 163–171. https://doi.org/10.1021/cm402179h.
(80) Cortizo-Lacalle, D.; Mora-Fuentes, J. P.; Strutyński, K.; Saeki, A.; Melle-Franco, M.; Mateo-Alonso, A. Monodisperse N-Doped Graphene Nanoribbons Reaching 7.7 Nanometers in Length. *Angew. Chem. Int. Ed.* **2018**, *57* (3), 703–708. https://doi.org/10.1002/anie.201710467.
(81) Wei, H.; Liu, Y.; Gopalakrishna, T. Y.; Phan, H.; Huang, X.; Bao, L.; Guo, J.; Zhou, J.; Luo, S.; Wu, J.; et al. B–N–B Bond Embedded Phenalenyl and Its Anions. *J. Am. Chem. Soc.* **2017**, *139* (44), 15760–15767. https://doi.org/10.1021/jacs.7b07375.
(82) Giustra, Z. X.; Liu, S.-Y. The State of the Art in Azaborine Chemistry: New Synthetic Methods and Applications. *J. Am. Chem. Soc.* **2018**, *140* (4), 1184–1194. https://doi.org/10.1021/jacs.7b09446.
(83) Pan, J.; Kampf, J. W.; Ashe, A. J. The Ligand Properties of 2-Vinyl-1,2-Azaboratabenzene. *J. Organomet. Chem.* **2009**, *694* (7), 1036–1040. https://doi.org/10.1016/j.jorganchem.2008.10.043.
(84) Giustra, Z. X.; Yang, X.; Chen, M.; Bettinger, H. F.; Liu, S.-Y. Accessing 1,2-Substituted Cyclobutanes through 1,2-Azaborine Photoisomerization. *Angew. Chem. Int. Ed. n/a* (n/a). https://doi.org/10.1002/anie.201912132.
(85) Zhao, P.; Nettleton, D. O.; Karki, R. G.; Zécri, F. J.; Liu, S.-Y. Medicinal Chemistry Profiling of Monocyclic 1,2-Azaborines. *ChemMedChem* **2017**, *12* (5), 358–361. https://doi.org/10.1002/cmdc.201700047.
(86) Stojanović, M.; Baranac-Stojanović, M. Mono BN-Substituted Analogues of Naphthalene: A Theoretical Analysis of the Effect of BN Position on Stability, Aromaticity and Frontier Orbital Energies. *New J. Chem.* **2018**, *42* (15), 12968–12976. https://doi.org/10.1039/C8NJ01529E.

(87) Liu, X.; Wu, P.; Li, J.; Cui, C. Synthesis of 1,2-Borazaronaphthalenes from Imines by Base-Promoted Borylation of C–H Bond. *J. Org. Chem.* **2015**, *80* (8), 3737–3744. https://doi.org/10.1021/jo5029437.
(88) Fox, J. M.; Huang, X.; Chieffi, A.; Buchwald, S. L. Highly Active and Selective Catalysts for the Formation of α-Aryl Ketones. *J. Am. Chem. Soc.* **2000**, *122* (7), 1360–1370. https://doi.org/10.1021/ja993912d.
(89) Xu, L.; Li, P. Direct Introduction of a Naphthalene-1,8-Diamino Boryl [B(Dan)] Group by a Pd-Catalysed Selective Boryl Transfer Reaction. *Chem. Commun.* **2015**, *51* (26), 5656–5659. https://doi.org/10.1039/C5CC00231A.
(90) Ding, S.; Zhao, Y.; Ma, Q.; Tian, S.; Liu, J.; Yu, F. New Method for Preparing Asymmetric Boron Reagent Bpin-Bdan. CN106946916 (A), July 14, 2017.
(91) Körner, C.; Starkov, P.; Sheppard, T. D. An Alternative Approach to Aldol Reactions: Gold-Catalyzed Formation of Boron Enolates from Alkynes. *J. Am. Chem. Soc.* **2010**, *132* (17), 5968–5969. https://doi.org/10.1021/ja102129c.
(92) Yamamoto, Y.; Matsubara, H.; Yorimitsu, H.; Osuka, A. Base-Free Palladium-Catalyzed Borylation of Aryl Chlorides with Diborons. *ChemCatChem* **2016**, *8* (14), 2317–2320. https://doi.org/10.1002/cctc.201600456.
(93) Yamamoto, Y.; Matsubara, H.; Murakami, K.; Yorimitsu, H.; Osuka, A. Activator-Free Palladium-Catalyzed Silylation of Aryl Chlorides with Silylsilatranes. *Chem. – Asian J.* **2015**, *10* (1), 219–224. https://doi.org/10.1002/asia.201402595.
(94) Coutts, S. J.; Adams, J.; Krolikowski, D.; Snow, R. J. Two Efficient Methods for the Cleavage of Pinanediol Boronate Esters Yielding the Free Boronic Acids. *Tetrahedron Lett.* **1994**, *35* (29), 5109–5112. https://doi.org/10.1016/S0040-4039(00)77040-7.
(95) Yuen, A. K. L.; Hutton, C. A. Deprotection of Pinacolyl Boronate Esters via Hydrolysis of Intermediate Potassium Trifluoroborates. *Tetrahedron Lett.* **2005**, *46* (46), 7899–7903. https://doi.org/10.1016/j.tetlet.2005.09.101.
(96) Bagutski, V.; Ros, A.; Aggarwal, V. K. Improved Method for the Conversion of Pinacolboronic Esters into Trifluoroborate Salts: Facile Synthesis of Chiral Secondary and Tertiary Trifluoroborates. *Tetrahedron* **2009**, *65* (48), 9956–9960. https://doi.org/10.1016/j.tet.2009.10.002.
(97) Molander, G. A.; Trice, S. L. J.; Kennedy, S. M.; Dreher, S. D.; Tudge, M. T. Scope of the Palladium-Catalyzed Aryl Borylation Utilizing Bis-Boronic Acid. *J. Am. Chem. Soc.* **2012**, *134* (28), 11667–11673. https://doi.org/10.1021/ja303181m.
(98) Dong, J.-L.; Yu, L.-S.-H.; Xie, J.-W. A Simple and Versatile Method for the Formation of Acetals/Ketals Using Trace Conventional Acids. *ACS Omega* **2018**, *3* (5), 4974–4985. https://doi.org/10.1021/acsomega.8b00159.
(99) Patra, T.; Bag, S.; Kancherla, R.; Mondal, A.; Dey, A.; Pimparkar, S.; Agasti, S.; Modak, A.; Maiti, D. Palladium-Catalyzed Directed Para C−H Functionalization of Phenols. *Angew. Chem. Int. Ed.* **2016**, *55* (27), 7751–7755. https://doi.org/10.1002/anie.201601999.
(100) Kristensen, J.; Lysén, M.; Vedsø, P.; Begtrup, M. Synthesis of Ortho Substituted Arylboronic Esters by in Situ Trapping of Unstable Lithio Intermediates. *Org. Lett.* **2001**, *3* (10), 1435–1437. https://doi.org/10.1021/ol015598+.
(101) J. Cooper, D.; N. Owen, L. Cytotoxic Compounds. Part VII. α-Aryl-α-Halogenoacetophenones, Their Enol Acetates, and Some Related Compounds. *J. Chem. Soc. C Org.* **1966**, *0* (0), 533–540. https://doi.org/10.1039/J39660000533.

(102) Pichette Drapeau, M.; Fabre, I.; Grimaud, L.; Ciofini, I.; Ollevier, T.; Taillefer, M. Transition-Metal-Free α-Arylation of Enolizable Aryl Ketones and Mechanistic Evidence for a Radical Process. *Angew. Chem. Int. Ed Engl.* **2015**, *54* (36), 10587–10591. https://doi.org/10.1002/anie.201502332.
(103) Srinivasan, R.; Pheng Tan, L.; Wu, H.; Yang, P.-Y.; A. Kalesh, K.; Q. Yao, S. High-Throughput Synthesis of Azide Libraries Suitable for Direct "Click" Chemistry and in Situ Screening. *Org. Biomol. Chem.* **2009**, *7* (9), 1821–1828. https://doi.org/10.1039/B902338K.
(104) Nahm, S.; Weinreb, S. M. N-Methoxy-n-Methylamides as Effective Acylating Agents. *Tetrahedron Lett.* **1981**, *22* (39), 3815–3818. https://doi.org/10.1016/S0040-4039(01)91316-4.
(105) Kim, J. G.; Jang, D. A Convenient One-Pot Method for the Synthesis of N-Methoxy-N-Methyl Amides from Carboxylic Acids. *Bull. Korean Chem. Soc.* **2010**, *31* (1), 171–173. https://doi.org/10.5012/bkcs.2010.31.01.171.
(106) Jammula, S. R.; Anna, V. R.; Tatina, S.; Krishna, T.; Sreenivas, B. Y.; Pal, M. A New Strategy for Accessing (S)-1-(Furan-2-Yl)Pent-4-En-1-Ol: A Key Precursor of Ipomoeassin Family of Compounds and C1–C15 Domain of Halichondrins. *Tetrahedron Lett.* **2016**, *57* (35), 3924–3928. https://doi.org/10.1016/j.tetlet.2016.07.059.
(107) Zacuto, M. J.; Dunn, R. F.; Figus, M. One-Step Synthesis of 1-Chloro-3-Arylacetone Derivatives from Arylacetic Acids. *J. Org. Chem.* **2014**, *79* (18), 8917–8925. https://doi.org/10.1021/jo5016486.
(108) Lawrence, K.; Flower, S. E.; Kociok-Kohn, G.; Frost, C. G.; James, T. D. A Simple and Effective Colorimetric Technique for the Detection of Boronic Acids and Their Derivatives. *Anal. Methods* **2012**, *4* (8), 2215–2217. https://doi.org/10.1039/C2AY25346A.
(109) Lait, S. M.; Rankic, D. A.; Keay, B. A. 1,3-Aminoalcohols and Their Derivatives in Asymmetric Organic Synthesis. *Chem. Rev.* **2007**, *107* (3), 767–796. https://doi.org/10.1021/cr050065q.
(110) Erker, G.; Wingbermühle, D.; Grehl, M.; Fröhlich, R. Borylation of a Stable Primary Enamine. *Chem. Ber.* **1994**, *127* (7), 1331–1332. https://doi.org/10.1002/cber.19941270725.
(111) Aguilera-Sáez, L. M.; Belmonte-Sánchez, J. R.; Romero-González, R.; Vidal, J. L. M.; Arrebola, F. J.; Frenich, A. G.; Fernández, I. Pushing the Frontiers: Boron-11 NMR as a Method for Quantitative Boron Analysis and Its Application to Determine Boric Acid in Commercial Biocides. *Analyst* **2018**, *143* (19), 4707–4714. https://doi.org/10.1039/C8AN00505B.
(112) Nocentini, A.; Supuran, C. T.; Winum, J.-Y. Benzoxaborole Compounds for Therapeutic Uses: A Patent Review (2010- 2018). *Expert Opin. Ther. Pat.* **2018**, *28* (6), 493–504. https://doi.org/10.1080/13543776.2018.1473379.
(113) Ager, D. J.; Prakash, I.; Schaad, D. R. 1,2-Amino Alcohols and Their Heterocyclic Derivatives as Chiral Auxiliaries in Asymmetric Synthesis. *Chem. Rev.* **1996**, *96* (2), 835–876. https://doi.org/10.1021/cr9500038.
(114) Mancilla, T.; Contreras, R.; Wrackmeyer, B. New Bicyclic Organylboronic Esters Derived from Iminodiacetic Acids. *J. Organomet. Chem.* **1986**, *307* (1), 1–6. https://doi.org/10.1016/0022-328X(86)80169-3.

(115) Bardhan, M.; Misra, T.; Chowdhury, J.; Ganguly, T. Comparative Studies by Using Spectroscopic Tools on the Charge Transfer (CT) Band of a Novel Synthesized Short-Chain Dyad in Isotropic Media and in a Gel (P123). *Chem. Phys. Lett.* **2009**, *481* (1), 142–148. https://doi.org/10.1016/j.cplett.2009.09.054.
(116) Brustad, E.; Bushey, M. L.; Lee, J. W.; Groff, D.; Liu, W.; Schultz, P. G. A Genetically Encoded Boronate Amino Acid. *Angew. Chem. Int. Ed Engl.* **2008**, *47* (43), 8220–8223. https://doi.org/10.1002/anie.200803240.
(117) António, J. P. M.; Russo, R.; Carvalho, C. P.; Cal, P. M. S. D.; Gois, P. M. P. Boronic Acids as Building Blocks for the Construction of Therapeutically Useful Bioconjugates. *Chem. Soc. Rev.* **2019**, *48* (13), 3513–3536. https://doi.org/10.1039/C9CS00184K.
(118) Akgun, B.; Hall, D. G. Boronic Acids as Bioorthogonal Probes for Site-Selective Labeling of Proteins. *Angew. Chem. Int. Ed.* **2018**, *57* (40), 13028–13044. https://doi.org/10.1002/anie.201712611.
(119) Svoboda, K.; Yasuda, R. Principles of Two-Photon Excitation Microscopy and Its Applications to Neuroscience. *Neuron* **2006**, *50* (6), 823–839. https://doi.org/10.1016/j.neuron.2006.05.019.
(120) Yoshida, J.; Suga, S.; Suzuki, S.; Kinomura, N.; Yamamoto, A.; Fujiwara, K. Direct Oxidative Carbon−Carbon Bond Formation Using the "Cation Pool" Method. 1. Generation of Iminium Cation Pools and Their Reaction with Carbon Nucleophiles. *J. Am. Chem. Soc.* **1999**, *121* (41), 9546–9549. https://doi.org/10.1021/ja9920112.
(121) Suga, S.; Suzuki, S.; Yoshida, J. Reduction of a "Cation Pool": A New Approach to Radical Mediated C−C Bond Formation. *J. Am. Chem. Soc.* **2002**, *124* (1), 30–31. https://doi.org/10.1021/ja0171759.
(122) Suga, S. Cation-Pool Method. In *Encyclopedia of Applied Electrochemistry*; Kreysa, G., Ota, K., Savinell, R. F., Eds.; Springer: New York, NY, 2014; pp 154–159. https://doi.org/10.1007/978-1-4419-6996-5_342.
(123) Weigert, F. J. Polyamines from Cyanobutadienes. *J. Org. Chem.* **1978**, *43* (4), 622–626. https://doi.org/10.1021/jo00398a021.
(124) Suissa, M. R.; Rømming, C.; Dale, J. Synthesis and Conformation Studies of a Dodecaazanonacyclotetratetracontane. *Chem. – Eur. J.* **1999**, *5* (10), 3055–3065. https://doi.org/10.1002/(SICI)1521-3765(19991001)5:10<3055::AID-CHEM3055>3.0.CO;2-N.

Appendices

Appendix 1: Representative NMR Spectra

^{1}H NMR Spectrum for Compound 2-4 (acetonitrile-d_3, 498 MHz)

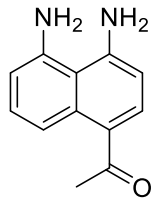

^{13}C NMR Spectrum for Compound 2-4 (acetonitrile-d_3, 176 MHz)

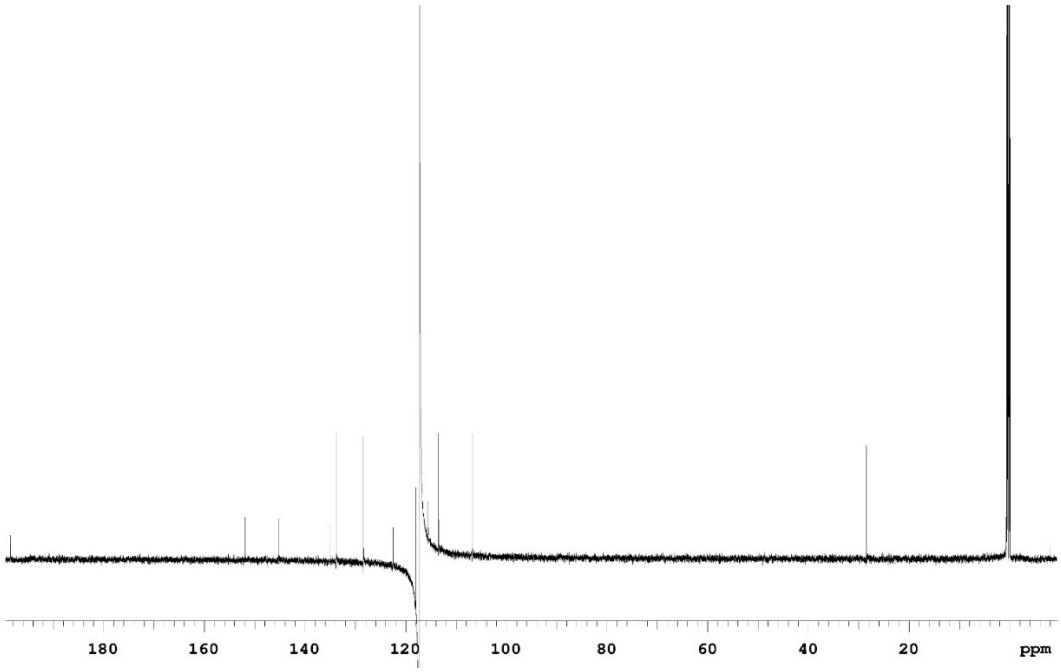

^{1}H NMR Spectrum for Compound 2-5 (acetonitrile-d_3, 400 MHz)

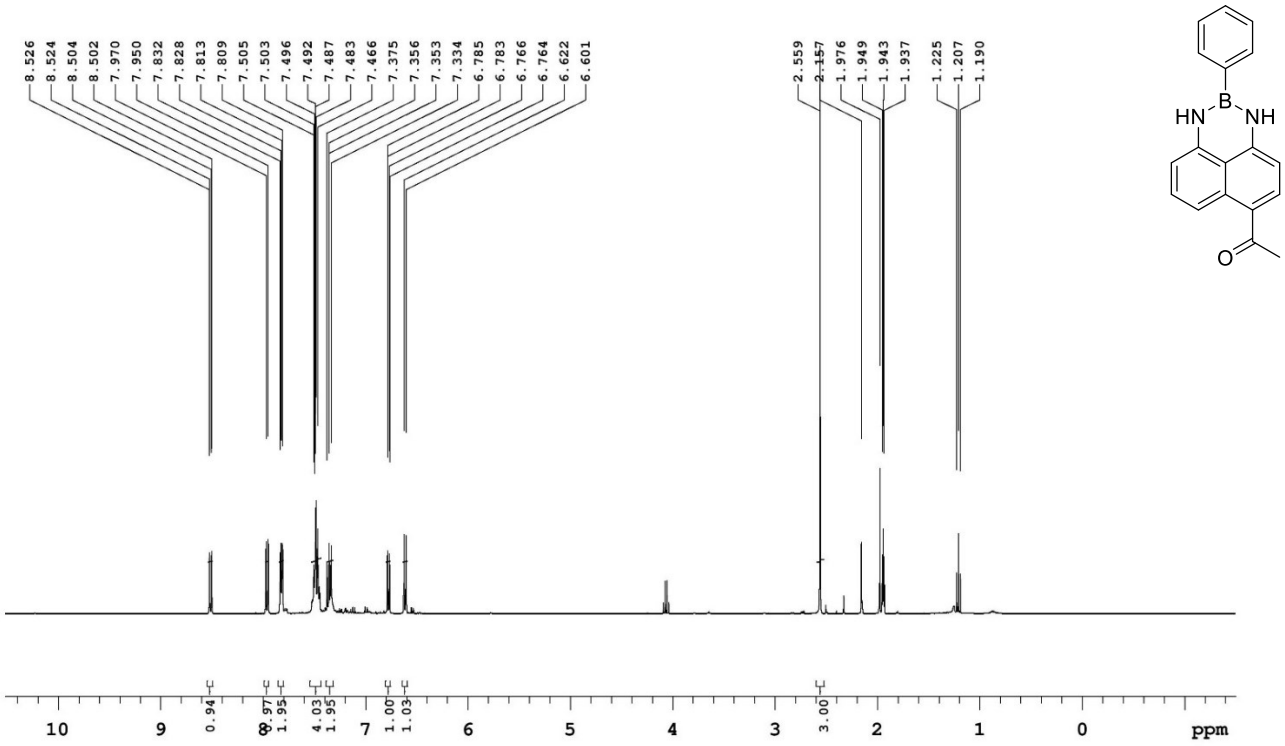

^{13}C NMR Spectrum for Compound 2-5 (acetone-d_6, 176 MHz)

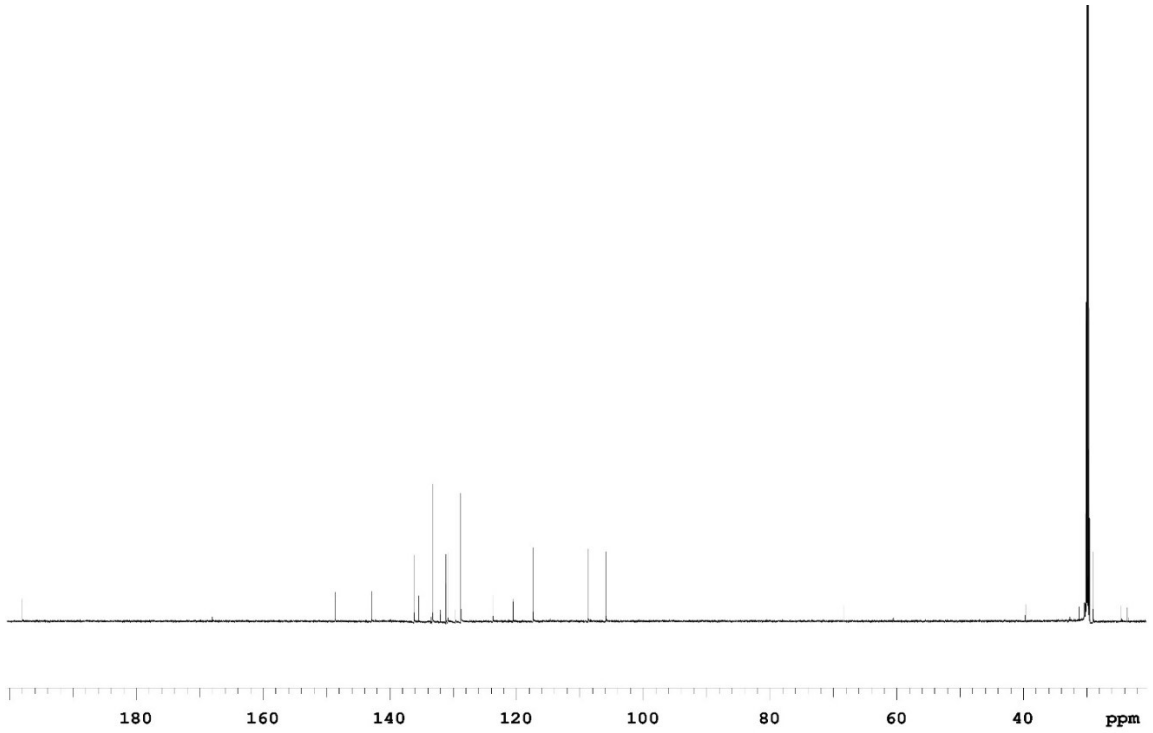

^{1}H NMR Spectrum for Compound 2-14 (acetone-d_6, 400 MHz)

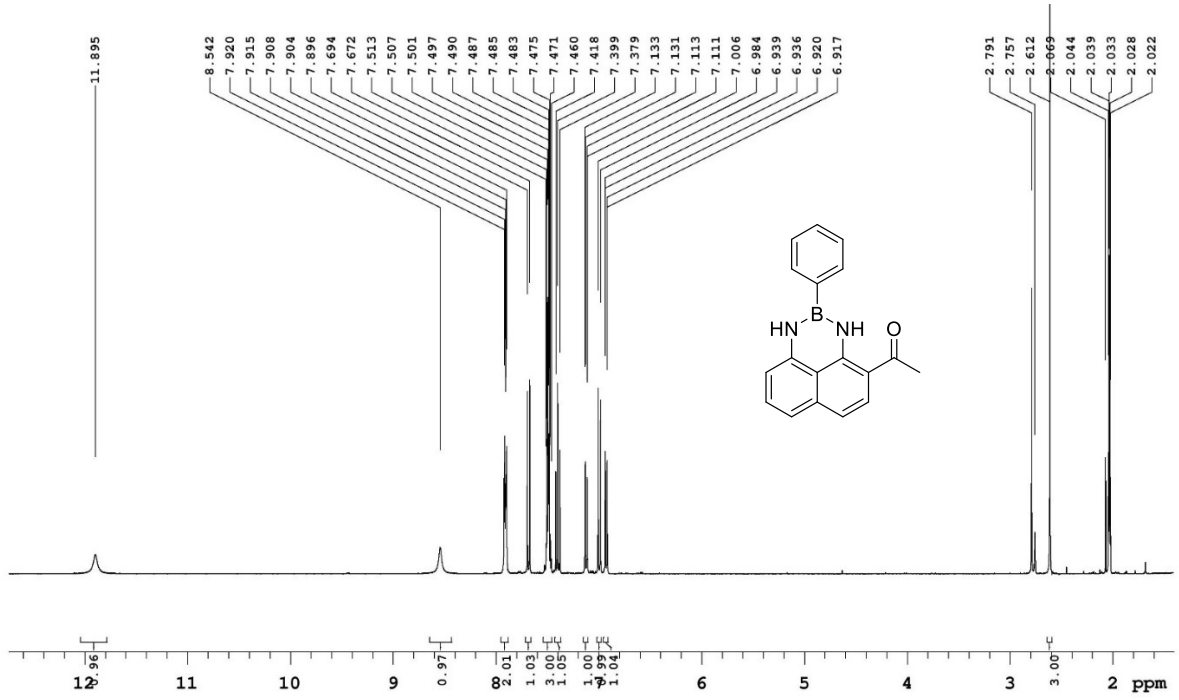

^{13}C NMR Spectrum for Compound 2-14 (acetone-d_6, 176 MHz)

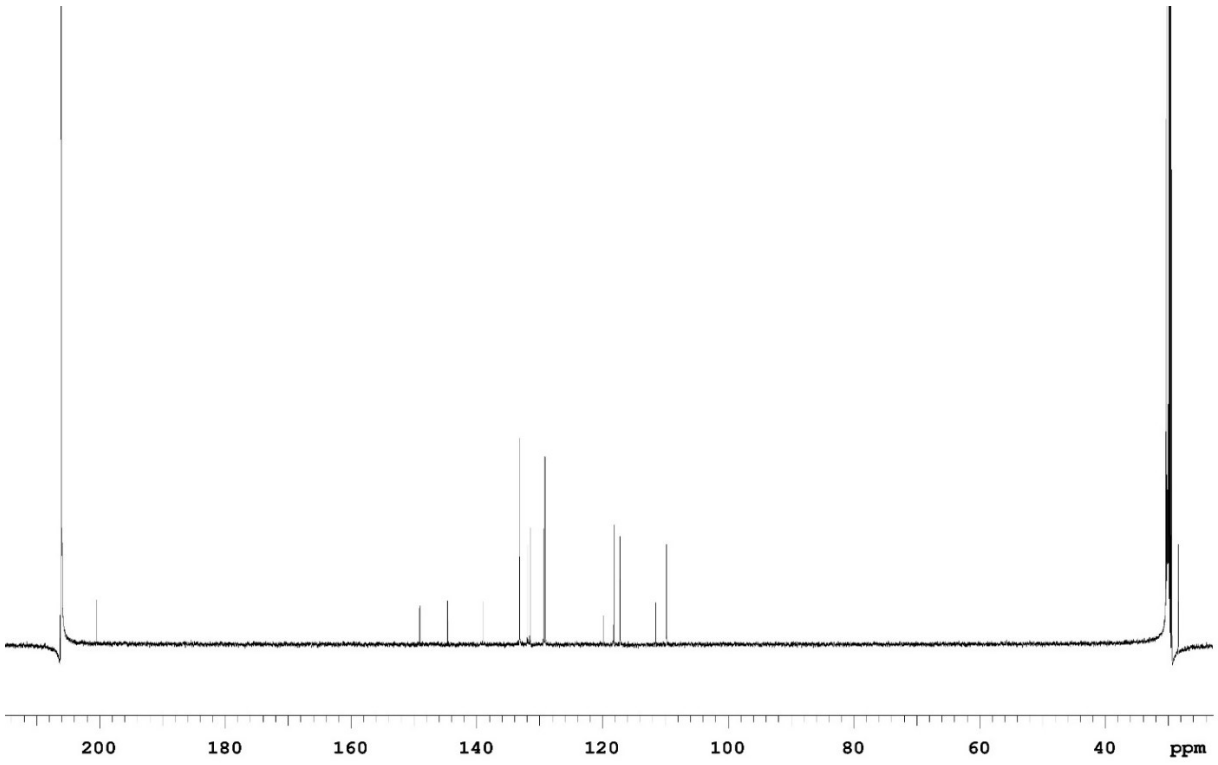

^{1}H NMR Spectrum for Compound 2-15 (acetone-d_6, 498 MHz)

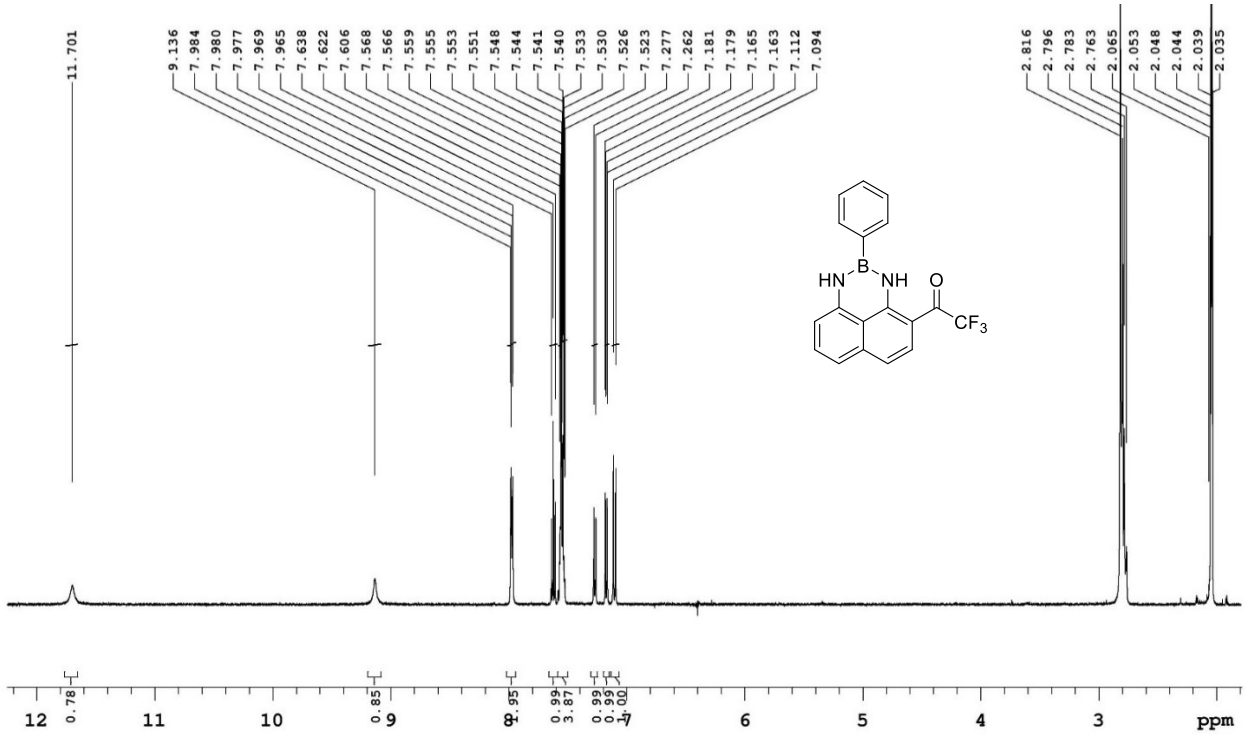

^{13}C NMR Spectrum for Compound 2-15 (acetone-d_6, 176 MHz)

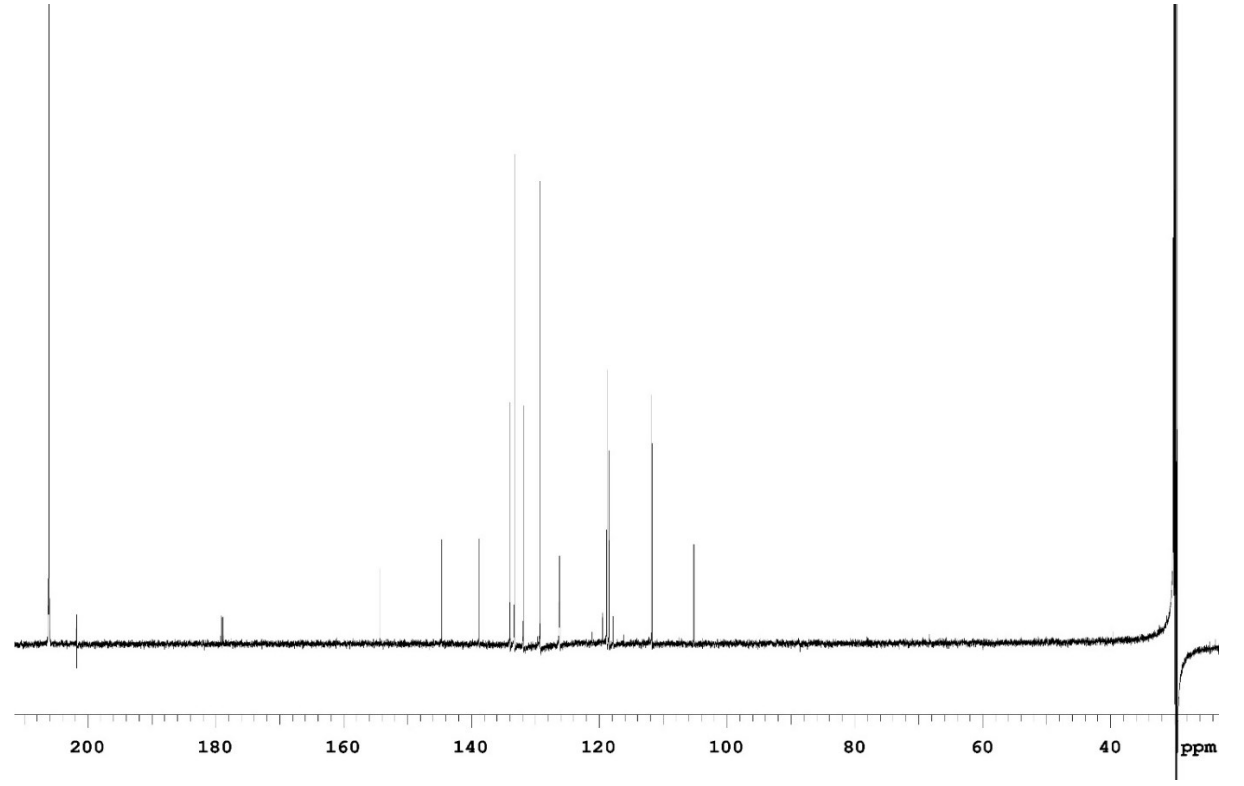

^{1}H NMR Spectrum for Compound 3-15 (400 MHz, $CDCl_3$)

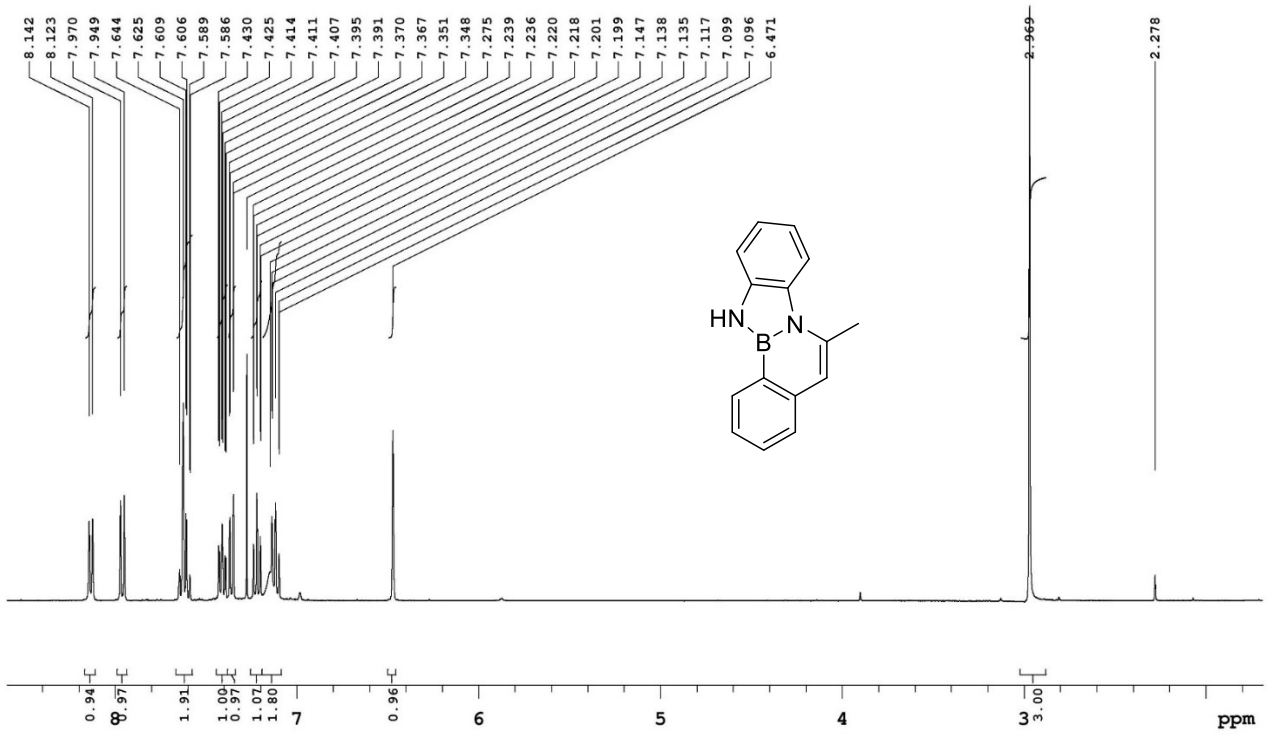

^{13}C NMR Spectrum for Compound 3-15 (176 MHz, $CDCl_3$)

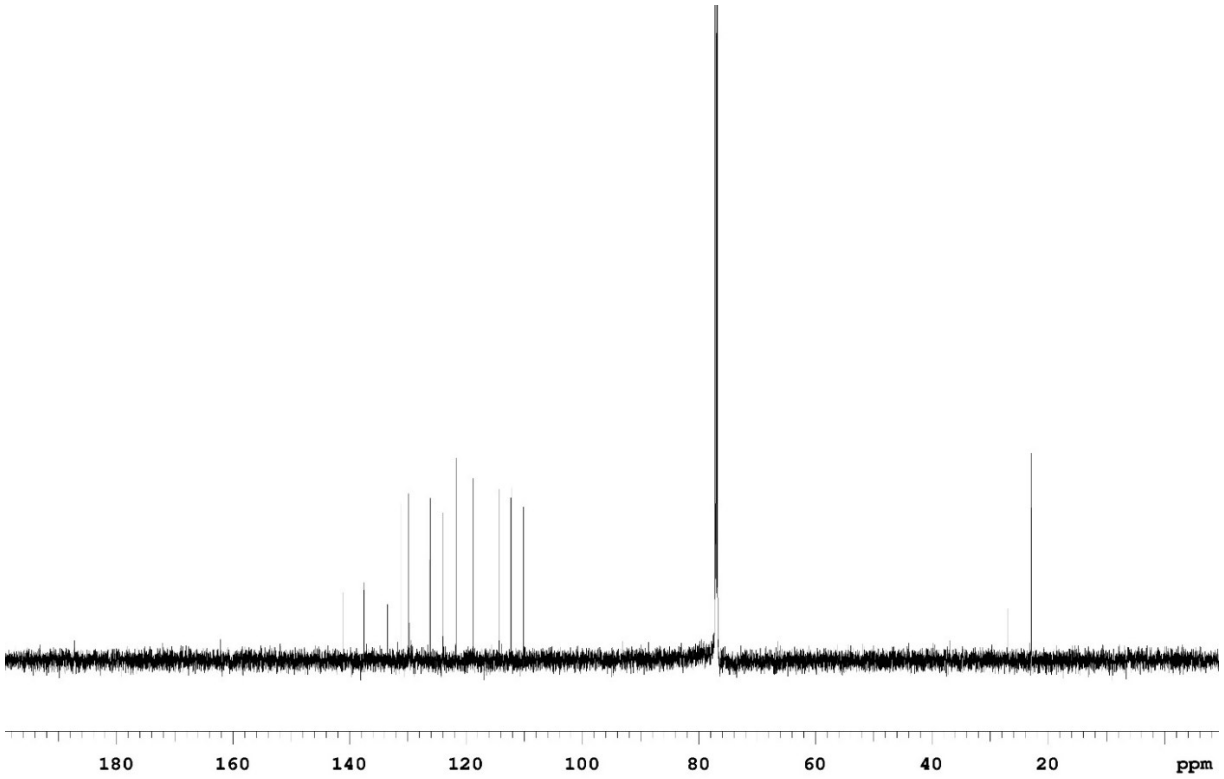

^{1}H NMR Spectrum for Compound 3-19 (400 MHz, $CDCl_3$)

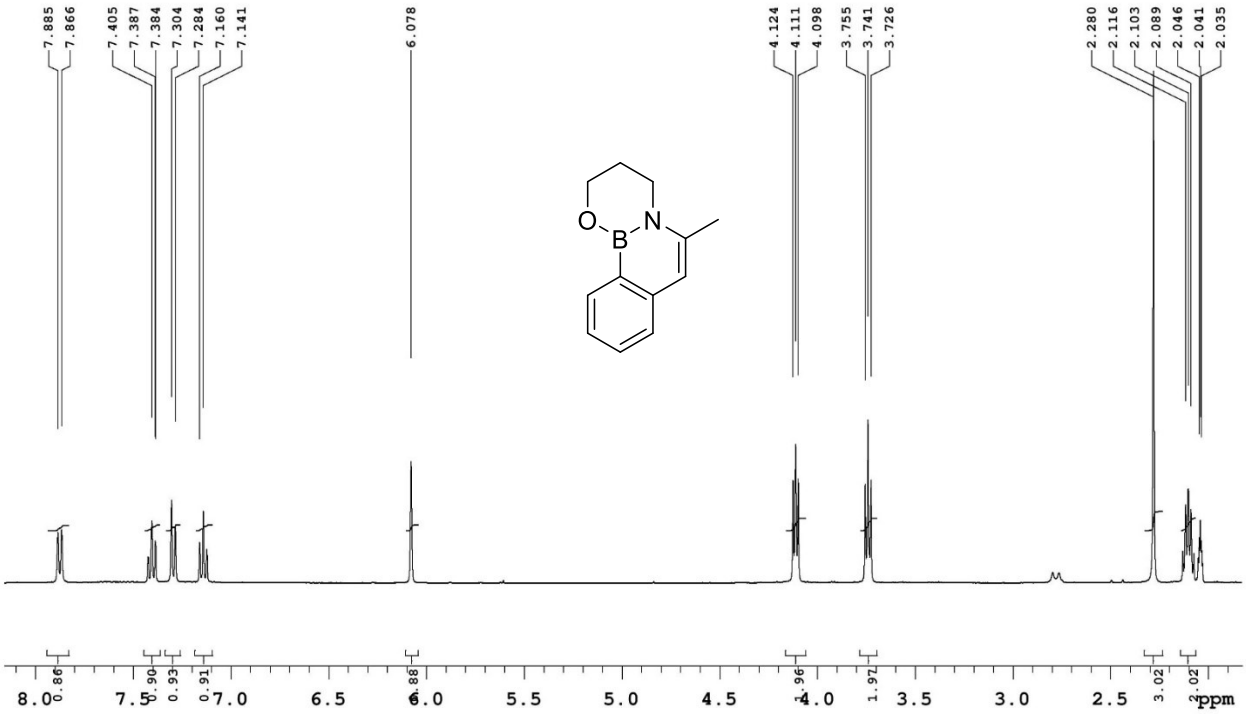

^{13}C NMR Spectrum for Compound 3-19 (177 MHz, $CDCl_3$)

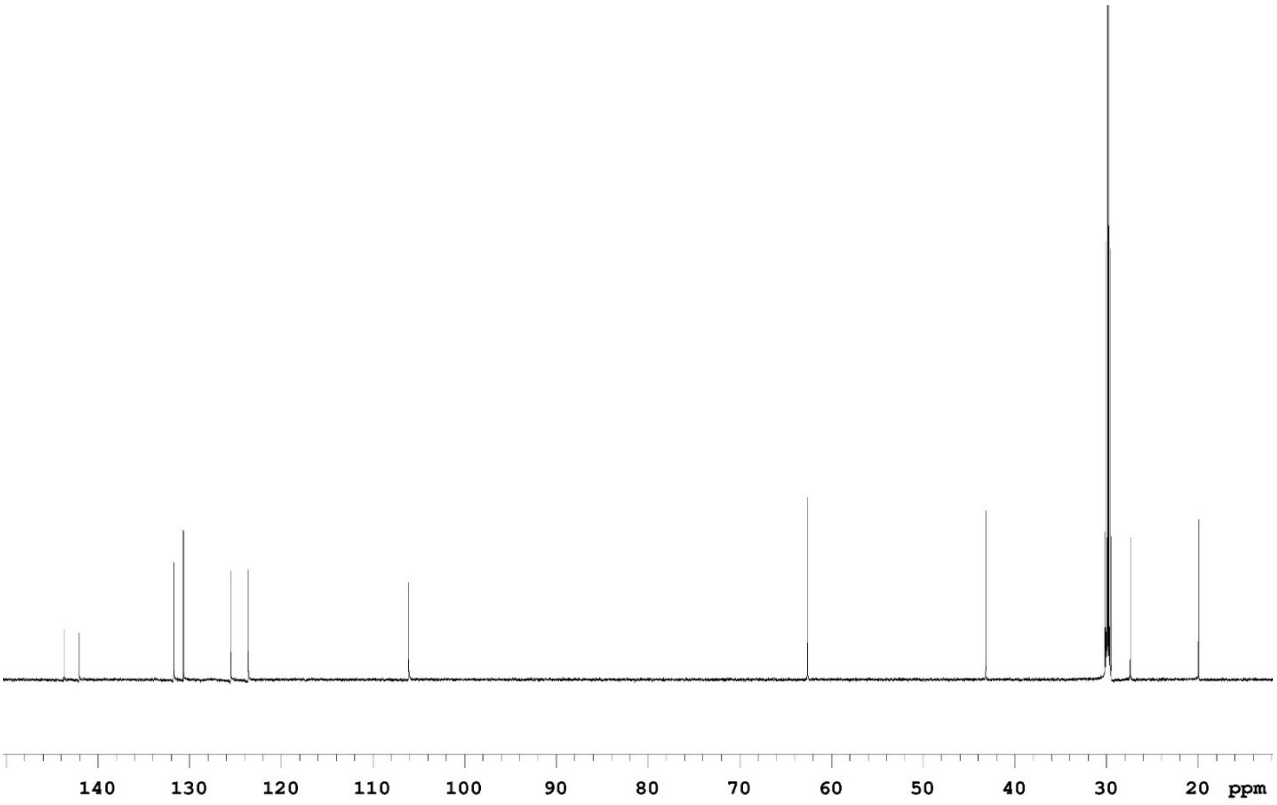

Appendix 2: Crystal Structure Reports

X-Ray Crystallographic Data for 2-14

XCL Code: DGH1902 **Date:** 26 June 2019

Compound: 1-(2-phenyl-2,3-dihydro-1H-naphtho[1,8-de][1,3,2]diazaborinin-4-yl)ethanone

Formula: $C_{18}H_{15}BN_2O$

Supervisor: D. Hall **Crystallographer:** Y. Zhou

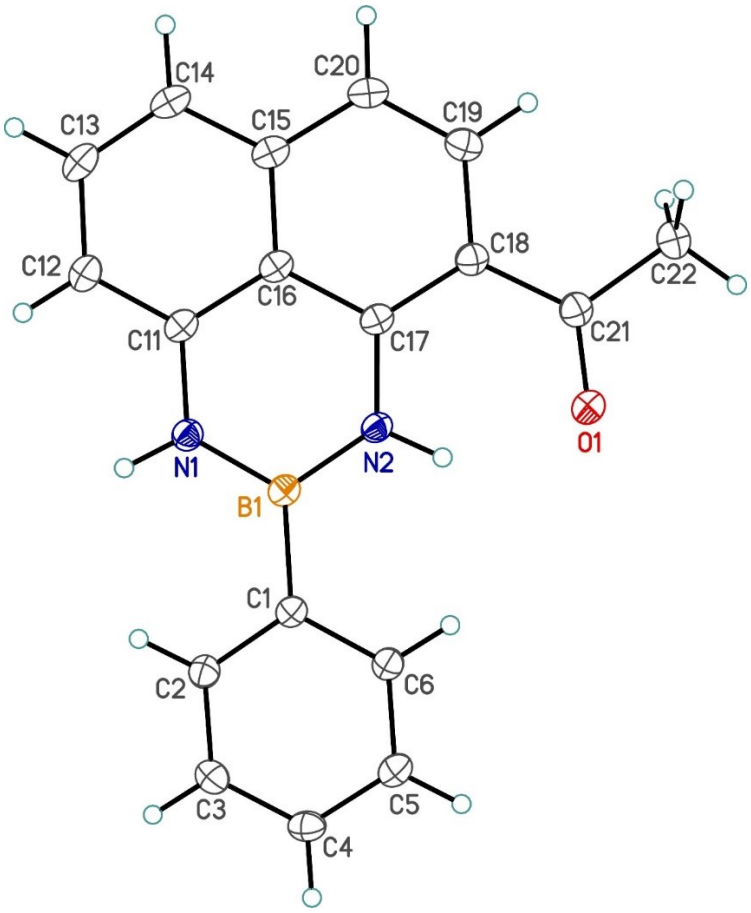

For further information regarding this X-ray, please contact the X-ray crystallography laboratory at the University of Alberta:

Dr. Yuqiao Zhou **E-Mail:** yuqiao4@ualberta.ca

Dr. Michael J. Ferguson **E-Mail:** Michael.Ferguson@ualberta.ca Lab: E3-09; Office: E3-13 Gunning/Lemieux Chemistry Centre

Phone: +1 780 492 2485; **Fax:** +1 780 492 8231

X-Ray Crystallography Laboratory, Department of Chemistry, University of Alberta, Edmonton, Alberta, T6G 2G2, Canada.

X-Ray Crystallographic Data for 2-15

XCL Code: DGH1911 **Date:** 5 September 2019

Compound: 2,2,2-trifluoro-1-(2-phenyl-2,3-dihydro-1*H*-naphtho[1,8-*de*][1,3,2]diazaborinin-4-yl)ethanone

Formula: $C_{18}H_{12}BF_3N_2O$

Supervisor: D. G. Hall **Crystallographer:** M. J. Ferguson

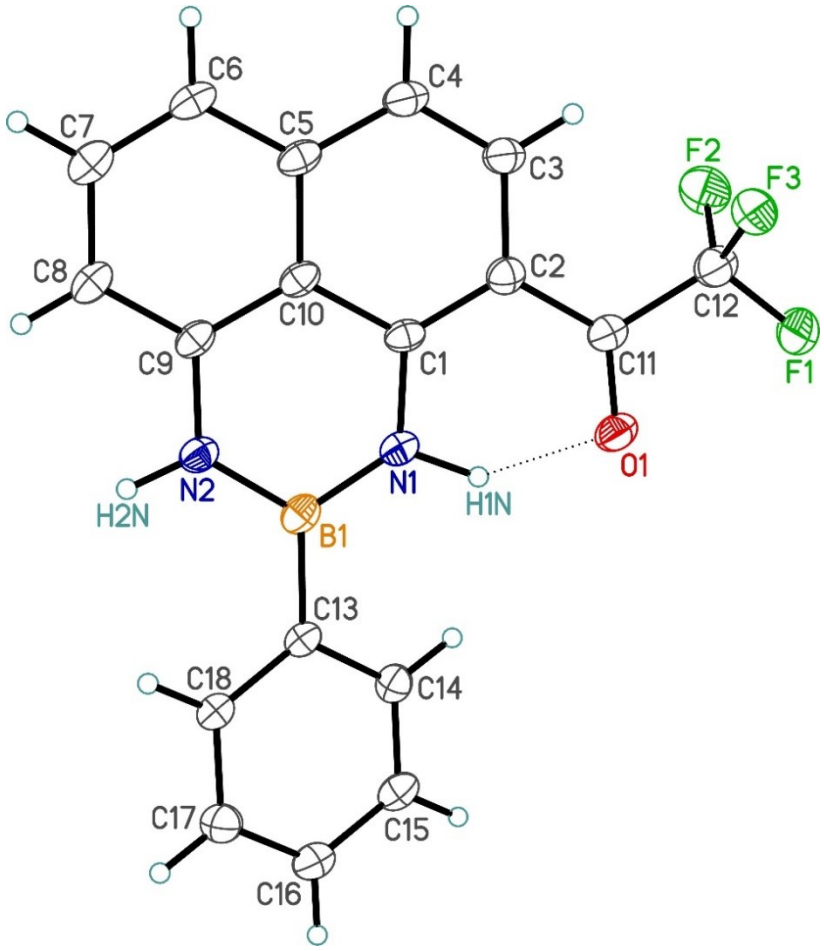

For further information regarding this X-ray, please contact the X-ray crystallography laboratory at the University of Alberta:

Dr. Michael J. Ferguson **E-Mail:** Michael.Ferguson@ualberta.ca Lab: E3-09; Office: E3-13 Gunning/Lemieux Chemistry Centre

Phone: +1 780 492 2485; **Fax:** +1 780 492 8231

X-Ray Crystallography Laboratory, Department of Chemistry, University of Alberta, Edmonton, Alberta, T6G 2G2, Canada.

X-Ray Crystallographic Data for 3-19

XCL Code: DGH1905 **Date:** 12 July 2019

Compound: 6-methyl-3,4-dihydro-2*H*-[1,3,2]oxazaborinino[2,3-a][2,1]benzazaborinine

Formula: $C_{12}H_{14}BNO$

Supervisor: D. Hall **Crystallographer:** Y. Zhou

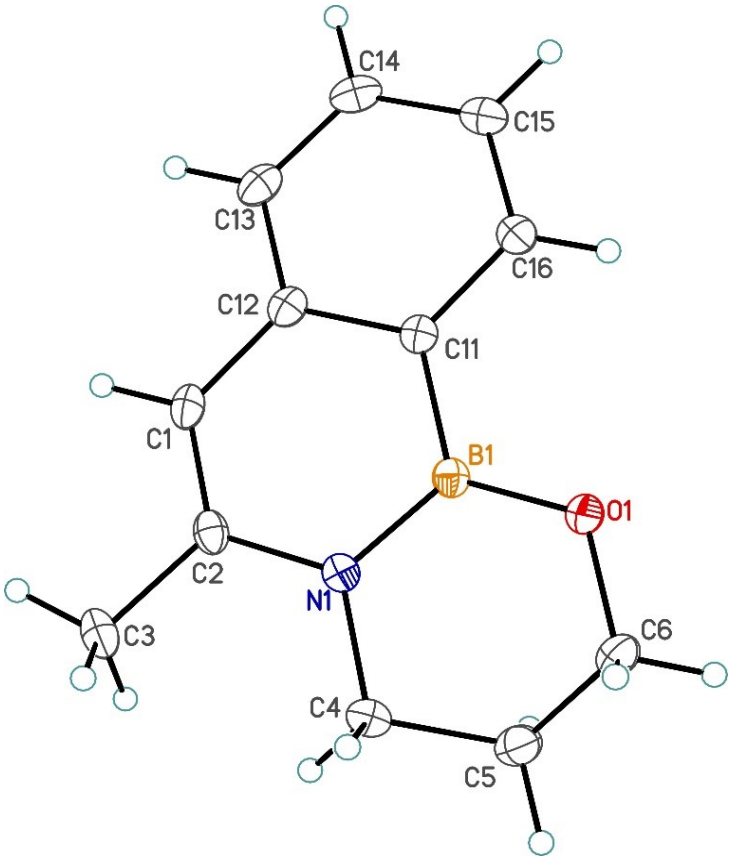

For further information regarding this X-ray, please contact the X-ray crystallography laboratory at the University of Alberta:

Dr. Yuqiao Zhou **E-Mail:** yuqiao4@ualberta.ca

Dr. Michael J. Ferguson **E-Mail:** Michael.Ferguson@ualberta.ca Lab: E3-09; Office: E3-13 Gunning/Lemieux Chemistry Centre

Phone: +1 780 492 2485; **Fax:** +1 780 492 8231

X-Ray Crystallography Laboratory, Department of Chemistry, University of Alberta, Edmonton, Alberta, T6G 2G2, Canada.